Synthesis of Carboxylated Dithiafulvenes and Tetrathiafulvalene Vinylogues as Redox-Active Ligands

by

©Hadeel Adows

A thesis submitted to the School of Graduate Studies in partial fulfillment of the requirements for the degree of

Master of Science

Department of Chemistry

Memorial University of Newfoundland

December 2016

St. John's Newfoundland

Abstract

The excellent electron-donating properties of dithiafulvene (DTF) derivatives and tetrathiafulvene vinylogues (TTFVs) make them versatile building components in the synthesis of functional organic optoelectronic materials and devices. The recent synthesis and characterization studies on functionalized DTF and TTFV derivatives have disclosed promising applicability in the development of advanced optoelectronic, photonic, and redox-active nanomaterials. To cast more light in this aspect, the central theme of this MSc thesis is based upon the design and synthesis of a new class of DTF and TTFV derivatives containing carboxylate esters and carboxylic groups as active ligands for metal coordination. The detailed research is diversified into two projects. In the first project, the ability of these carboxylated DTFs and TTFVs to reduce Au(III) species in organic media was investigated by various spectroscopic and microscopic analyses (e.g., UV-Vis-NIR, cyclic voltammetry, SEM, and DLS). It was found that a carboxylic DTF was able to directly reduce Au(III) to Au(0) in dipolar aprotic solvents (DMF, DMSO), and the resulting Au(0) could be further stabilized by the carboxylic DTF as nanoparticles with sizes of tens of nanometers. The finding point to a useful approach for the preparation of functionalized gold nanoparticles with redox-activity. In the second project, the carboxylic TTFV derivative was investigated as a ligand for complexation with a number of metal cations, with the attempt to form redox-active coordination polymers or metal-organic frameworks (MOFs). The

detailed reactivity and properties were characterized by IR, single-crystal and power X-ray differaction analyses.

Acknowledgements

First and above all, I praise Allah for providing me this opportunity and granting me the capability to undertake this work. I would like to express my sincere thanks to my great supervisor Dr. Yuming Zhao for his encouragement, thoughtful guidance and support during my research work and thesis writing. His kindness and words always motivate me to work hard and made my thesis work such a remarkable learning experience to me. Also, I would like to extend my thanks to my supervisory committee, Dr. Sunil Pansare and Dr. Robert Davis for their valuable time and assistance throughout my program and reading my thesis. Prof. Louise Dawe (Wilfrid Laurier), Dr. Hillary Jenkins (McMaster), and Prof. Rik Tykwinski (Erlangen) are acknowledged for assistance in X-ray analysis.

Most importantly, I would like to express my deepest gratitude to my dad Mohammed , my mom Salwa and to my brothers and sisters for their encouragement and support . This thesis work is dedicated to a special person, my husband Yahya who has been consistently supportive to me during my study, I am truly thankful for having him in my life and also to my lovely kids, Mayas, Ajwan, and Relam for their love and patience, I do not think I could have done this without them.

Moreover, a tremendous gratitude to all the staff and faculty at Chemistry Depart-

ment, and CREAIT members of the chemistry department and to Memorial University for creating such a great educational and friendly environment for students. Also, the Saudi Cultural Bureau is sincerely acknowledged for the generous funding support of my study and research.

Table of Contents

List of Figures

List of Schemes

List of Abbreviations and Symbols

APPI	atmospheric pressure photo ionization
aq	aqueous
AuNPs	gold nanoparticles
ca.	circa
calcd	calculated
cm	centimeter(s)
CV	cyclic voltammetry
d	doublet
MOF	metal organic framework
DTF	dithiafulvene or dithiafulvenyl
Et	ethyl
exTTF	π-extended tetrathiafulvalene
FTIR	Fourier transform infrared
g	gram(s)

h	hour(s)
HRMS	high resolution mass spectrometry
Hz	hertz
IR	infrared
ITO	indium tin oxide
J	coupling constant
m	multiplet
m/z	mass to charge ratio
MALDI-TOF	matrix assisted laser desorption/ionization-time of flight
Me	methyl
mg	milligram(s)
MHz	megahertz
min	minute(s)
mL	milliliter(s)
mmol	millimole(s)
mol	mole(s)
m.p.	melting point
MS	mass spectrometry
mV	millivolt(s)

mW	milliwatt(s)
nm	nanometer(s)
NMR	nuclear magnetic resonance
ppm	parts per million
PXRD	powder X-ray diffraction
s	singlet
satd	saturated
SWNT	single-walled nanotubes
t	triplet
TFA	trifluoroacetic acid
THF	tetrahydrofuran
TLC	thin-layer chromotography
DMF	dimethylformamide
SEM	scanning electron microscope
DLS	dynamic light scattering
TTF	tetrathiafulvalene
TTFAQ	anthraquinone-type π-extended tetrathiafulvalene
TTFV	tetrathiafulvalene vinylogue
UV-Vis	ultraviolet-visible

V	volt(s)
XRD	X-ray diffraction
δ	chemical shift
ϵ	molar attenuation coefficient
λ_{max}	maximum absorption wavelength

Chapter 1

Introduction

1.1 Background of Tetrathiafulvalene

Tetrathiafulvalene (TTF), also named 2,2′-bis(1,3-dithiole), is a remarkable organic $\pi-$electron donor with a relatively simple heterocyclic molecular architecture (Figure 1.1).[1] For many decades, TTF has attracted enormous attention in the fields of organic electronic materials and supramolecular chemistry, since its first synthesis in the early 1970s by Fred Wudl and co-workers.[2] There were also studies on similar sulfur-based $\pi-$conjugated donors in the early 1970s; for example, the synthesis of unsubstituted TTFs by Coffen[3] and Hunig.[4] However, it was Wudl who first demonstrated that high electrical conductivity could be achieved from TTF radical cation–a finding that soon opened the door to the famous organic metals and organic superconductors in the following years. In 1973, the first "organic metal", which is a charge-transfer complex of tetrathiafulvalinium tetracyanoquinodimethane (TTF-TCNQ), was synthesized and characterized to show an unprecedented high electrical conductivity for organic-based solids.[5] After the ground-breaking work by Wudl, an impressive array of novel organic $\pi-$conjugated materials have been developed, in

which TTF was utilized as a redox-active building block.[6]

In the gas phase, the TTF molecule takes a non-planar boat-like shape with a C_{2v} symmetry according to density functional theory (DFT) studies.[7,8] In the solid state, however, TTF has been known to adopt a planar geometry with either an orange monoclinic α form[1,9] or a yellow triclinic β form resulting from different crystallization conditions.[10,11] Figure 1.1 shows the X-ray structure for the α form of TTF recently re-investigated by Bastanov in 2006.[1] The molecule takes a planar geometry with the bridging C=C bond at a length of 1.34 Å and the central S–C–S bond angle at 114°.

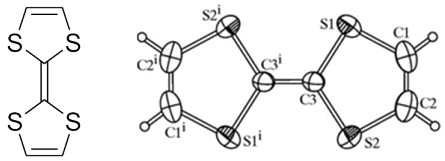

1

Figure 1.1: The chemical structure of TTF **1** (left) and an ORTEP plot of TTF showing the α form at 290 K.[1]

When substituents are attached to the dithiole units, the molecular structure of TTF may change depending on the nature of the substituents. For example, a recent crystallographic study by Zuo and co-workers[12] showed that tetrakis(methylthio)-substituted TTF **2** (Scheme 1.1) took a slightly twisted conformation in the neutral state. Using a weakly coordinating anion, $[Al(OC(CF_3)_3]^-$, Zuo and co-workers obtained stabilized radical cation and dication of **2** by oxidation reactions, and they further determined their structures by single crystal X-ray diffraction analysis. Unlike the neutral state, the radical cation and dication of TTF **2** were found to adopt a planar shape and the central bridging C–C bond between the two dithiole groups was steadily elongated as the oxidation state increased. The excellent electron-donating ability of TTF is mainly ascribed to the transformation of its non-aromatic dithiole units to stable aromatic dithiolium ions upon releasing one or two electrons.[13] In gen-

eral, a simple TTF molecule readily undergoes two steps of single-electron transfers when oxidized chemically or electrochemically, leading to the formation of TTF radical cation and dication respectively (E_{ox1} = +0.34 V, E_{ox2} = +0.78 V vs Ag/AgCl in CH_3CN). However, with increased $\pi-$conjugation the redox behavior of more $\pi-$extended TTF derivatives can be switched to simultaneous two-electron transfers rather than stepwise single-electron transfers–a case where the oxidation potential of the TTF to $TTF^{\bullet+}$ is higher than that of TTF to TTF^{2+} (i.e., redox potential inversion).

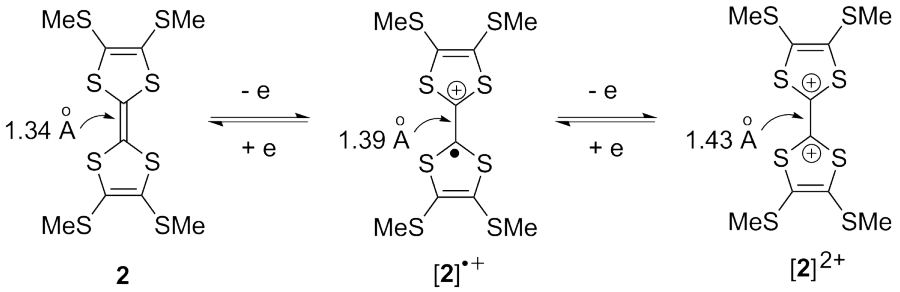

Scheme 1.1: Sequential oxidation of tetrakis(methylthio)-substituted TTF **2** into its radical cation and dication salts.

Indeed, the rich redox activity of TTF has made it a very popular molecular building block for many applications in materials science and nanotechnology; for example, electrically conducting materials, host−guest chemistry, organic electronic devices, and molecular machinery.[14] In modern TTF chemistry, a great number of TTF derivatives, particularly $\pi-$extended TTF analogues has been synthesized and investigated in order to control and manipulate the electronic, photonic, and redox properties. It has been well-documented in the literature that connecting $\pi-$conjugated functional groups to the two dithiole rings of TTF can result in dramatically changed structural and electronic properties. Systematic adjustment of the substituents attached to the TTF framework has been the most widely applied strategy for designing new functional TTF derivatives. Many synthetic efforts have hence been made for the syn-

thesis and characterization of new $\pi-$extended TTF analogues (exTTFs), in which $\pi-$extension of conjugated molecular frameworks was commonly attained by annulation of the dithiole rings with arenes or insertion a $\pi-$bridge between them. With the extension of $\pi-$conjugation, TTF derivatives can form much better stabilized charge-transfer salts as a result of decreased charge repulsion. Also, the increased dimensionality and enhanced π-staking allow favored solid-state structures and ordering to be achieved for improved electronic performance. The versatility in tuning the molecular structures and properties of exTTFs has led to rapid growth in the development of new molecular materials and devices using TTF and its derivatives as the active functional building components.[15]

1.2 $\pi-$Extended Tetrathiafulvalenes

For decades, progress in synthetic TTF chemistry has been continuously made by the synthetic community which has in turn inspired the design of a vast array of $\pi-$extented TTF analogues (hereafter referred to as exTTFs) in order to explore novel electronic and photonic properties and applications arising from their structural complexity and diversity. Many derivatives of TTF have been known to show excellent redox performance and intriguing structural switchability regulated by different oxidation states. These properties have led to extensive applications of exTTFs as key molecular building blocks in constructing functional molecular devices including switches, shuttles, tweezers, chemosensors, molecular wires, logic gates, and related electronic devices.[16] The common strategy for creating $\pi-$extended TTF analogues is to linearly lengthen the vinyl bridge in the parent TTF structure with various conjugated $\pi-$units inserted between the two dithiole heterocycles (see Figure 1.2A). Alternatively, annulation of aromatic rings to the dithiole units presents a straightfor-

ward design approach to achieve exTTFs (Figure 1.2B). Finally, insertion of an arene unit (e.g., quinodimethane) has been widely used to generate novel exTTFs.[17]

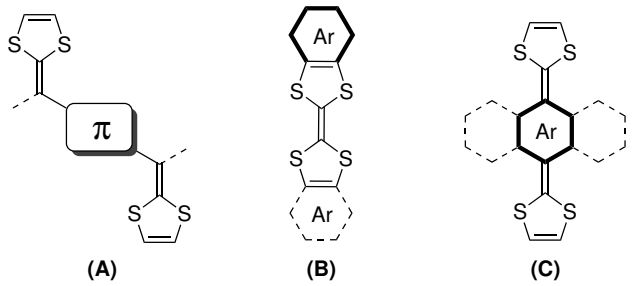

Figure 1.2: Schematic illustration of three general strategies for extending the $\pi-$backbone of TTF. (A) Linearly $\pi-$extension, (B) Annulation of the dithioles, and (C) fusion of TTF with an aromatic central core.

Figure 1.3 lists a collection of representative exTTF analogues which were synthesized and investigated over the past few decades. An example of attaching $\pi-$conjugated arenes to the dithiole rings can be seen in compounds **3** and **4**. Dibenzo-TTF **3** and its dervaitves have been known to have an oxidation potential higher than the parent TTF by 250 mV, due to the electron-withdrawing effect engendered by the annulated benzene rings.[18] A vast number of $\pi-$extended TTF analogues has been reported, which contain a generic structure of two dithiole rings connected by $\pi-$conjugated units, such as vinylene,[19] thiophene,[20] acetylene,[21] and other heterocyclic structures (represented by compounds **5**-**9**). Besides vinyl and aryl bridges, acene-linked exTTF systems with a quinoid-type central structure; for example, 9,10-bis(1,3-dithiol-2-ylidene)-9,10-dihydroanthracene (TTFAQ, **6** R=H), constitutes another important class of exTTFs in modern TTF chemistry.[18]

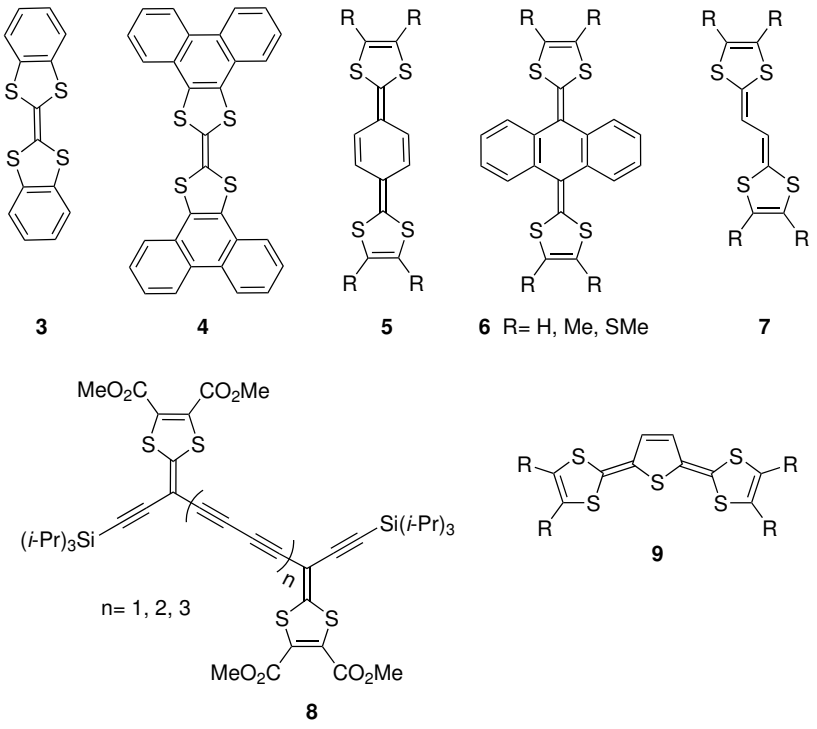

Figure 1.3: Selected examples of $\pi-$extended TTF analogues reported in the literature.

1.3 Tetrathiafulvalene Vinylogues

Of many classes of exTTFs, tetrathiafulvalene vinylogues (TTFVs) have received growing attention in recent research. TTFVs are π-extended analogues of TTF with the vinyl groups located between the two dithiole rings of TTF. The simplest example of TTFVs is compound **7** (Figure 1.3), which has a planar structure and excellent electron-donating properties. However, the most commonly seen TTFVs are those with aryl substituents attached to the vinylic positions, such as compound **10** in Scheme 1.2). Herein the presence of aryl groups offers stabilization effects to make the aryl-substituted TTFVs synthetically accessible and tunable.[18,22] The $\pi-$extension in TTFVs can greatly increase the stability of the oxidized species (radical cation and dication) by enhancing delocalization of the positive charges upon oxidation to minimize repulsion and facilitate intermolecular interactions and stacking with improved dimensionality and solid-state ordering.[17] In this context, the family of aryl-substituted TTFVs has been continuously expanded in the past few years. In particular, the Zhao group has been actively working in this area with the goal of exploiting their excellent electron donating ability, highly tunable redox activity, and unique redox-regulated conformational switching behavior.[16,17,23]

A simple example of aryl-substituted TTFVs is the diphenyl-TTFV **10** (Scheme 1.2). Compared with the unsubstituted TTF **7** which has a planar shape, the structure of **10** generally prefers a pseudo-*cis* conformation to minimize the steric crowding among the dithiole and phenyl rings. Upon chemical or electrochemical oxidation, a dication of **10** can be directly formed through a simultaneous two-electron transfer process. This redox behavior is a result of the potential for oxidation of diphenyl TTFV to dication $TTFV^{2+}$ being lower than that of its radical cation—a scenario generally referred to as "potential inversion". In the dication, electrostatic repulsion between the two dithiolium rings offers a major driving force to have the molecule

adopt a fully *trans* conformation (Scheme 1.2), in which the two dithiolium rings are co-planar and the two phenyl rings are nearly perpendicular to the plane of the central double bond.[16] In a sense, the phenyl-TTFV and related TTFV systems can be viewed as a class of "molecular switches", the conformations of which can be readily interchanged between pseudo-*cis* to *trans* through reversible redox reactions. Recent studies have demonstrated that the structural and electrochemical properties of aryl-substituted TTFVs can vary significantly with the nature of the aryl substituents; in particular, the electronic properties (i.e., donor, acceptor) and steric hindrance are two key factors.[17]

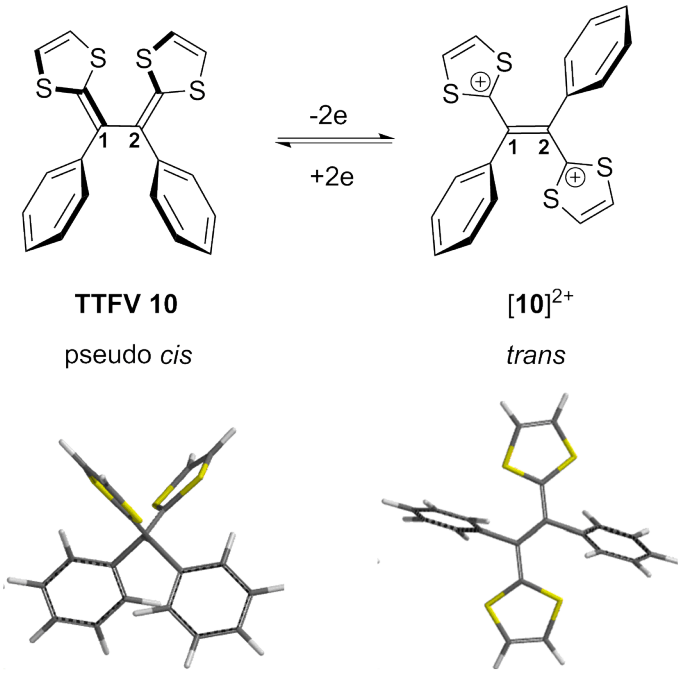

Scheme 1.2: Redox-regulated conformational switching property of diphenyl-TTFV **10**. The bottom shows the geometries of **10** in the neutral (viewed along the C1–C2 bond) and dicationic states optimized at the semi-empirical AM1 level using the Spartan'10 software. Adapted with permission from ref 87.

1.4 Application of TTFVs in Materials Chemistry

The application of TTFVs as a class of functional $\pi-$conjugated molecular building blocks has been continuously developed over the past two decades. Like other TTF derivatives, TTFVs have often been used as the active components in modern molecular electronic and optoelectronic materials and devices, playing key roles in regulating the electronic and structural performance. Indeed, their versatile redox activity and controllable conformational switching properties have allowed a large number of molecular and supramolecular systems to be designed and tested, for example, redox-active ligands,[24,25] chemical sensors,[26–28] supramolecular hosts for fullerenes[29] and single-walled carbon nanotubes (SWNTs).[30] Moreover, complex macromolecular structures based on TTFV have been recently synthesized, ranging from shape-persistent macrocycles[31] to $\pi-$conjugated polymers.[32] Altogether, the studies on TTFV and its derivatives have created a fascinating and vibrant research topic in recent research on advanced organic materials. The following subsections highlight the examples representing the state-of-the-art of TTFV-based molecular materials and devices reported in the literature, to which the Zhao group has made a major contribution over the past six years.

1.4.1 TTFV-Based Macrocycles

The non-planar shapes of phenyl-subsituted TTFVs are usually not deemed to be ideal for making cyclized products. Nevertheless, it has been found that macrocyclization reactions between TTFVs and other arene building blocks can happen under carefully controlled conditions. A recent collaborative study by the Bodwell and Zhao groups has established an effective method to create TTFV-containing macrocycles via oxidative dithiafulvenyl (DTF) coupling (Scheme 1.3).[33] Herein a redox-active pyrene-

TTFV macrocycle **12** was synthesized by a two-step method using a bis(DTF)pyrene **11** as precursor. Initially, bis(DTF)pyrene **11** was mixed with an oxidant (iodine) in CH_2Cl_2 for 45 min and worked up to give a solid mixture of a dimerized intermediate and unreacted **11**.[33] The resulting mixture was then subjected to grinding for 1.5 h with iodine in the solid state using a mortar and pestle and addition of diatomaceous earth (DE) was added to facilitate the grinding process. After two steps of treatment, TTFV-pyrene macrocycle **12** was formed in a good yield of 37%. The cyclic voltammetric analysis of **12** show similar redox activity to those of typical TTFVs. Furthermore, macrocycle **12** was found to act as an electron-rich supramolecular host giving rise to strong binding to nitrobenzene. The results suggested potential application in chemical sensing for nitroaromatic explosives.

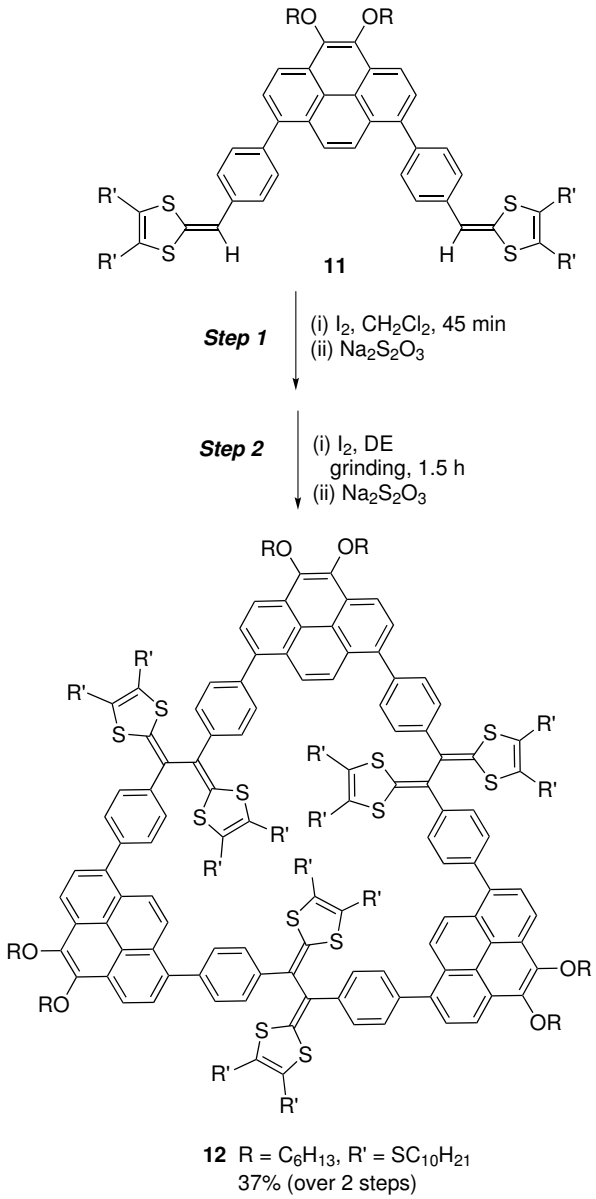

Scheme 1.3: Two-step synthesis of a redox-active pyrene-TTFV macrocycle **12**.

TTFV-based macrocyclic systems can also be prepared by using transition-metal catalyzed cross-coupling reactions as the key step. In 2011, the Zhao group reported the synthesis of a class of TTFV-alkyne based shape-persistent macrocycles (SPMs) (see Figure 1.4).[31,34] Macrocycles **13a-b** were prepared through a three-fold alkynyl homocoupling reaction (i.e., Hay coupling) using phenylacetylenic TTFV precursors under the catalysis of Cu(I) and Pd(II). Macrocycle **13a** was successfully purified as a stable product and its structrual, electronic, and redox properties were well characterized by various spectroscopic methods. Cyclic voltammetric analysis of **13** showed that the oxidation potential of the TTFV moiety in **13a** was slightly greater than its phenylacetylenic TTFV precursor, which can be explained by the locked pseudo *cis* TTFV conformation in macrocyclic structure. The bigger TTFV-macrocycle **13b** was found to be unstable in the solid state, due to the presence of very reactive tetrayne moeities. As a result, it was only characterized by UV-Vis and MALDI-TOF MS analyses in diluted solutions.

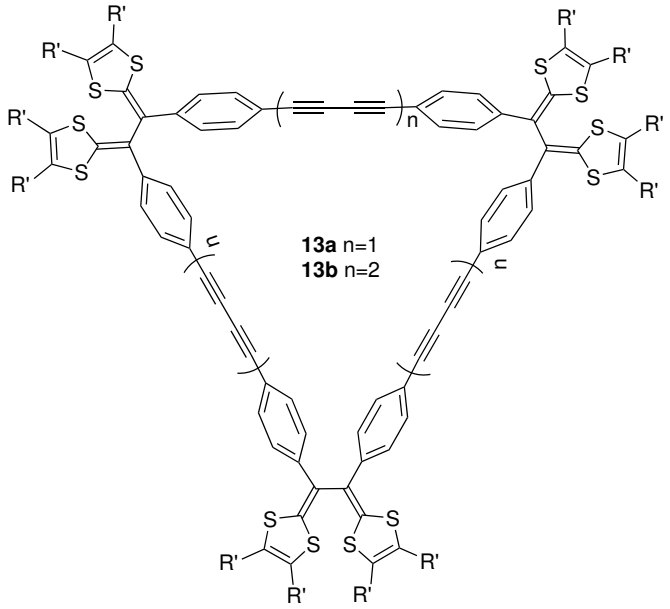

Figure 1.4: Structures of TTFV-alkyne macrocycles **13a-b**.

1.4.2 TTFV-Based Foldamers for Wrapping SWNTs

The landmark work by Ijima and co-workers on carbon nanotubes (CNTs) in 1991[35] is considered to be one of the most influential scientific papers in modern nanotechnology. The field of nanotube chemistry has, since then, rapidly grown and the applications of CNTs have been found in many different areas, such as electronics,[36,37] optics,[38] environment,[39] biology,,[40] and medicinal science.[41] Conceptually, CNTs can be viewed as graphitic sheets rolling up in a cyclindral structure. Depending on the layers, CNTs can be single-walled, double walled, and multi-walled. Also, the different ways of rolling up the graphitic sheet can result in zigzag, armchair, and chiral CNTs, the electronic properties of which range from semiconducting to metallic. Single-walled carbon nanotubes (SWNTs) are the most popularly employed building nanocarbon materials in modern nanoscale electronic and optoelectronic devices, owing to their unique structural and electronic properties. In particular, the electronic types (semiconducting and conducting) of SWNTs are directly related to their diameter and chirality. Presently, synthetic methods for preparing bulk quantities of SWNTs produce mixtures of tubes with various electronic types and structures. This technical bottleneck has greatly impeded the application of SWNTs in advanced electronic devices where the structural homogeneity of SWNTs is highly desired. For years, how to effectively produce and/or separate SWNTs according to electronic type, diameter, and chiralty has taken the central stage of the research on SWNT-based science and technology.

Reversible dispersion and release of SWNTs by conjugated polymer dispersants offers a promising solution to this challenging problem. Recently, rationally designed conjugated polymers with selectivity for electronic type, diameter, and chirality of SWNTs have been reported. For example, the Zhao group designed a class of TTFV foldamers **14** which can reversibly wrap and unwrap around SWNTs under redox

control (Figure 1.5).[30]

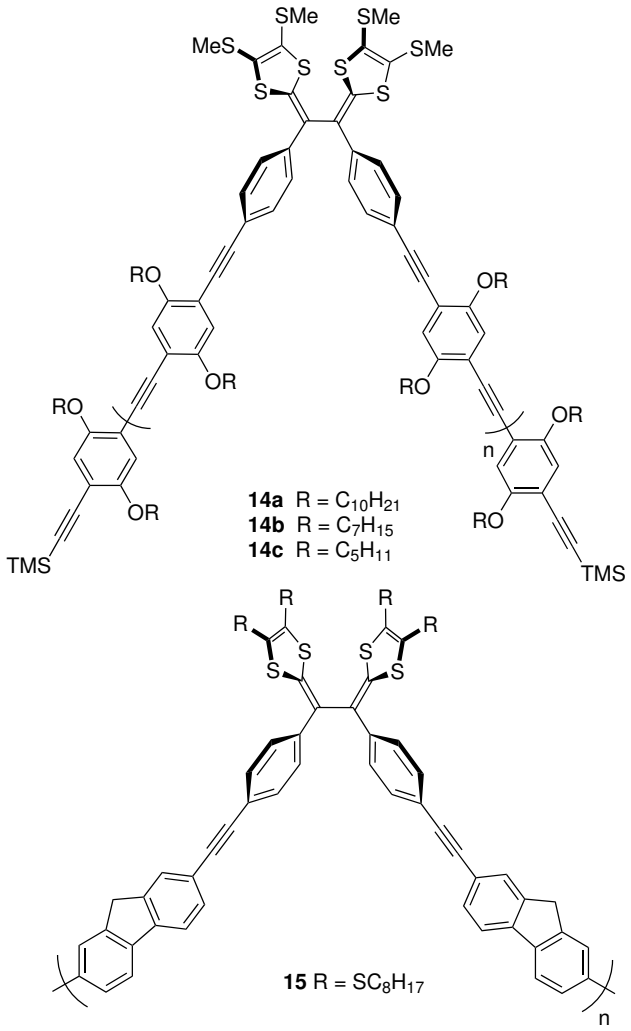

Figure 1.5: TTFV-based conjugated co-polymers **14** and **15** as selective dispersants for SWNTs.

It was found that the pseudo *cis* conformation of TTFV allowed the polymers to adopt a folded structure in the neutral state, favoring the wrapping of SWNTs through $\pi-$stacking. Upon oxidation or protonation with a strong acid (e.g., TFA), the polymers were ionized to change their conformations from folding to a linear structure. As such their interactions with SWNTs were destroyed, resulting in the dissociation of the polymer-SWNT supramolecular assemblies. In 2010, Adronov and Zhao reported

a modifed TTFV-fluorene co-polymer **15** as reversible selective SWNT dispersants, taking advantage of the high selectivity of fluorene units for semiconducting SWNTs. With this co-polymer, semiconducting SWNTs with narrowly distributed chiral indexes were successfully separated and enriched from commercial SWNT samples by simple dispersion and releasing methods in organic solvents.

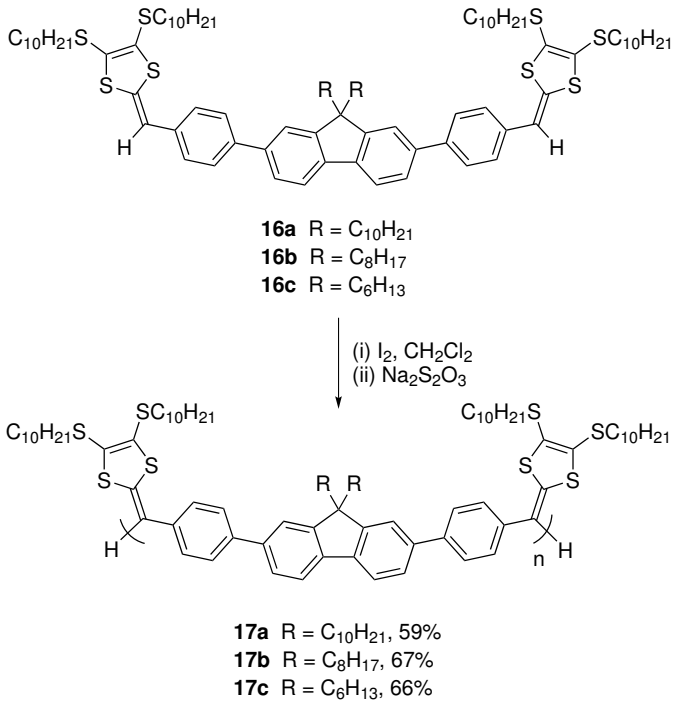

Scheme 1.4: Synthesis of monodispersed TTFV-fluorene co-oligomers **17** via controlled oxidative coupling reactions.

In 2015, a class of monodispersed π-conjugated TTFV co-oligomers was developed by the Zhao group (Scheme 1.4).[42] The TTFV− fluorene oligomers were prepared by controlled oxidative polymerization reactions of bis(DTF)-endcapped fluorenes **16** in CH_2Cl_2 at room temperature. The obtained TTFV-fluorene co-oligomers **17** as characterized by NMR, gel permeation chromatography (GPC), and cyclic voltammetry, showed a narrow polydispersity degree with an average chain length of pentamer to hexamer (n = 5–6). Interestingly, the co-oligomers were also found to effectively inter-

act with SWNTs through $\pi-$stacking, leading to stable SWNT-oligomer suspensions in organic solvents. Raman analysis showed that the SWNTs dispersed with these oligomers exhibited a narrow vibrational band in the radial breathing mode (RBM) region, suggesting a good diameter selectivity for SWNTs.

1.4.3 TTFV-Based Molecular Tweezers as Chemosensors

The preferred pseudo *cis* conformation of most aryl-substituted TTFV derivatives makes it possible to produce tweezer-like molecular systems (i.e., molecular tweezers) to give special functions such as supramolecular hosts or molecular receptors. In this context, the class of acetylenic phenyl-TTFVs has been explored by the Zhao group in recent years, taking advantage of the facile reactivity of the alkynyl groups attached in terms of cross-coupling and cycloaddition reactions. One notable synthetic tool in modern materials chemistry is "click chemistry", which emerged in the early 2000s. So far, numerous efficient reactions have been recognized as "click reactions" for conjugation of diverse functional groups with systems ranging from synthetic polymers, biological substrates, metal surfaces, to inorganic nanoparticles in a reliable and modular way. Among them, the Cu-catalyzed alkynyl-azide coupling (CuAAC) consitutes the most popularly used "click reaction" in the recent literature.

A TTFV-phenylboronic acid hybrid **18** (Figure 1.6) was designed and synthesized by the Zhao group in 2013 via the "click reaction" between an alkynyl-TTFV and an azido-substituted phenylbornate precursor under the CuAAC conditions.[26] The two phenylboronic acid groups in this molecular tweezer were designed to serve as effective receptors for saccharides and the redox-active TTFV central unit as an electrochemically active reporter for the binding events of saccharides with **18**. Overall, molecular tweezers **18** was demonstrated to work as an electrochemical probe for various monosaccharides under physiological conditions.

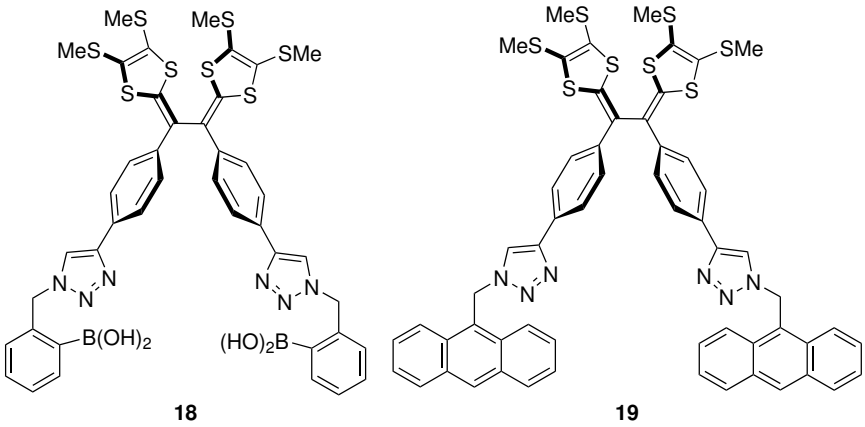

Figure 1.6: TTFV-based molecular tweezers **18** and **19**.

By a similar synthetic approach, a class of arene-substituted TTFV molecular tweezers was synthesized using the CuAAC reaction in the key ligation step. Compound **19** (Figure 1.6) is an interesting member in this family, because it was found to selectively bind with C_{70} fullerene in the presence of a large excess of C_{60} fullerene (>1000 fold).[29] In fluorescence spectroscopic titration, the binding of **19** with C_{70} fullerene was observed to give enhanced emission arising from the attached anthracene fluorophore. The fluorescence turn-on phenomenon can be explained by the electron-transfer between TTFV and C_{70} fullerene. As such, this type of molecular tweezers can work as highly sensitive fluorescence sensors for fullerenes, with the fluorescence responsiveness dependent on the arene fluorophores connected to the TTFV unit.

1.4.4 TTFV-Based Molecular Rotors

The redox-controlled conformational switching behavior of TTFVs can be utilized in the design of molecular machines. For example, a molecular rotor (Scheme 1.5) was reported by Chen and Zhao in 2014.[43] In this molecular machine, two triptycenyl groups were connected to a phenyl-TTFV central unit. Triptycene has been long recognized as a "molecular cogwheel" which in combination with other hindered arene

groups can form molecular rotary devices, such as molecular gears, molecular motors, molecular brakes, and so on. In the TTFV-based molecular rotor, the conformational change associated with the reversible electron transfer upon the oxidation/reduction of the TTFV unit would lead to two types of concerted (geared) molecular rotation, namely disrotation in the neutral state and conrotation in the dicationic state. A dynamic NMR study on this molecular rotor was carried out to show that the rotational speed of the triptycenyl groups is much faster in the oxidized state than in the neutral state. The study represents the first example of redox-regulated molecular rotation in the literature and has the potential to be further developed into redox or electrochemically controlled molecular rotary machines.

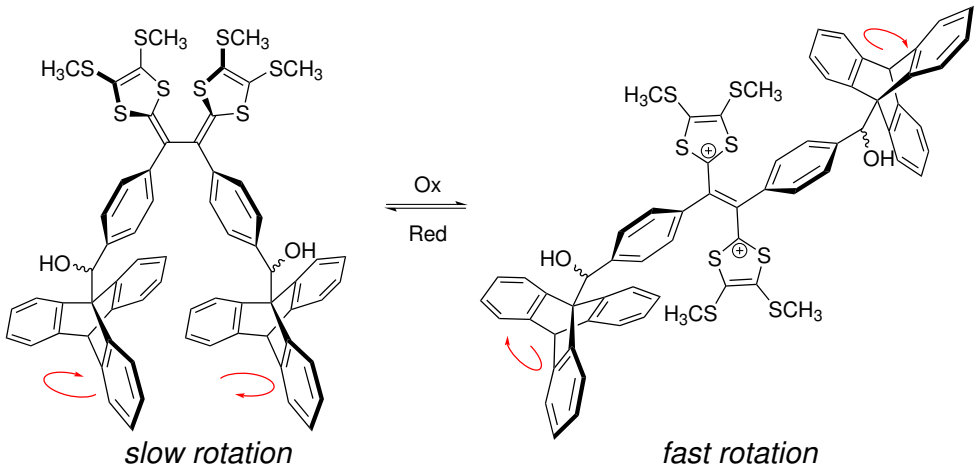

Scheme 1.5: Redox-regulated rotary motion of a bis(9-triptycyl)-TTFV system.

1.4.5 TTFV-based Redox-Active Ligands

When a rigid $\pi-$conjugated system is functionalized with multiple organic ligand groups, such as pyrdinyl and carboxyl, the resulting hybrids can show the ability to coordinate with various metal ions to form structrally complex metal-organic assemblies. This has indeed become a topic of enormous interest over the past few years, given the rapid development of metal-orgnaic frameworks (MOFs) as a new type of

porous functional materials. In the current literature, the design of TTFV-based redox-active ligands has been rarely known, but this type of ligands are expected to be intriguing in view of the redox swtiching properties of TTFV. An early example of TTFV-based ligands was reported by the Lorcy group (compound **20**, Figure 1.7).[24] In this work, pyridyl substituents were attached to TTFV and compound **20** was then coordinated with $Mo(CO)_6$ to form a cyclic complex **22**. The structure of complex **22** was elucidated by single-crystal X-ray diffraction analysis, showing a square-shaped macrocyclic architecture. The self-assembly into such a "molecular square" was driven by two key factors: (1) complementarity of angle, size, and orientation of TTFV ligand, and (2) the *cis*-shaped $Mo(CO)_4$ fragment. Furthermore, cyclic voltammetric analysis on **22** was conducted to show that the redox properties the complex are mainly coming from the TTFV moiety, while the Mo centers do not contribute as much.

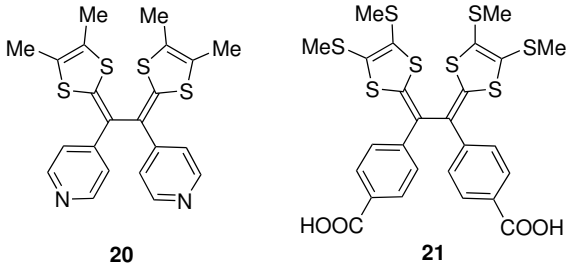

Figure 1.7: TTFV-based redox-active ligands **20**, **21**, and a square-shaped complex of **20** and Mo ions.

Another TTFV-based redox ligand was carboxylated TTFV **21** (Figure 1.7) recently reported by Wang and Zhao. This ligand was intended to complex with various transition metals using its carboxyl ligands attached. A more detailed discussion on the synthesis and characterization of this compound can be found in the introductory section of Chapter 3.

1.5 Synthetic Methods for Dithiafulvenes (DTFs) and Tetrathiafulvalene Vinylogues (TTFVs)

DTFs and TTFVs have been widely used as electron-donating $\pi-$building blocks in the preparation of various functional π-conjugated molecular and macromolecular systems. In many of the cases, the key synthetic steps involved the formation of C–C and C=C bonds, as well as the five-membered dithiole rings. The retrosynthesis as demonstrated in Scheme 1.6[23] presents one of the most concise and commonly employed strategies for the construction of TTFVs, where two important precursors thione **23** and aldehyde **24** need to be first prepared or procured from commercial sources. With these two synthons, a Wittig-type olefination reaction is conducted to prepare the DTF intermediate **25**. DTF **25** is then subjected to an oxidative dimerization to give TTFV **26**. This is a straightforward C–C bond forming reaction, in which the R group directly connected to the vinyl unit plays an important role. Typically aryl groups are known to facilitate the dimerization by offering stablization to the radical cation intermediates involved in this reaction.

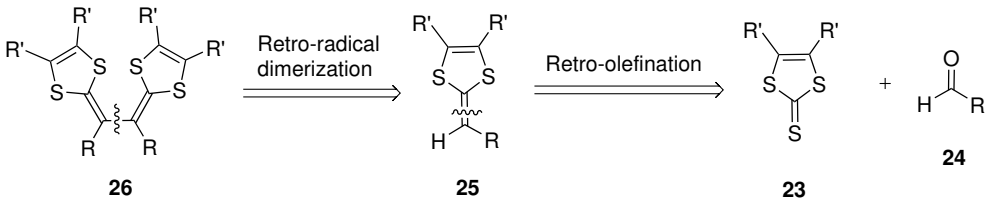

Scheme 1.6: A general retrosynthetic strategy for TTFVs.

Following the synthetic strategy mentioned above, the preparation of 1,3-dithiole-2-thiones must be performed at the very beginning of the synthesis, since most of them are not commercially available. One of the commonly used methods for preparation of the 1,3-dithiole-2-thione precursor was developed by Hoyer's group in 1979.[44] This method is indeed very versatile in making bis(alkylthio)-substituted 1,3-dithiole-2-thione, for example, compound **23** shown in Scheme 1.7. It is also worth noting that this reaction can be readily conducted on a large scale using commercially available carbon disulfide and an alkali metal, such as sodium or potassium. Mechanistically, the reaction begins by the reduction of carbon disulfide with sodium metal to produce a dithiolate intermediate. The resulting dithiolate intermediate can be stabilized by complexation with Zn(II) ion in the presence of quaternary ammonium cations, affording a stable red-colored salt **27**. Depending on the substituents desired, salt **27** can be further reacted with various alkyl halides to yield the 1,3-dithiole-2-thione products with different alkylthio groups (RS–) attached to the dithiole ring.

The detailed reaction mechanism for the formation of the dithiolate intermediate in the first step of the thione synthesis is also illustrated in Scheme 1.7.[45] At first, reduction of CS_2 by sodium metal generates CS_2 radical anion, which undergoes a fast dimerization to give an dithiolate anion. The anionic intermediate then attack another molecule of CS_2, followed by cyclization to form a five-membered ring dithiolate intermediate. Another sequence of nucleophilic attack to CS_2, followed by elimination and reduction with sodium then affords the dithiolate, which is ready to be stabilized by

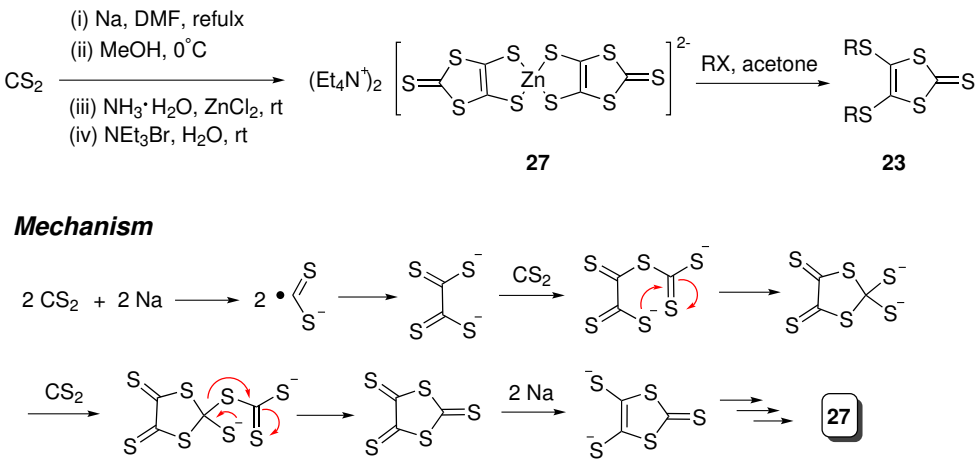

Scheme 1.7: Synthesis of 1,3-dithiole-2-thione **23** and the mechanism accounting for the formation of dithiolate intermediate **27**.

complexation with with Zn(II) ion. The resulting zincate anion in combination with tetrabutylammonium cation produces a red-colored solid salt, which is very stable and can be store for a long time without decomposition. Treatment of this salt with a chosen alkyl halide (electrophile) can easily produce 1,3-dithiole-2-thione precursor with desired substituent in good yield.

Once the 1,3-dithole-2-thione precursor is made, DTF can be prepared by coupling it with a suitable aldehyde through an olefination reaction. Wittig-type reactions are generally used at this stage, and there have been several synthetic pathways developed for this purpose. So far the most preferable methodology is the phosphite-promoted olefination reaction[46,47] developed by the Bryce group (see Scheme 1.8). The significant advantage of this olefination method lies in that it is a one-pot synthesis, in which the 1,3-dithiole-2-thione precursor is mixed with an easily accessible aldeyhyde or ketone in excess trialkylphosphite (e.g., $P(OMe)_3$, $P(OEt)_3$) to directly undergo olefination. The drawback of this reaction is that it requires a very high reaction temperature, which is not suitable for making some thermally unstable products.

After the DTF synthesis, the construction of TTFV can be readily performed

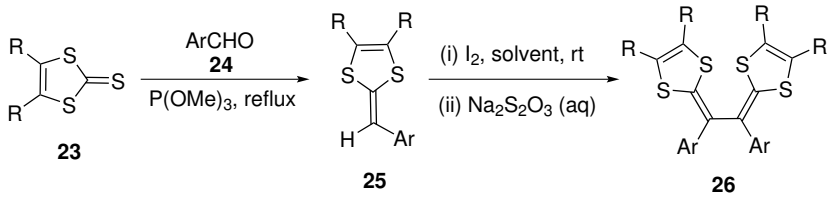

Scheme 1.8: Synthetic sequence for making DTFs and TTFVs.

through a direct oxdiative dimerization reaction (Scheme 1.8). The mechanism of oxidative dimerization reaction of DTF is shown in Scheme 1.9. The first step is the oxidation of the DTF through single electron transfer using an oxidant (e.g., iodine, Ag(I), Fe(III), etc.) to form DTF radical cation. During the dimerization process, a new C–C bond is formed to combine the two molecules of DTF radical cation together. The resulting dicationic intermediate then undergoes a deprotonation to give the TTFV product which is further oxidized under the oxidative conditions to yield a stable TTFV dication. Once the oxidative dimerization is finished, the TTFV dication will be reduced by addition of a reducing agent such as sodium thiosulfate to regenerate the neutral TTFV product.

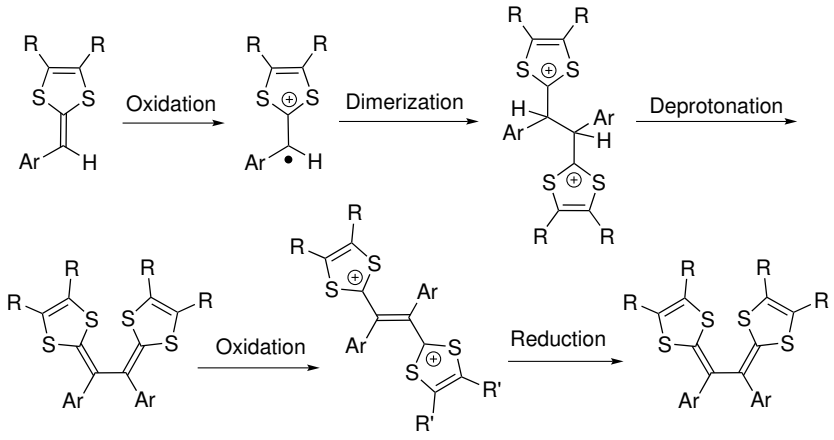

Scheme 1.9: Mechanism of the oxidative dimerization reaction of DTF.

1.6 Brief Introduction to Gold Nanoparticles

Metal nanoparticles have attracted enormous interest over the past few decades, owing to their unique chemical and physical properties stemming from the so-called "quantum size effect" as well their large surface areas. For these reasons, metal nanoparticles have been extensively investigated as novel nanomaterials for a wide range of applications in optics, electronics, catalysis and biology.[48] Of the numerous metal nanoparticles, gold nanoparticles (AuNPs)–also commonly referred to as gold colloids–have stood out as the most fascinating and widely studied ones. So far the applications of AuNPs have encompassed the fields of diagnostics, therapeutics, catalysis, optical sensing, materials science and nanotechnology.[49]

Historically the interest in gold particles that could transmit red color began in around the 5th or 4th century when Egyptians, Greeks and Romans used them as colored pigments for decorative purposes in buildings, ceramics, and glassware. An example of combining gold and silver particles is the famous Lycurgus Cup preserved in the British Museum. This cup is believed to be made in the fourth century by Romans (see Figure 1.8).[50] The unique feature of this cup lies in its colour changes: when the light transmits through the cup the color is red, and it becomes green when in the reflected light. This unusual property led scientists to perform chemical analysis, which showed that the cup carries a very small amount of gold (about 40 parts per million) and silver (about 300 parts per million). The crystalline nature of the silver and gold particles and their fine dispersion found in the glass suggest that colloidal metals were precipitated out in the solution during the heating process of the glass making.

Figure 1.8: Photographic images of the Lycurgus cup by courtesy of the British Museum. Copied from Wagner et al., *Nature* **2000**, *407*, 691–692 with permission.

In the Middle ages, gold was used for treatment of heart and venereal problems, dysentery, epilepsy, and tumors.[48] Nowadays, a great development has been made in the synthesis of AuNPs with different morphologies and sizes, making AuNPs highly tunable nanomaterials for a variety of applications. Moreover, surface modifications can be easily performed on AuNPs during their synthesis, allowing the access to nanogolds in different shapes, structures, and functionalities. For example, the preparation of gold nanospheres[51] nanorods,[52] nanoshells,[53] and nanocages[54] has been reported, and in general the gold-based nanoobjects have a dimension range from 1 to 100 nm.[55]

Since ancient times, AuNPs have been known to be intense red in color, the origin of which is due to the photophysical response, namely surface plasmon resonance (SPR), of metal nanoparticles to irradiation, which does not exist in non-metallic particles. In principle, when a AuNP is exposed to light, the free electrons on the gold metal are collectively oscillating in the conduction band induced by the oscillating electromagnetic field of the light.[55] The electron oscillation surrounding the surface of the particle leads to charge dissociation with respect to the ionic lattice and this pro-

duces a dipole oscillation along the direction of the electric field. Once the maximum extent of oscillation reaches a specific frequency, known as surface plasmon resonance (SPR), strong absorption and scattering of the incident light take place. The SPR phenomenon can be measured by UV–Vis absorption analysis. For AuNPs, the SPR usually results in an absorption band around 520 nm in the visible region, depending on the size of AuNPs measured. Figure 1.9 illustrates the dependence of SPR bands on the shapes of AuNPs, changing from spherical to rod-like.[56] It has been known that the size, shape, surface area, and agglomeration state of AuNPs all play significant roles in the electric field density on the Au surface. When AuNPs are enlarged in diameter, their optical properties change notably as observed for the differently sized gold nanospheres. Besides dimension, when an anisotropy is added to the nanoparticle, such as growth of nanorods, the optical properties of the nanoparticle also change dramatically.

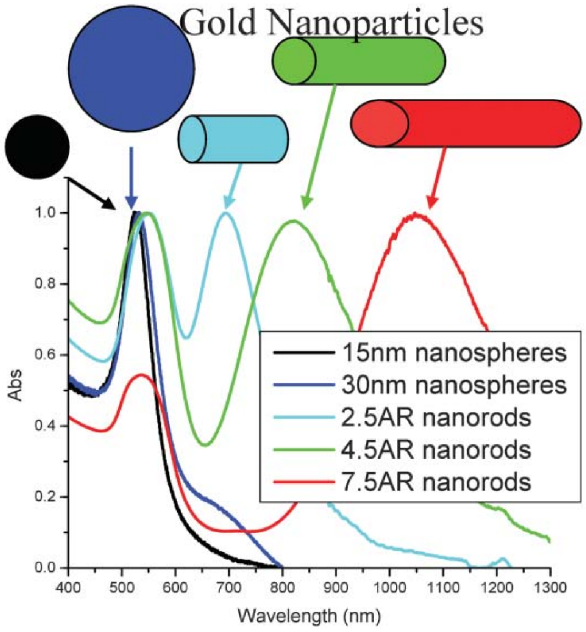

Figure 1.9: UV-Vis absorption behavior of nanogolds in various sizes and shapes. Adopted with permission from ref 56.

Furthermore, as mentioned above, AuNPs show a strong absorption SPR band in the visible region of the spectrum, typically around 500 nm to 600 nm. When the particle diameter increases, the maximum absorption wavelength increases as well (see Figure 1.10). As such, UV-Vis analysis is often used in lieu of the tedious electron microscopic methods (e.g., SEM, TEM) to determine the size of AuNPs. Also, the aggregation state of AuNPs in solution can cause dramatic color changes (e.g., from red to blue/purple) associated with broadening of the SPR band and decrease in absorption intensity. All these unique spectroscopic features can be used to monitor and characterize the growth of AuNPs proceeding under different chemical conditions.

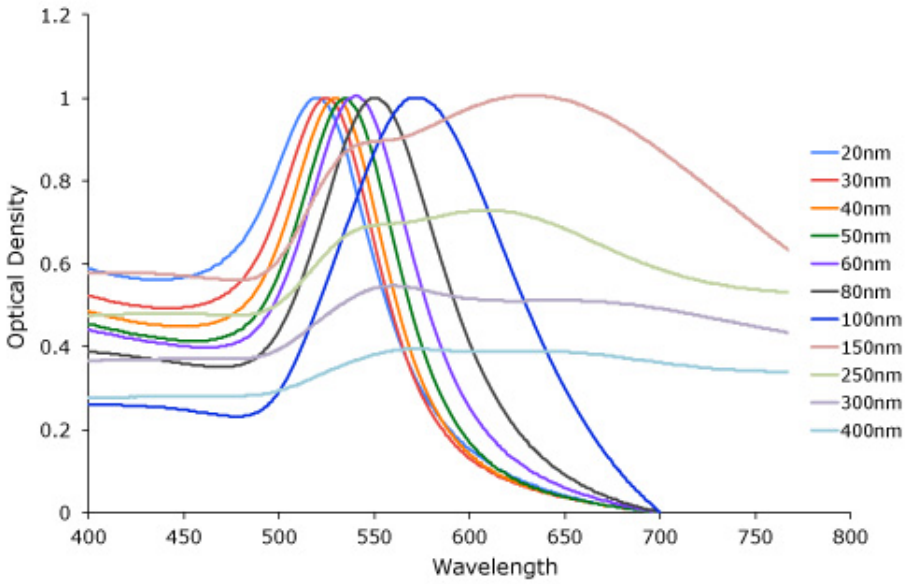

Figure 1.10: Size and aggregation state dependant SPR absorption of AuNPs. Adopted from http://www.cytodiagnostics.com/store/pc/Introduction-to-Gold-Nanoparticle-Characterization-d3.htm with permission.

1.7 Synthesis of AuNPs

Numerous synthetic methods have been developed to generate AuNPs with control over size, shape, solubility, stability, and functionality. In most of the AuNP synthetic methods, capping reagents such as surfactants or polymers are added to prevent aggregation and precipitation of the AuNPs out of solution. In 1951, the observation of the deep red color after the reduction of an aqueous solution of chloroaurate ($AuCl_4^-$) with phosphorus in carbon disulfide was reported by Faraday.[57] Later work developed by Turkevich resulted in a popular method for the preparation of AuNPs through citrate reduction of $HAuCl_4$ in water.[58] In this straightforward approach citric acid acts as both reducing and stabilizing agent, and it provides AuNPs with a diameter around 20 nm. Among the numerous AuNP synthesis methods developed so far, the Brust and Schiffrin method reported in 1994 stands out as the most popularly employed one and it has made a tremendous impact on the field of AuNP chemistry.[59]

1.7.1 The Brust−Schiffrin Method

The novelty of the Brust−Schiffrin method[59] lies in a biphasic synthetic process along with the use of a thiol to protect AuNPs. It is particularly useful for the production of small AuNPs with narrow, controllable dispersity. The detailed processes involved in this method are illustrated in Figure 1.11. In the beginning, $AuCl_4^-$ ion is transferred from an aqueous phase to toluene with the aid of a phase-transfer reagent, tetraoctylammonium bromide (TOAB). In the organic phase, $AuCl_4^-$ is reduced to Au(I) species by dodecanethiol. After the addition of $NaBH_4$, Au(I) is further reduced into Au(0) and the color of the solution changes from orange to dark brown. AuNPs generated in the organic phase possess diameters in the range of ca. 1.5−5.0 nm. The thiol ligands protect the resulting AuNPs from aggregation by forming a self-assembling

layer on the particle surface. The thiol-functionalized AuNPs can be redispersed in other organic solvents without any aggregation or decomposition. Moreover, the Burst-Schifrrin method allows the particle size to be readily adjusted by varying the preparation conditions, such as type of thiol, Au/thiol ratio, temperature, pH, and reduction rate.[60]

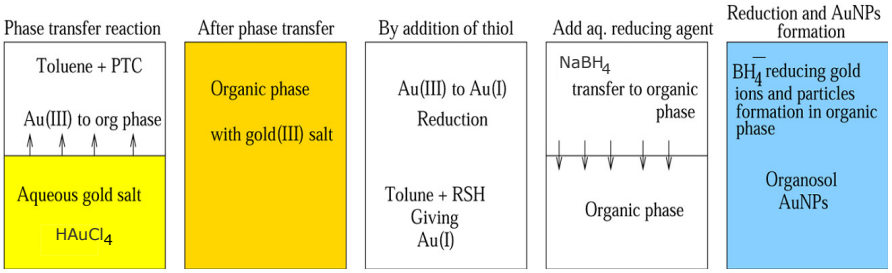

Figure 1.11: Schematic illustration of the Brust−Schiffrin method for two-phase synthesis of AuNPs. Adapted with permission from Perala, S. R. K.; Kumar, S. *Langmuir* **2013**, *29*, 9863—9873. Copyright (2013) American Chemical Society.

Recently, many mechanistic studies have been conducted to cast new insights into the detailed reduction processes involved in the two phase system of the Brust−Schiffrin method.[61] Initially the chloroauric acid ($HAuCl_4$) is transferred to the organic phase (toluene) by tetraoctylammonium bromide (TOAB), a phase transfer catalyst (PTC), through the following reaction:[59]

$$H^+AuCl_4^-(aq) + (R_8)_4\ N^+Br^-\ (org) \rightarrow (R_8)_4\ N^+\ AuX_4^-\ (org)\ HX\ (aq) \qquad \textbf{(eq. 1)}$$

where X represents the halide group (Br or Cl). The next stage is the reduction of Au^{3+} to Au^{2+} by alkanethiol (RSH) as shown in the following reaction:[59,62,63]

$$(R_8)_4\ N^+\ AuX_4^- + 3RSH \rightarrow AuSR + RSSR + (R_8)_4\ N^+ + 4X^- + 3H^+ \qquad \textbf{(eq. 2)}$$

The organic phase at this step is composed of TOAB, dialkyl disulfide (RSSR),

Au^{1+} in the form of $-$(AuSR)n$-$polymer in which AuX_4^- may be complexd with TOA ion or an excess of RSH. The reduction of Au^{3+} and Au^{1+} to Au^0 by sodium borohydride is expected to take place through the following reaction:[62,63]

$$\text{-(AuSR)n-} + BH_4^+ + RSH + RSSH \rightarrow Au_x\ (SR)y \qquad \textbf{(eq. 3)}$$

$$(R_8)_4\ N^+\ AuX_4^- + BH_4^+ + RSH + RSSH \rightarrow Au_x\ (SR)y \qquad \textbf{(eq. 4)}$$

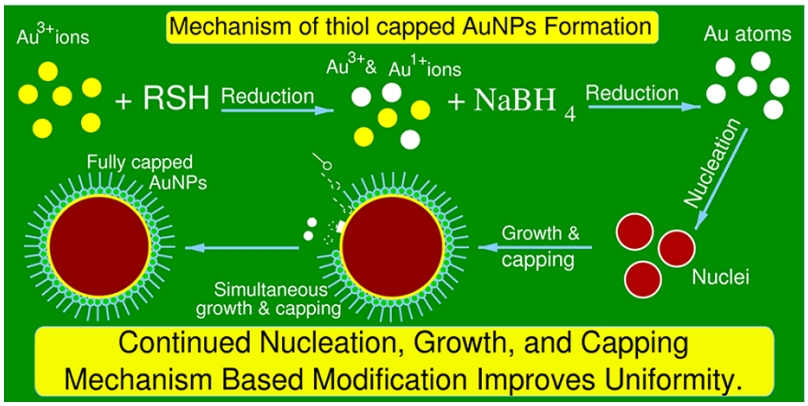

Figure 1.12: The mechanism for the formation of thiol capped AuNPs through the Brust$-$Schiffrin method. Adapted with permission from Perala, S. R. K.; Kumar, S.*Langmuir* **2013**, *29*, 9863—9873. Copyright (2013) American Chemical Society.

Despite the numerous reports in the current literature, the mechanism of AuNP synthesis and size control is not yet fully disclosed. For example, the nucleation of Au(0) seeds and their growth into AuNPs is a rather complex process, and a population balance model shows that the particle formation in the Brust$-$Schiffrin synthesis can be controlled by continuous nucleation, growth, and capping of particles throughout the synthesis process.

1.8 Objectives and Outline of This Thesis

The excellent electron donating properties of DTF and TTFV derivatives allow them to be used as versatile functional building blocks in organic/inorganic hybrid materi-

als. Innovation in the methods for their synthesis (e.g., metal-catalyzed coupling, click chemistry) has facilitated access to various complex redox-active nanomaterials and molecular devices. The main objective of this MSc dissertation is aimed at developing new applications of DTF and TTFV-based small molecules as redox-active building blocks/ligands for making complex metal-organic hybrid materials. As mentioned in Section 1.4.5, a class of carboxylated TTFV derivatives (e.g., compound **21**) was synthesized and investigated by a former group member, Yunfei Wang. To further his study, a new class of carboxylated DTF and TTFV derivatives was designed in the beginning of this thesis work. In these compounds, each of the phenyl groups carries two carboxyl groups at the meta positions instead of the mono-carboxyl subsitution in Yunfei's work. The inclusion of multiple carboxyl groups in the DTF and TTFV building blocks was expected to bring about new redox and structural properties as well as enhanced coordination reactivity towards metal ions.

Taking advantage of the redox activities of carboxylated DTFs and TTFVs as well as their compatibility with polar organic media, reduction of Au(III) with these $\pi-$conjugated electron donors was envisaged and it was anticipated that this reaction should, in principle, deliver Au(0) as the product. Moreover, the presence of carboxyl and methylthio groups should offer effective ligands to stabilize AuNPs. Based on this hypothesis, Chapter 2 reports a systematic study on the redox reactions between $HAuCl_4$ and the newly designed carboxylic DTF and DTF ligands in various polar organic solvents. Apart from the redox activity, exploration of the coordination chemistry of the carboxylic DTF and TTFV derivatives is described in Chapter 3, with the aim of preparing TTFV-based redox-active coordination polymers and metal-organic frameworks (MOFs). This part of the work is also a continuation of Yunfei Wang's project. So far, there has been no successful synthesis of TTFV-based MOFs reported in the literature. Investigations in this direction should lead to better

understanding of how to rationally design and control this new type of microporous organic-inorganic hybrid materials. Finally, Chapter 4 provides a summary of the two MSc projects conducted and discusses on some interesting research directions for the future work.

Chapter 2

Redox Interactions of Au(III) with Carboxylated Dithiafulvenes and Tetrathiafulvalene Analogues

2.1 Introduction

Gold nanoparticles (AuNPs), owing to their unique electronic, magnetic, and chemical properties, have found a wide range of applications in the fields of biology, catalysis, chemical sensing, and nanomedicine.[64–67] The preparation of AuNPs is usually done through the reduction of Au(III) species such as $HAuCl_4$ with a reducing agent (e.g., citrate,[68–70] $NaBH_4$,[71,72] and block copolymers[73–76]), and suitable ligands are also applied to stabilize the resulting AuNPs as well as to exert control over their dimensions and functionality. For example, the well-known Brust-Schiffrin two-phase method[77–79] has provided facile synthetic access to highly stable, monodispersed, and flexibly functionalized AuNPs. On the other hand, direct reduction of $HAuCl_4$ into AuNPs by using $\pi-$conjugated electron donors as reductants in organic media has been rarely

reported in the literature. In the early 2000s, Chujo and co-workers[80,81] first utilized $\pi-$conjugated polymers containing electron-rich dithiafulvene (DTF) units to convert $HAuCl_4$ into narrowly distributed AuNPs, taking advantage of the reductive nature of DTF and the protective effect of the oxidized polymers on AuNPs.[82] Small DTF-based molecules **28a-b** (Scheme. 2.1) were later on studied by the groups of Chujo[83] and Granados[84] respectively to reduce $HAuCl_4$ in acetonitrile. In both reports, electron transfers from DTF to Au(III) were observed, which led to the formation of AuNPs. The stabilization of AuNPs was briefly ascribed to the capping effects of oxidized DTFs (DTF_{ox}) on the surface of AuNPs via S–Au interactions (Scheme. 2.1A); however, the proposed models for DTF_{ox}–Au interactions have not been clearly verified by experimental evidence. A key scenario that has been overlooked in the previous studies on DTF_{ox}-stabilized AuNPs systems is the oxidative dimerization reaction of DTFs as illustrated in Scheme 2.1B. This reaction occurs readily in an oxidative environment, affording the dication of tetrathiafulvalene vinylogue ($TTFV^{2+}$) as stable product.[85–87] Over the past few years, the DTF oxidative dimerization has been actively utilized by the Zhao group and others as an efficient synthetic tool in preparing $\pi-$conjugated polymers,[88–90] redox-active ligands,[91,92] macrocycles,[93,94] chemosensors,[94–97] and functional molecular devices.[98,99]

With this type of chemistry in mind, research work described in this chapter has been dedicated to addressing some fundamentally important questions related to the DTF–Au(III) redox interactions. (1) Does the DTF unit undergo dimerization after redox interaction with Au(III) or just simply stay as the DTF radical cation bound to certain Au species? (2) Do DTF and TTFV have similar or different effects on Au(III) reduction? (3) Does the nature of organic solvent(s) play any significant role in the DTF/TTFV-Au(III) interactions as well as subsequent AuNP formation?. To address these issues, we have designed and synthesized a new class of DTF compounds

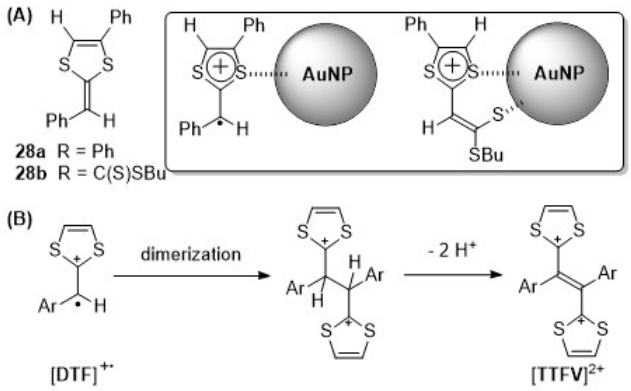

Scheme 2.1: (A) Structures of DTF dervitives **28a-b** and proposed interactions with Au(0) nanoparticels. (B) Dimerzation reaction of two DTF radical cations into a TTFV dication.

31a-b together with their TTFV derivatives **32a-b** (Scheme. 2.2). The presence of carboxyl groups in these compounds was primarily aimed at enhancing their solvation in polar organic solvents, wherein reduction of Au(III) to Au(0) was supposed to occur effectively. In addition, the ability of carboxyl groups to bind with metal surface as well as to form supramolecular assemblies via hydrogen bonds was anticipated to yield beneficial effects on stabilizing the reduced Au(0) species in the form of AuNPs.

2.2 Results and Discussion

2.2.1 Synthesis of Carboxylated DTFs and TTFVs

The synthesis of carboxyl-TTFV **32b** and its DTF precursor **31b** could be readily conducted through well-established procedures for similar, aryl-substituted, TTFV derivatives. As shown in Scheme 2.2, the synthesis of DTF began with the reaction between thione **30** and dimethyl-5-formylisophthalate **29** in the presence of trimethylphosphite at 105 °C. This olefination reaction was complete within 3 hours, affording DTF **31a** in 88% yield after silica gel chromatography. The resulting compound **31a** then underwent an oxidative dimerization in CH_2Cl_2 at room temperature

using iodine as oxidant, which was afterwards reduced by sodium thiosulfate as reducing agent to give TTFV **32a** in 86% yield as a stable yellow solid. Compound **32a** was subjected to saponification reaction in a solution of NaOH in water and MeOH at 75 °C to produce the desired product carboxyl-TTFV **32b** in 75% yield. In non-polar organic solvents, compound **32b** showed relatively poor solubility due to its polar carboxylic groups. However, good solublity was achieved in polar organic solvents, such as MeOH, EtOH, THF, DMF, and DMSO. Carboxyl-DTF **31b** was prepared under similar saponification conditions in a good yield of 87%.

Besides the $SC_{10}H_{21}$-subsituted DTF and TTFV derivatives, the SMe-sbustituted DTF **34** and TTFV **35** were also prepared in order to investigate their single-crystal structural properties in view of their much better crystallinity than the $SC_{10}H_{21}$-subsituted analogues.

2.2.2 Characterization of Carboxylated DTFs and TTFVs

Carboxylated DTFs **(31a-b)** and $TTFVs_{ox}$ **(32a-b)** were first subjected to routine NMR, IR, and MS analysis to confirm their molecular structures. The electrochemical redox behavior of compounds **31a-b**, **32a-b** and **34**, **35** was then characterized by cyclic voltammetric (CV) analysis, and Figure 2.1 shows the detailed cyclovoltammograms of these compounds. All compounds have been investigated in different solvents based on the solubility of the compounds under the CV experimental conditions. In general, the CV profile for DTF **31a** (Figure 2.1A) shows an anodic peak at + 0.89 V and a cathodic peak in the reverse scan at + 0.59 V in the first cycle of scans, which is indicative of a single-electron oxidation of the DTF moiety in **31a** to $[DTF]^{\cdot+}$ radical cation. The cathodic peak at + 0.59 V it is due to a bielectronic reduction of TTFV dication accumulated on electrode surface via the immediate dimerization reaction of $[DTF]^{\cdot+}$. On the second cycle of CV scan, a new anodic peak is seen at + 0.67 V.

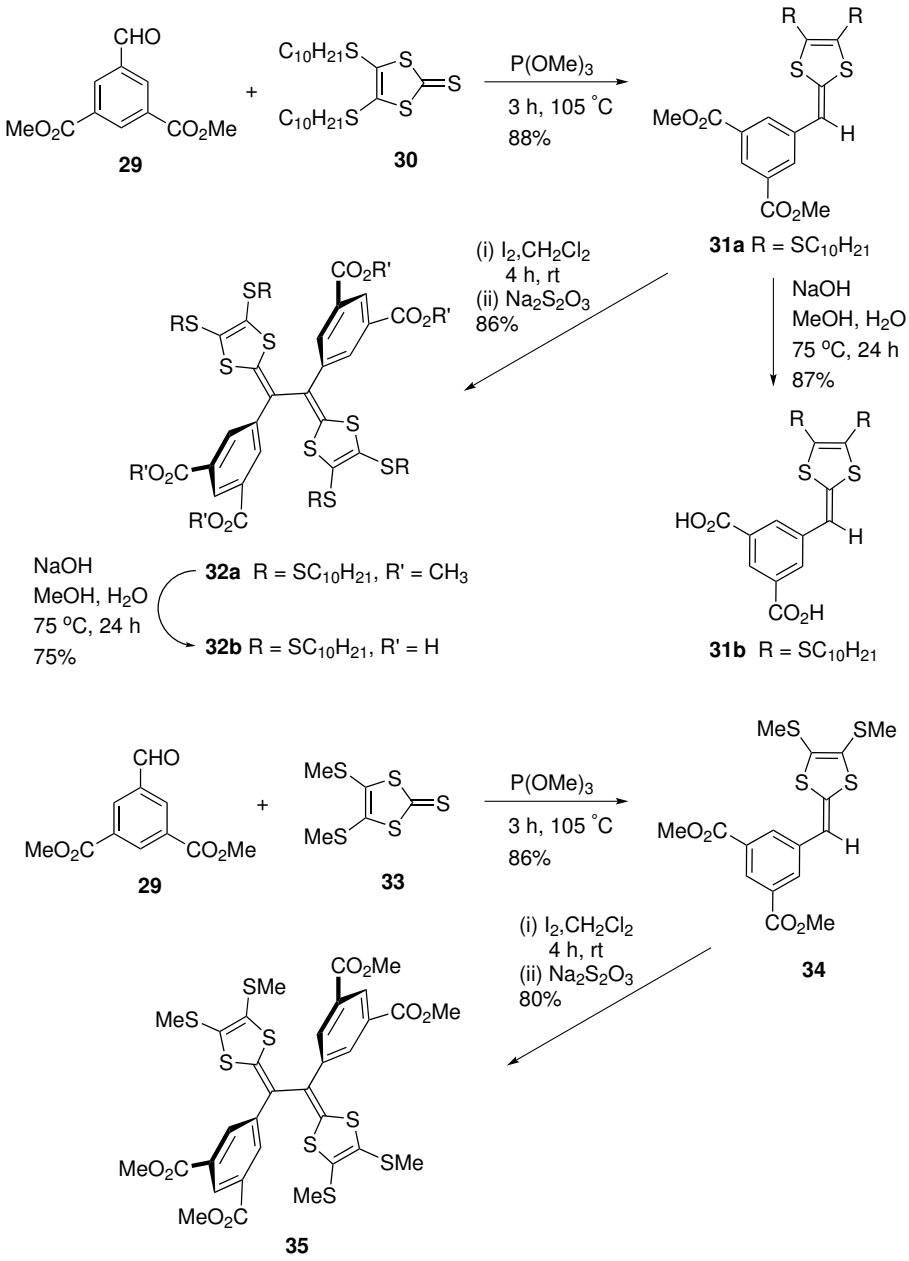

Scheme 2.2: Synthesis of carboxylated DTF and TTFV derivatives **31**, **32**, **34**, and **35**.

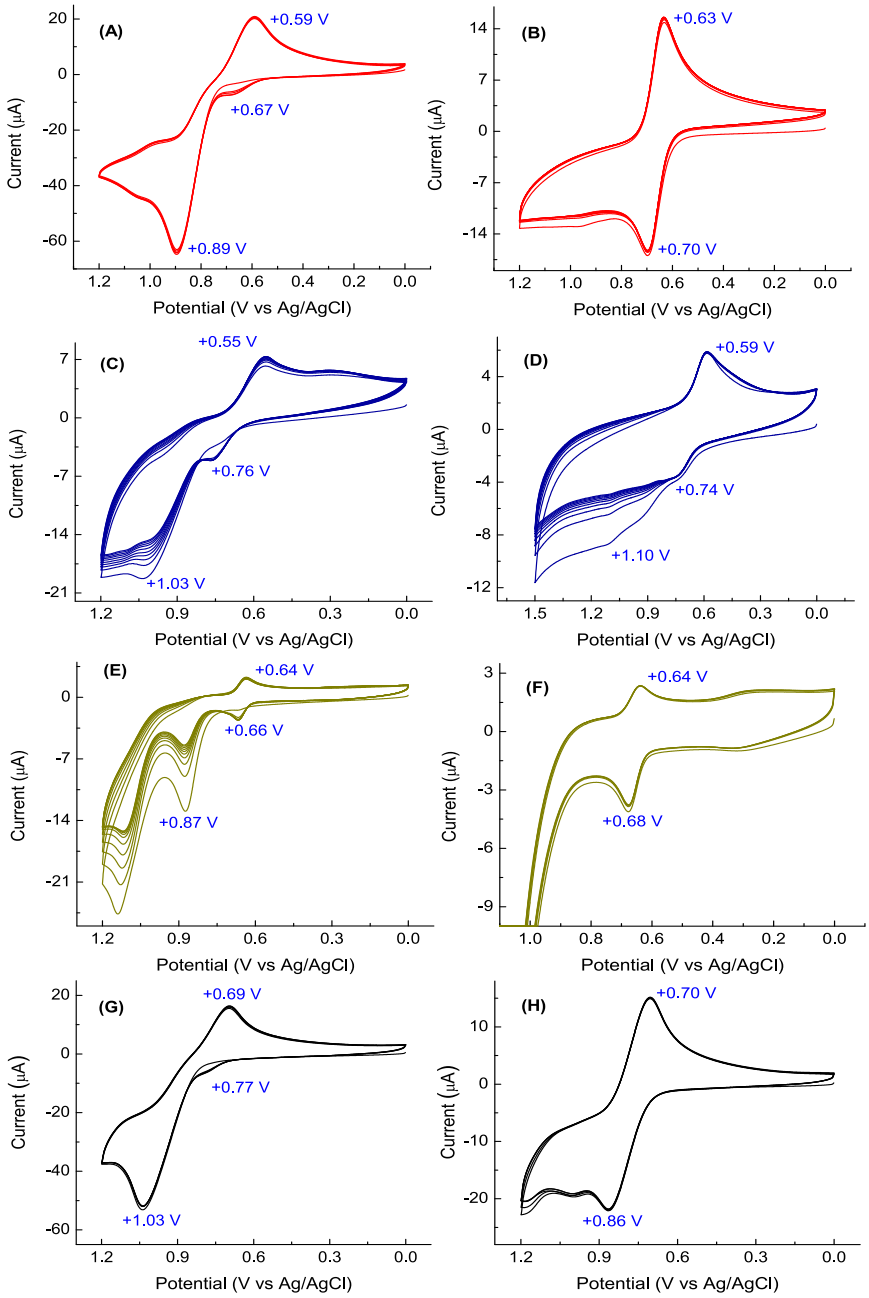

Figure 2.1: Cyclic voltammograms of (A) DTF **31a** in CH_2Cl_2, (B) TTFV **32a** in CH_2Cl_2, (C) DTF **31b** in $CHCl_3$, (D) TTFV **32b** in $CHCl_3$, (E) DTF **31b** in DMSO, (F) TTFV **32b** in DMSO, (G) DTF **34** in CH_2Cl_2, (H) TTFV **35** in CH_2Cl_2. All CV data were measured at room temperature. Experimental conditions: supporting electrolyte: Bu_4NBF_4(0.10 M), working electrode: glassy carbon, counter electrode:Pt wire, reference electrode: Ag/AgCl (3 M NaCl), scan rate: 100 mV/s.

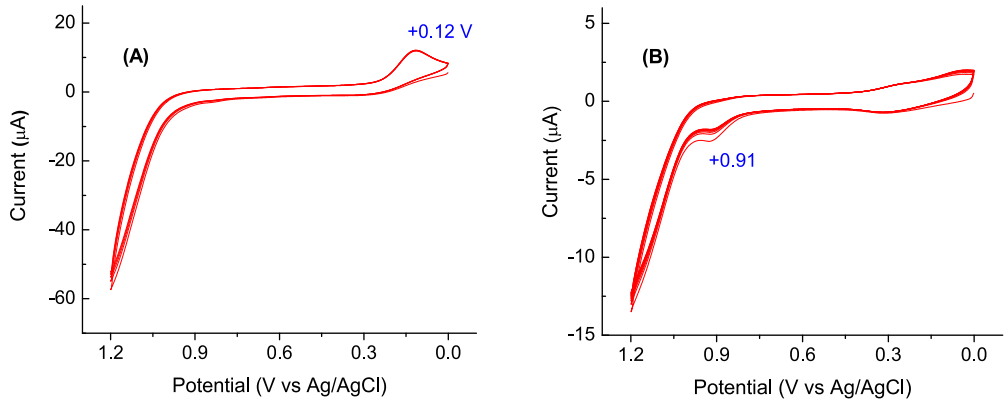

Figure 2.2: Cyclic voltammograms of (A) DTF **31b**/$HAuCl_4.3H_2O$ in DMSO (B) TTFV **32b**/ $HAuCl_4 \cdot 3\,H_2O$ in DMSO measured at room temperature. Experimental conditions: supporting electrolyte: Bu_4NBF_4 (0.10 M), working electrode: glassy carbon, counter electrode: Pt wire, reference electrode: Ag/AgCl (3 M NaCl), scan rate: 50 mV/s.

In the cyclic voltammogram of TTFV **32a**, a reversible redox couple can be clearly seen at Epa= + 0.70 V and Epc= + 0.63 V (Figure 2.1B), which is due to the two-electron redox processes taking place on the TTFV unit. This result further confirms the assignment of the TTFV dication peak in the CV profile of **31a** (Figure 2.1A). Similar redox behavior has been observed in carboxyl DTF **31b** and DTF **34** with a slight difference in redox potentials (Figure 2.1C,D). The voltammograms of TTFV **32a** and carboxyl TTFV **32b** both show a clear reversible redox wave pair due to simultaneous two-electron redox processes at the TTFV units.

To further understand the redox properties of the carboxylated DTF and TTFV derivatives after interacting with $HAuCl_4$, the solutions of DTF **31b** and TTFV **32b** in DMSO were mixed with $HAuCl_4$ for 24 h. The resulting solutions were then subjected to CV analysis and Figure 2.2 shows the detailed voltammograms. After interactions with $HAuCl_4$ the redox properties of DTF **31b** and TTFV **32b** are drammatically altered. Detailed assignments of the redox featurs still await more systematic inves-

tigations in the future work, since there have been no clear studies reported in the literature so far on this aspect.

2.2.3 Oxidative UV-Vis-NIR Titration Results

To obtain a deeper insight into the redox activity of caroxylated DTF and TTFV, UV-Vis-NIR spectroelectrochemical analysis was conducted in $CHCl_3$ and CH_3CN (Figure 2.3). Experimentally, a solution of DTF **31b** and TTFV **32b** in $CHCl_3$ and DTF **31b** in CH_3CN were prepared and then titrated with a mixture solution of $PhI(OAc)_2$/ CF_3SO_3H, (1: 4) molar ratio, $[PhI(OAc)_2] = 2.60 \times 10^{-2}$M) using a microsyringe. In each step of the titrations, a different molar equivalent of oxidant was added to **31b** and **32b** respectively. The mixture solution was allowed to stand for ca. 5 min before a UV -Vis-NIR absorption spectrum of the solution was recorded. As shown in Figure 2.3A, the absorption band of DTF **31b** in $CHCl_3$ at 365 nm is observed to decrease in intensity. In the meanwhile, a new broad low-energy band peaking emerges at ca. 557 nm to 784 nm and become much stronger in intensity. This broad band is attributed to the formation of dication $[TTFV]^{2+}$ produced upon the oxidation. The absorption spectrum of DTF **31b** in CH_3CN (Figure 2.3C) demonstrates similar spectral variations to those in $CHCl_3$ with slight shifts in absorption bands. UV-Vis-NIR titration analysis of TTFV **32b** was carried out only in $CHCl_3$ due to its poor solubility in CH_3CN. The spectra show an absorption band at 369 nm related to the TTFV **32b** (Figure 2.3B) with a significant decrease in intensity. In contract, a long wavelength band at ca. 482 nm to 800 nm is observed with a notable growth in intensity. This characteristic band can be ascribed to the formation of $[TTFV]^{2+}$ upon oxidation.

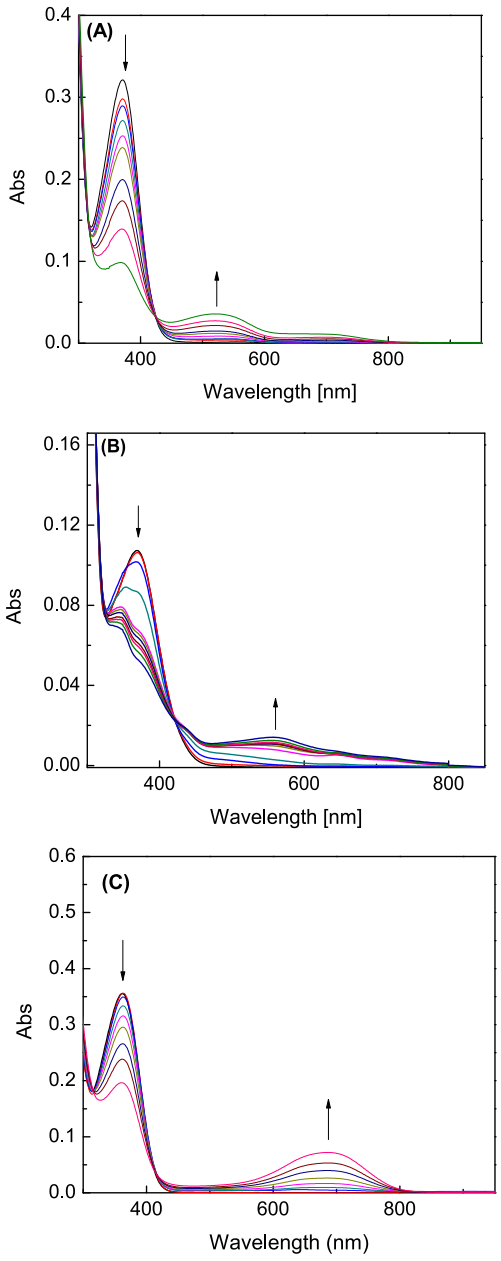

Figure 2.3: UV-Vis-NIR spectra monitoring the titration of (A) DTF **31b** in $CHCl_3$ (1.0×10^{-6} M), (B) TTFV **32b** in CH_3Cl (8.2×10^{-7} M), and (C) DTF **31b** in CH_3CN (1.6×10^{-5} M) titrated with $PhI(OAc)_2/CF_3SO_3H$ (1:4 molar ratio) as oxidant at room temperature.

2.2.4 X-ray Structural Analysis

DTF **34** and TTFV **35**, which are analogous to **31a** and **32a** respectively but differ in the substituents (SCH_3 instead of $SC_{10}H_{21}$) attached to the dithiole units, were synthesized and their crystal structures were successfully determined by single crystal X-ray diffraction analysis (Figure 2.4). In our previous crystallographic studies of other phenyl-substituted DTFs,[100,101] the dithiole ring and the phenyl group usually adopt a significant twist angle (ca. 20-40°) as a result of steric interactions. However, this is not the case in the structure of DTF **34**, wherein the dithiole ring and the phenyl group are virtually co-planar (Figure 2.4A). The planarization is driven by the strong electron-withdrawing effects of the two carboxyl groups to favour maximal $\pi-$electron delocalization. The structure of TTFV **35** (Figure 2.4B) also appears to be an anomaly in comparison with other known phenyl-substituted TTFVs.[87,95,99] Herein a nearly *trans* conformation is adopted instead of the pseudo-*cis* conformation typically seen in other phenyl-TTFVs. Such an outcome can be explained by the effect of dipole-dipole interactions; that is, the trans orientation allows the four polar carboxylate groups of **35** to be aligned opposite to one another to minimize the net dipole moment.

2.2.5 Reduction of $HAuCl_4$ by Carboxylated DTFs and TTFVs

The interactions of **31a-b** and **32a-b** with $HAuCl_4{\cdot}3H_2O$ were investigated in four selected polar organic solvents (CH_3CN, THF, DMF, and DMSO), except that TTFV **32b** was not tested in CH_3CN due to its poor solubility in it. In the experiments, compounds **31a-b** and **32a-b** were mixed with $HAuCl_4$ in the solvents mentioned above at room temperature. When DTF **31a** was mixed with $HAuCl_4.3H_2O$ in CH_3CN, the color of the solution immediately turned into green and gradually developed into a

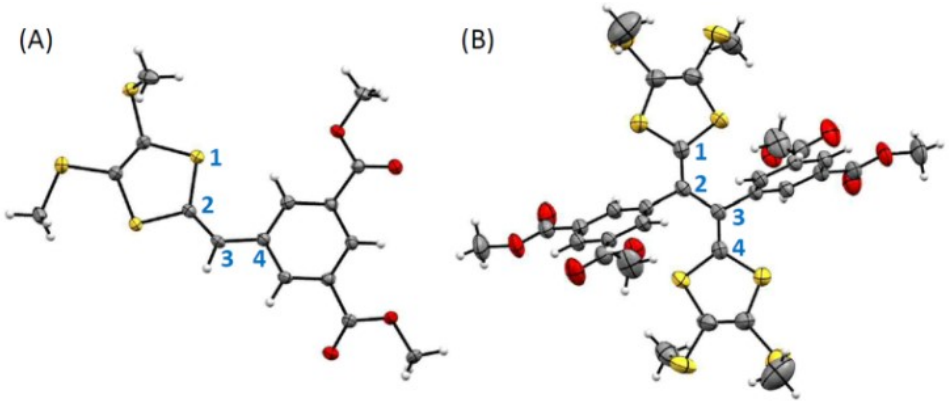

Figure 2.4: ORTEP plots (50% probability displacement ellipsoids) of (A) DTF **34** (torsion angle S1-C2-C3-C4 = 1.9°, CCDC # 1503852) and (B) TTFV **35** (torsion angle C1-C2-C3-C4 = 156.8°, CCDC# 1503853).

deep blue colour after standing at room temperature for 24 h (see Figure 2.5). UV-Vis-NIR absorption spectral analysis (Figure 2.6) shows a strong low-energy band at 690 nm, which is consistent with the characteristic absorption band of the TTFV dication.[102,103] Slow evaporation of the mixture of **31a** and $HAuCl_4$ in CH_3CN yielded single crystals of TTFV dication $[\mathbf{32a}]^{2+}$ associated with $[AuCl_4]$ as counterion (Figure 2.7), confirming that $HAuCl_4$ induced the dimerization of DTF **31a** in CH_3CN as an oxidant.

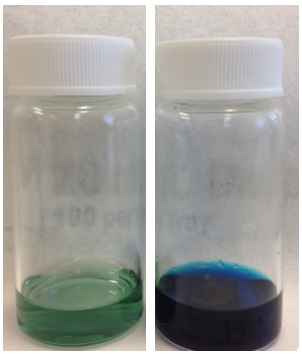

Figure 2.5: Photographic images of DTF **31a** mixed with $HAuCl_4.3H_2O$ in CH_3CN at room temperature for 24 h.

Similar UV-Vis-NIR absorption features were observed in the mixture of DTF

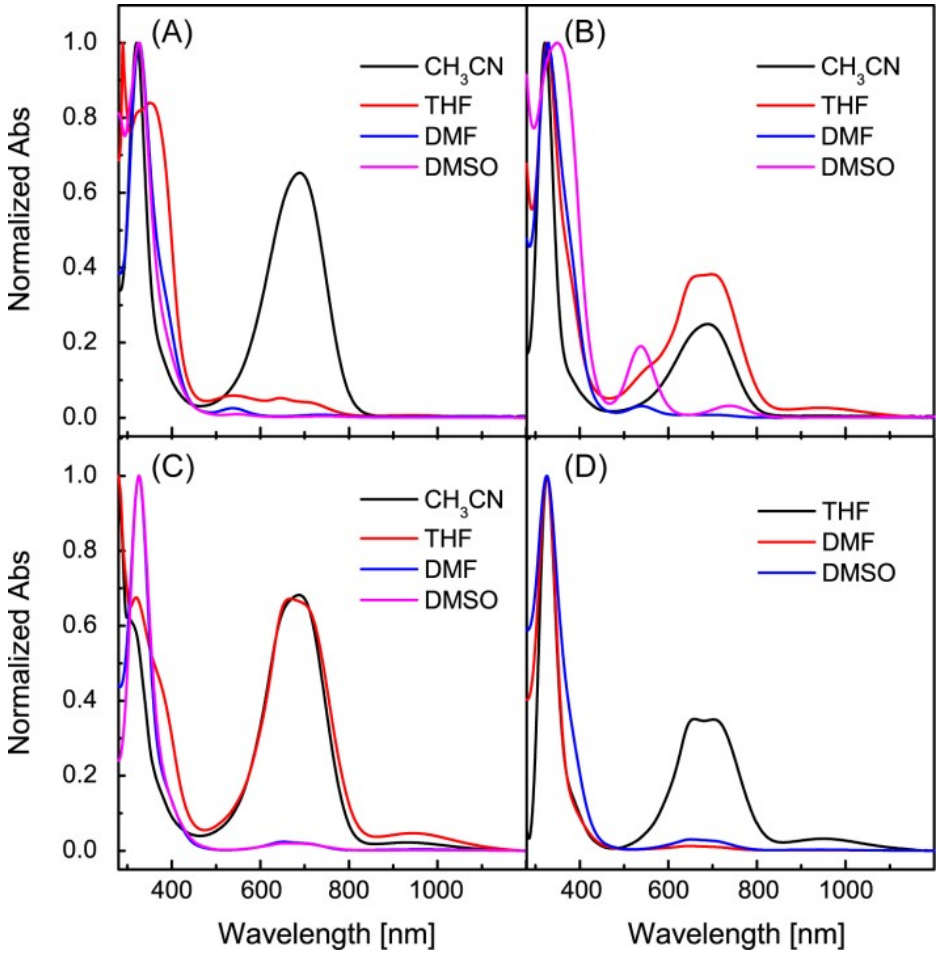

Figure 2.6: Normalized UV-Vis-NIR spectra of $HAuCl_4$ after mixing with (A) DTF **31a**, (B) DTF **31b**, (C) TTFV **32a**, and (D) TTFV **32b** respectively in various polar organic solvents for 24 h.

31b with $HAuCl_4$ in CH_3CN (Figure 2.6B), while for both cases of **31a** and **31b** in CH_3CN there is no evidence for the formation of AuNPs from their UV-Vis absorption spectra. Furthermore, scanning electron microscopic (SEM) analysis on the mixtures of **31a**/**31b** and $HAuCl_4$ after complete evaporation of CH_3CN did not reveal any significant amount of Au(0) species. It is hence postulated that DTF **31a** and **1b** reduced $HAuCl_4$ mainly into Au(II) and/or Au(I) species in CH_3CN. The mixture of **31a** with $HAuCl_4$ in THF shows a spectral envelop comprised of three peaks at 541, 647, and 718 nm in the Vis-NIR region (Figure 2.6A). In addition, there is a

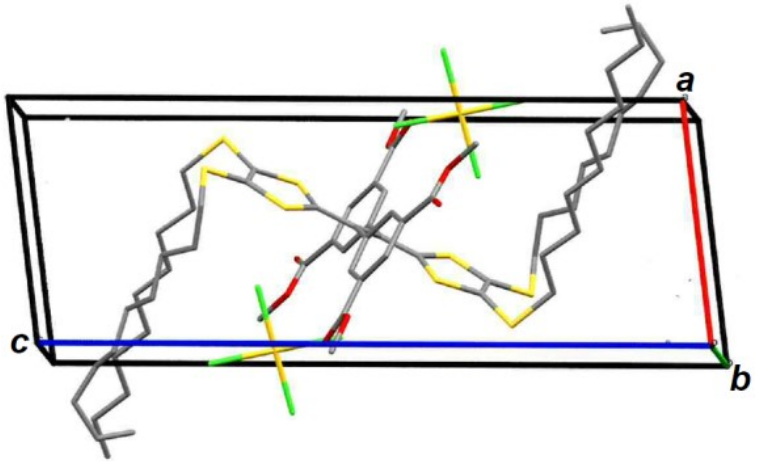

Figure 2.7: X-ray structure of $[32a^{2+}] \cdot [AuCl^{-}_{4}]_2$ in the unit cell, viewed along the b axis (CCDC# 1503854).

weak absorption tail (ca. 830 to 1100 nm) discernible. These features can be more distinctively seen in the spectrum of **31b** and $HAuCl_4$ mixed in THF (Figure 2.6B). The peak at 541 nm agrees with the surface-plasmon band (SPB) of AuNPs with diameters of tens of nm,[64,104] while the longer-wavelength bands can be assigned to the dication and radical cation of TTFVs resulting from oxidative dimerization, which is evidenced by the fact that they bear great resemblance to the spectra of TTFVs **32a** and 32b after interacting with $HAuCl_4$in THF (see Figure 2.6C and D).The most intriguing observation came from the mixtures of DTFs **31a** and **31b** with $HAuCl_4$ in strongly aprotic dipolar solvents DMF and DMSO. The solutions of DTF **31a** in DMF and DMSO gave a greenish tinge when $HAuCl_4$ was added and then gradually developed into a pinkish colour after standing for a few hours. UV-Vis-NIR analysis shows absorption bands at ca. 540 and 740 nm, suggesting the formation of AuNPs and TTFV dications. However, the relative intensities of these bands are rather weak. For the solutions of DTF **31b** mixed with $HAuCl_4$ in DMF and DMSO, the SPB bands of AuNPs appear to be more prominent. Particularly, the DMSO solution of **31b** mixed with $HAuCl_4$ gave a deep red color after standing for a few hours at room

temperature and the colour could sustain for several weeks without any significant changes. The outcomes suggest that stabilized AuNPs were generated by reducing $HAuCl_4$ with DTF **31b** in DMSO.

Further comparison of the Vis-NIR absorption profile of DTF **31b**/$HAuCl_4$ in DMSO with that of TTFV **32b**/$HAuCl_4$ (Figure 2.8) exposes markedly different absorption behavior. The spectrum of **32b**/$HAuCl_4$ exhibits the characteristic bands of the TTFV dication and radical cation at 653, 728, and 952 nm, whereas the spectrum of **31b**/$HAuCl_4$ gives a conspicuous AuNP SPB band at 538 nm along with a relatively weak broad peak centred at 739 nm. The exact assignment of the latter peak cannot be clearly made at this juncture and further studies are underway. Possibly it is due to the TTFV dication resulting from related redox reactions. On the other hand, the formation of AuNP aggregates[105] may also account for this longer-wavelength absorption band (vide infra).

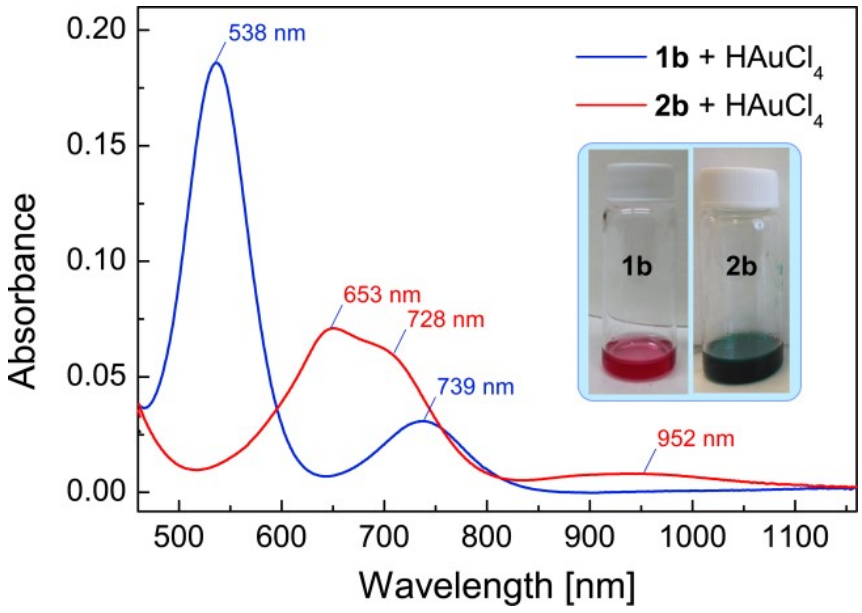

Figure 2.8: Vis-NIR spectra comparing the absorption profiles of DTF **31b** and TTFV **32b** mixed with $HAuCl_4$ in DMSO. Inset: photoimages of the two solutions.

2.2.6 SEM and DLS Analyses

The morphology of the synthesized gold particles were investigated by the scanning electron microscopy (SEM). In the experiments, each sample solution was carefully placed on a sample holder stub with a double-sided carbon tape and then kept for 24 h to be air dried prior to SEM imaging. In addition, a dynamic light scattering (DLS) study was undertaken to determine size distribution of the nanoparticles formed in the solutions. In the DLS experiments, a quartz cuvette was rinsed with high purity solvent prior to use to avoid dust contamination that may lead to an accurate result. The sample solutions of carboxyl DTF **31b**/$HAuCl_4.3H_2O$ in DMSO went through multiple filtration steps using filters with a pore size of 0.2 μm. The filtrates were then respectively placed in the cuvette and kept still until the temperature reached 25°C.

SEM analysis of the residue of DTF **31a**/$HAuCl_4$ in DMSO after evaporation shows the formation of a significant amount of micron-sized Au(0) particles with very good crystallinity (Figure 2.9A). For the mixture of DTF **31b**/$HAuCl_4$, both AuNPs and their much larger aggregates (ca. 10 μm) were observed via SEM imaging. In additon, SEM analysis of mixture of DTF **31a-b** and TTFV **32a-b** /$HAuCl_4.3H_2O$ in CH_3CN and THF did not show any formation of gold nanoparticles or crystalline Au(0) particles, compared to those observed in highly polar solvents such as DMSO. When THF and CH_3CN were used as solvents, the dimerization reaction seems to be faster in these two media unlike that in a much higher polar solvent such as DMSO. During the DLS measurements, it was found that a large aggregates of spherical AuNPs were formed. After ultrasonication for 50 min, the large aggregates could be dissembled into smaller nanoparticles (Figure 2.9D), indicating that the inter-particle attractions are likely non-covalent forces (e.g., H-bonding).

The rationalization for this observation is as follows. The surface of AuNPs is

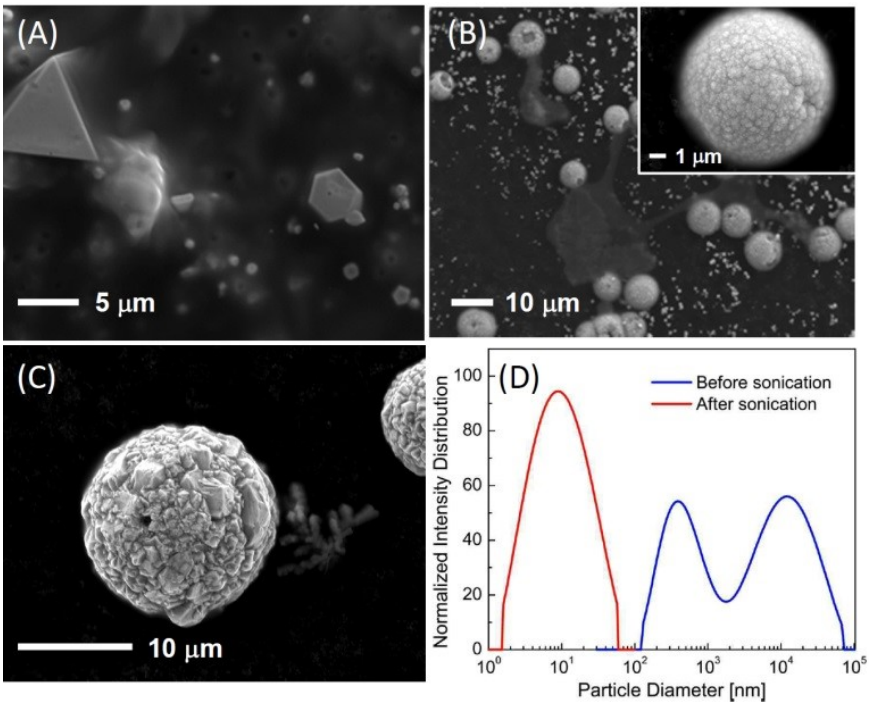

Figure 2.9: SEM images of the residues resulting from evaporating the DMSO solutions of $HAuCl_4$ mixed with (A) DTF **31a**, (B) DTF **31b**, and (C) TTFV **32b** respectively. (D) Size distribution of particles dispersed in the DMSO solution of **31b**/$HAuCl_4$ before and after ultrasonication for 50 min at room temperature.

capped by DTF **31b** and/or their oxidized forms (e.g., TTFV dication), and the carboxyl groups present in these species facilitate inter-particle attraction through dipole-dipole and hydrogen bonding interactions. In the case of TTFV 32b/$HAuCl_4$ in DMSO, micron-sized Au(0) particles were observed in the SEM analysis. Nevertheless, the crystallinity of these particles is much poorer than those resulting from DTF **31a**/$HAuCl_4$. The different microscopic properties can be explained by the fact that TTFV **32b** is a stronger electron donor (reductant) than DTF **31a** and hence reduces Au(III) into Au(0) at a much faster reaction rate. In general, a fast reduction rate would disfavour the formation of crystalline Au(0) particles.

Moreover, SEM images were taken for the solutions before and after ultrasonication. The nanoparticles obtained after ultrasonication show an average diameter of

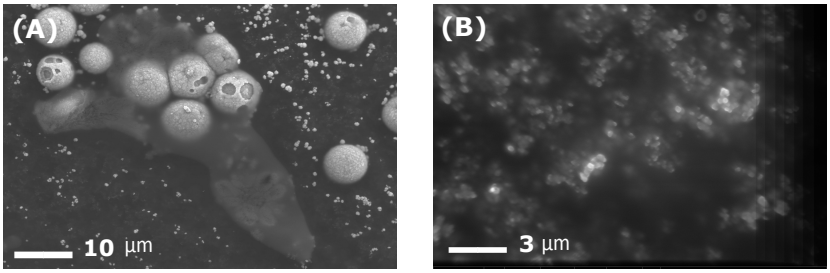

Figure 2.10: SEM images of $HAuCl_4$ mixed with DTF **31a** in DMSO taken before (left) and after (right) ultrasonication.

32 nm (see Figure 2.10). The normalized intensity distribution in DLS measurement is given in Figure 2.9D. After ultrasonication, the average particle diameter appears to be slightly larger than that determined by SEM imaging. This can be explained by the fact that DLS measures the solvodynamic radius which is usually close to but larger than the exact geometrical radius of the nanoparticles measured.

2.2.7 Conclusions

The work in this chapter has investigated the redox interactions of carboxylated DTFs **31a-b** and TTFVs **32a-b** with $HAuCl_4$ in various polar organic solvents. Of these four organic π-donors, carboxylic DTF **31b** stands out as a very effective agent for generating stabilized AuNPs in DMSO and DMF. This finding deepens the understanding of DTFs and TTFVs redox activities and expands the synthetic toolbox for preparing AuNPs.

2.2.8 Experimental Procedures

Chemicals were purchased from commercial suppliers and used directly without purification. All reactions were conducted in standard, dry glassware and under an inert atmosphere of nitrogen unless otherwise noted. Evaporation and concentration were carried out with a water-aspirator. Flash column chromatography was performed with silica gel 60 (240-400 mesh). Thin-layer chromatography (TLC) was done with silica gel F254 coated on plastic sheets and visualized by UV light. Melting points were measured on an SRS OptiMelt melting point apparatus. ^{1}H and ^{13}C NMR spectra were measured on a Bruker Avance III 300 MHz multinuclear spectrometer. Chemical shifts (δ) are reported in ppm downfield relative to the signal of either the internal reference $SiMe_4$ or residual solvent $CHCl_3$ (7.26 ppm for ^{1}H and 77.2 ppm for ^{13}C). Coupling constants (J) are given in Hz. Infrared spectra (IR) were recorded on a Bruker Alfa spectrometer. HRMS analyses were performed on an Agilent 6230 TOF LC/MS instrument using an APPI ionizer and a QSTAR XL hybrid quadrupole/TOF mass spectrometer equipped with an o-MALDI ion source. UV-Vis-NIR absorption spectra were measured on a Cary 6000i spectrophotometer. Scanning Electron Microscopes (SEM) were performed on JEOL JSM-7100F (Vacc = 30 kV, Imax = 400 nA). The Delsa Nano S particle analyzer (Beckman Coulter, Inc.) was used for dynamic light scattering (DLS) studies, where sample solutions were filtered through a 0.20 m Millex-FG filter prior to the measurements. The calculations of the particle size distributions were performed with the Delsa Nano software 2.30 (Beckman Coulter, Inc). Cyclic voltammetric analyses were carried out in a standard three-electrode setup controlled by a BASi Epsilon potentiostat.

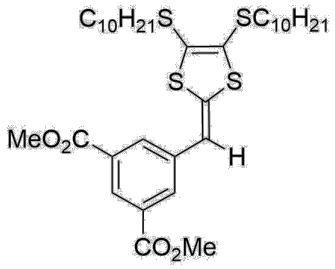

31a

DTF 31a: A mixture of dimethyl-5-formylisophthalate **29** (1.00 g, 4.50 mmol) and thione **30** (3.01 g, 8.79 mmol) in $P(OMe)_3$ (15 mL) was stirred and heated at 105 °C for 3 h. The excess $P(OMe)_3$ was removed by vacuum distillation.The residue was purified by silica column chromatography (CH_2Cl_2/hexanes, 1:4) to afford compound DTF **31a** (2.58 g, 3.36 mmol, 88%) as a yellow solid. m.p. > 145 °C (dec); ^{1}H NMR (300 MHz, $CDCl_3$) δ 8.44 (t, J = 1.5 Hz, 1H), 8.06 (d, J = 1.5 Hz, 2H), 6.51 (s, 1H), 3.96 (s, 6H), 2.83 (m, 4H), 1.69–1.59 (m, 4H), 1.45–1.22 (m, 28H), 0.91–0.81 (m, 6H) ppm; ^{13}C NMR (75 MHz, $CDCl_3$)δ 166.2, 137.1, 136.4, 131.4, 130.9, 128.3, 127.3, 124.7, 111.8, 52.4, 36.3, 36.1, 31.9, 30.9, 29.8, 29.7, 29.6, 29.5, 29.3, 29.2, 29.1, 28.57, 28.56, 22.7, 14.1 ppm; FTIR (neat) 2953, 2916, 2847, 1710, 1563, 1438, 1331, 1263, 1205, 1138, 1011, 886, 747 cm^{-1}; HRMS (APPI, positive) m/z calcd for $C_{34}H_{53}O_4S_4$ 653.2827, found 653.2814 $[M + H]^+$.

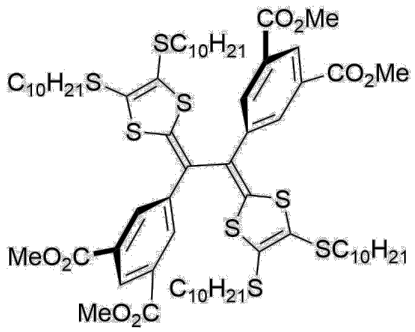

32a

TTFV 32a: DTF **31a** (0.50 g, 0.76 mmol) and I_2 (0.58 g, 2.28 mmol) were added in CH_2Cl_2 (100 mL) and the mixture was stirred at rt overnight. Then a satd $Na_2S_2O_3$ aq. solution (90 mL) was added and the mixture was stirred for another 3 h at rt. The organic layer was separated, washed with H_2O, dried over $MgSO_4$, and concentrated under vacuum. The residue was purified by silica column chromatography (EtOAc/hexanes, 1:8) to afford TTFV **32a**(0.40 g, 0.32 mmol, 86%) as a yellow gummy solid. ^{1}H NMR (300 MHz, $CDCl_3$) δ 8.46 (t, J = 1.5 Hz, 2H), 8.23 (d, J = 1.5 Hz, 4H), 3.92 (s, 12H), 2.93–2.67 (m, 8H), 1.68–1.52 (m, 8H), 1.44–1.19 (m, 56H), 0.90–0.85 (m, 12H) ppm ; ^{13}C NMR (75 MHz, $CDCl_3$) δ 166.0, 140.6, 138.1, 131.8, 131.2, 128.9, 128.8, 125.9, 121.5, 52.4, 36.3, 36.2, 31.93, 31.91, 29.65, 29.58, 29.4, 29.3, 29.2, 28.6, 28.5, 22.7, 14.1 ppm; FTIR (neat) 2922, 2852, 1728, 1436, 1327, 1240, 1134, 1002, 757, 721 cm^{-1}; HRMS (APPI, positive) m/z calcd for $C_{68}H_{103}O_8S_8$ 1303.5419, found, 1303.5424 $[M + H]^+$.

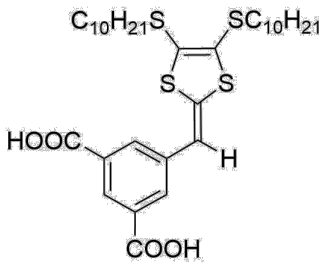

31b

DTF 31b: DTF **31a** (0.39 g, 0.59 mmol) and NaOH (0.76 g, 19 mmol) were added in MeOH/H_2O (240 mL, 3:1) and the mixture was stirred and heated at 75 °C overnight. The solvent MeOH was then removed under vacuum, and the residue was diluted to 50 mL with H_2O and acidified to pH 4 with HCl (aq). The precipitate formed was extracted with EtOAc, washed with H_2O, dried over $MgSO_4$, and concentrated under vacuum to afford compound **31b** (0.32 g, 0.51 mmol, 86%) as a yellow solid. m.p. $>$ 120 °C (dec); ^{1}H NMR(300 MHz, DMSO-d6) δ 8.26 (t, J = 1.5 Hz, 1H), 8.01 (d, J = 1.3 Hz, 2H), 6.94 (s, 1H), 2.92–2.80 (m, 4H), 1.62–1.51 (m, 8H), 1.43–1.15 (m, 28H), 0.85–0.78 (m, 6H) ppm (one carboxylic proton signal not observed because of rapid proton exchange); Meaningful ^{13}C NMR data was not acquired because of low solubility; FTIR (neat) 2920, 2849, 1687, 1559, 1436, 1301, 1262, 1217, 916, 795, 751, 608 cm^{-1}; HRMS (APPI, positive) m/z calcd for $C_{32}H_{49}O_4S_4$ 625.2514 found, 625.2513 $[M + H]^+$.

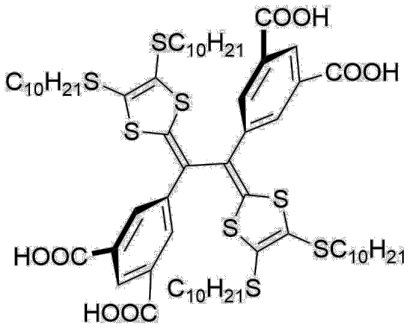

32b

TTFV32b: TTFV **32a** (0.10 g, 0.076 mmol) and NaOH (0.090 g, 2.3 mmol) were added in MeOH/H_2O(40 mL, 3:1) and the mixture was stirred and heated at 75 °C overnight. The solvent MeOH was then removed under vacuum, and the residue was diluted to 50 mL with H_2O and acidified to pH 4 with HCl (aq). The precipitate formed was extracted with EtOAc, washed with H_2O, dried over $MgSO_4$, and concentrated under vacuum to afford compound **32b** (0.060 g, 0.048 mmol, 75%) as a yellow solid. m.p. $>$ 246 °C (dec); ^{1}H NMR (300 MHz, acetone-d6) δ 8.53 (t, J = 1.5 Hz, 2H), 8.36 (d, J = 1.5 Hz, 4H), 2.98-2.78 (m, 8H), 1.72-1.61 (m, 8H), 1.50-1.22 (m, 56H), 0.91-0.83 (m, 12H) ppm (one carboxylic proton signal not observed because of rapid proton exchange); Meaningful ^{13}C NMR data was not acquired because of low solubility; FTIR (neat): 2922, 2851, 1729, 1528, 1436,1260, 1103, 1021, 720, 668,cm^{-1}; HRMS (APPI, negative) m/z calcd for $C_{64}H_{93}O_8S_8$ 1245.4642, found, 1245.4633 [M – H]$^-$.

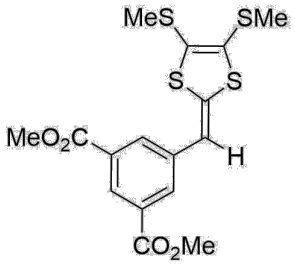

34

DTF 34: A mixture of dimethyl-5-formylisophthalate **29** (0.510 g, 2.25 mmol) and thione **30** (2.01 g, 8.87 mmol) in $P(OMe)_3$ (15 mL) was stirred and heated at 105 °C for 3 h. The excess $P(OMe)_3$ was removed by vacuum distillation. The residue was purified by silica column chromatography (CH_2Cl_2/hexanes, 1:2) to afford compound DTF **34** (1.97 g, 4.92 mmol, 86%) as a yellow solid. m.p. 167–198 °C; ^{1}H NMR (300 MHz, $CDCl^3$)δ 8.45 (m, 1H), 8.06 (m, 2H), 6.53 (s, 1H), 3.96 (s, 6H), 2.46 (s, 3H), 2.44 (s, 3H), ppm; ^{13}C NMR (75 MHz, $CDCl_3$) δ 166.4, 137.2, 136.2, 131.6, 131.1, 128.4, 127.5, 124.1, 112.4, 52.6, 19.3, 19.1 ppm; FTIR (neat) 2996, 2949, 2916, 1709, 1492, 1421, 1203, 1109, 725, 668, 547, 470 cm^{-1}; HRMS (APPI, positive) m/z calcd for $C_{16}H_{17O}O_4S_4$ 401,0010, found 401.0010 $[M + H]^+$.

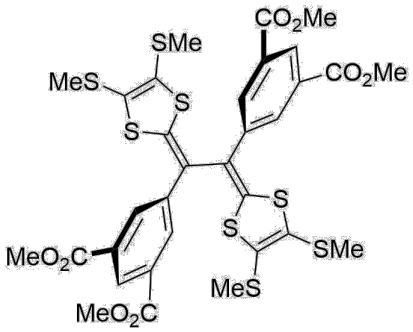

35

TTFV 35: A mixture of DTF **34** (0.34 g, 0.85 mmol) and I_2 (0.26 g, 3.07 mmol) in CH_2Cl_2 (100 mL) was stirred at rt overnight. Then a satd $Na_2S_2O_3$ aq. solution (90 mL) was added. The mixture was stirred for another 3 h at rt. The organic layer was separated, washed with H2O, dried over $MgSO_4$, and concentrated under vacuum. The residue was purified by silica column chromatography (EtOAc/hexanes, 1:1) to afford compound 4 (0.68 g, 1.3 mmol, 80%) as a yellow gummy solid. ^{1}H NMR (300 MHz, $CDCl_3$)δ 8.46 (m, 2H), 8.23 (m, 4H), 3.93 (s, 12H), 2.44 (s, 6H), 2.41 (s, 6H) ppm; Meaningful ^{13}C NMR data was not acquired because of low solubility; FTIR (neat) 2921, 2851, 1723, 1460, 1433, 1328, 1242, 1134, 1028, 720, 671, 467 cm^{-1}; HRMS (APPI, positive) m/z calcd for $C_{32}H_{31}O_8S_8$ 798.9785, found 798.9789 [M + H]$^+$.

Chapter 3

Towards the Synthesis of TTFV-Based Redox-Active MOFs

3.1 Introduction

A metal-organic framework, abbreviated as MOF, is a coordination polymer linked by organic ligands, with an open framework containing potential voids, which has the potential for host-guest chemistry. The coordination polymer is a term to describe an extended compound in a 1, 2 or 3-dimensional architecture assembled through coordination bonds. MOF contain polynuclear clusters with microcrystillenity engender a high porous materials. Moreover, bridging ligands stabilize these clusters and the networks are supported by strong covalent bonds within the organic component in MOFs.[106] An important feature of MOFs is that the linkers have to show the ability to coordinate to metal centers in either 1, 2 or 3 dimensions. Although coordination networks have been known for decades, MOFs became well recognised as an appealing class of porous materials only after the seminal work by Omar Yaghi's group in the mid-1990s.[107] The construction of MOFs was achieved by connecting metal-containing

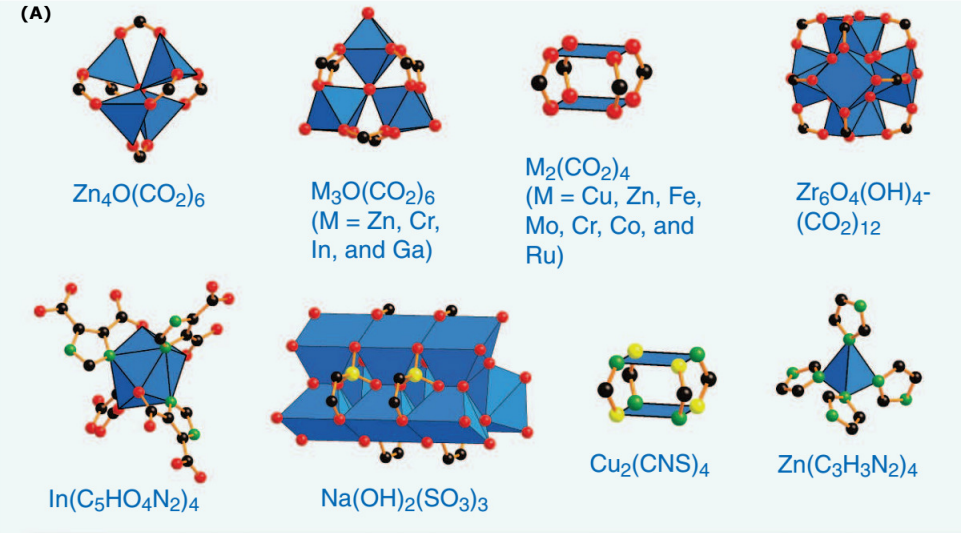

Figure 3.1: Exemplar of inorganic secondary building units (SBUs) for MOFs. Figure adopted from Yaghi et al., *Science* **2013**, *341*, 1230444 with permission.

units, secondary building units (SBUs), and organic linkers together through strong coordination bonds, and MOFs generally show open framework with enormous surface areas and excellent porosity. Fig. 3.1-3.2 lists the commonly used SBUs and ligands for the preparation of MOFs.[106,108]

The innovation of MOF chemistry started in 1999 when the most popular highly porous MOF-5 [Zn_4O(benzene−1,4−dicarboxylate)$_3$] was successfully designed and synthesized by Yaghi's group.[109] The novel prototype of MOFs features a $Zn_4O(CO_2)_6$ octahedral SBU, the who framework was assembled by linking the SBUs through 1,4-benzenedicarboxylate units (Fig. 3.3).[110]

In MOF synthesis, carboxylated arenes are commonly used linkers, given their versatile complexation ability with various metal ions. In addition, the selection of the organic linkers can be other types of metal ligands; for instance, cyanide[111] glutamate,[112] formate,[113] triazole,[114] oxalate,[115] 1,2,4,5-tetracarboxylates,[116] and squarates.[117] Recently, extensive research has been dedicated to controlling or fine-tuning the surface

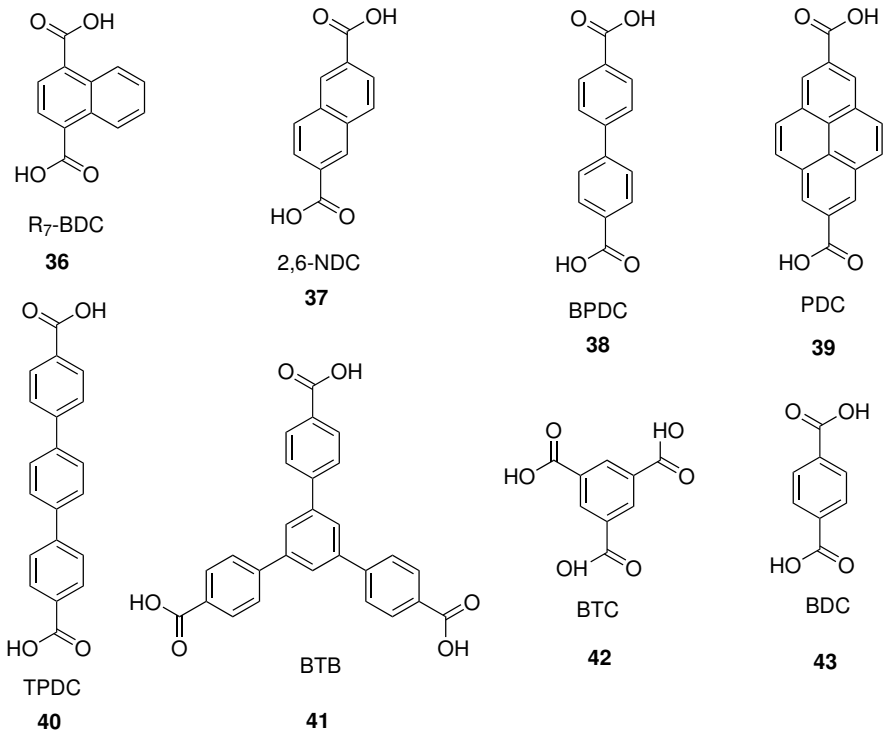

Figure 3.2: Commonly used carboxylic ligands for MOFs. Figure adopted from Yaghi et al., *Science* **2013**, *341*, 1230444 with permission.

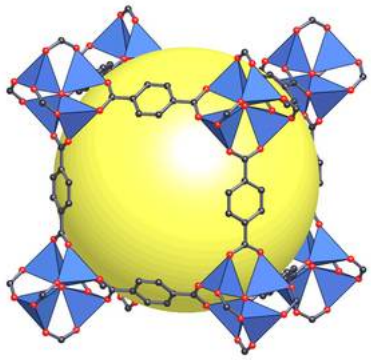

Figure 3.3: Single crystal structure of MOF-5 [Zn_4O(benzene−1,4−dicarboxylate)$_3$]. Color scheme is as follows: Zn (blue polyhedra), O (red spheres), C (black spheres). Figure copied from Yaghi et al., *Science*, **2002**, *295*, 469-472 with permission.

area, microscopic topology, and porosity of MOFs. The studies have demonstrated that rationally designed MOFs can serve as ideal materials for applications in gas storage, separations, and catalysis.[108] The variation in determined SBUs and organic linkers, geometry, size, and functionality led to a large number of MOFs being prepared and investigated up to now; however, the most widely studied MOFs so far in the literature are still the family of carboxylate-based MOFs. In general, a carboxylate ligand coordinates to a metal center via bonds involving two or more donor atoms.[118] The cationic charge afforded by the metal nodes used in MOFs can be neutralized by the anionic charge in the ligand which is important especially in host-guest interaction as these anions will decrease the space available in the inner channels and voids.[119] Carboxylate-based linear 1,4-benzenedicarboxylate, has been known as BDC, was invented by Yahgi and co-workers.[109] Similar to the popularly used ligand 4,4'-Bipyridine (4,4-bpy), BDC also has two Lewis basic moieties but its versatility is much higher than that of 4,4-bpy because of its multiple binding modes. (Figure 3.4) illustrates the three binding modes commonly observed for carboxylate-metal complexes.[106]

Over the past few years, the design and synthesis of MOFs with photo/redox-activity has received growing interest due to the intriguing application in advanced electronic and optoelectronic devices. Embedding functional chromophores and/or electron donors/acceptors in the structure of ligand has been an effective way to deliver novel functional MOFs; however, much challenge remains in the development of efficient and reliable synthetic methods for various functionalized ligands. In 2016, an interesting review article was published by D'Allessandro focusing on the latest development and studies of redox-active MOFs using new solid state techniques such as electrochemistry and spectroelectrochemistry.[120] MOFs constructed by connecting metal centers with typical organic linkers are often redox-inactive and therefore lack

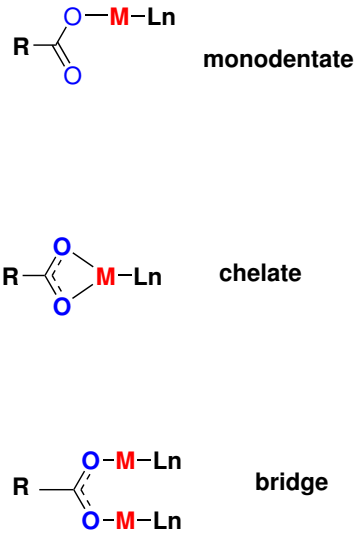

Figure 3.4: Common binding modes for carboxylates and metal ions: (a) monodentate, (b) chelate, (c) bridging interactions.

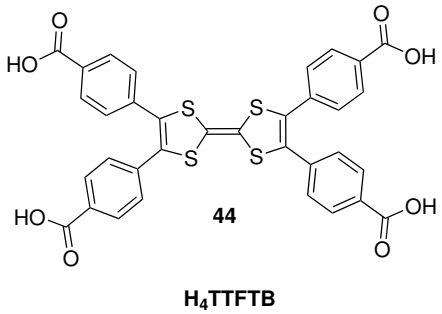

Figure 3.5: Chemical structure of the H_4TTFTB ligand.

of electrical conductivity and/or semi-conductivity. The emergence of redox-active MOFs has allowed studies on charge transfer phenomena within 3-dimensional coordination space. For instance, the redox-active tetratopic ligand tetrathiafulvalenetetrabenzoate (H_4TTFTB) (Figure 3.5) was synthesized and then used as the ligand to complex with Zn(II) ion forming a redox-active Zn_2(TTFTB) MOF (Figure 3.6). This new MOF contains circular stacks of TTF and benzoate lined within an extended 1-dimensional channel. The MOF was found to exhibit high charge mobility and permanent porosity.[121]

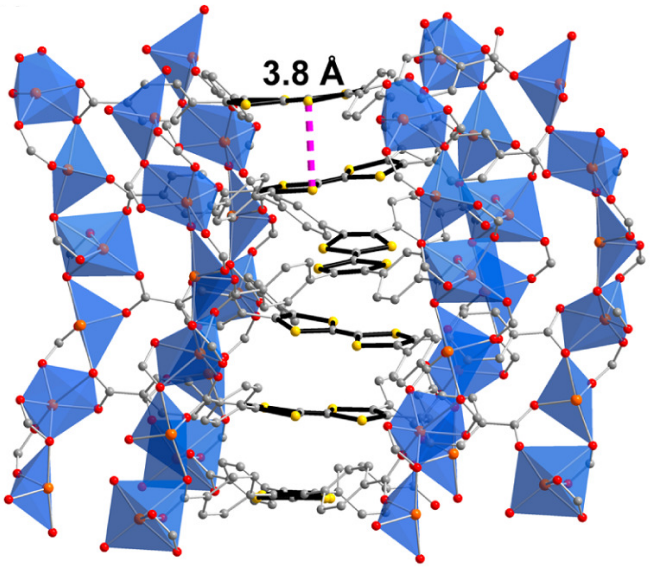

Figure 3.6: A side view of the crystal structure of Zn_2(TTFTB) MOF showing the helical stack of TTF groups with a highlight of the shortest intermolecular S···S contact. Reprinted with permission from ref 74. Copyright 2012 American Chemical Society.

Crystallographically as displayed in Figure 3.6, the extended metal-carboxylate chains are built from two free zinc atoms each of which shows two cases. One is a pseudo-octahedral coordination sphere of six oxygen atoms connected to carboxylates and another, four carboxylates and two *cis*-oriented water molecules. The TTF cores are not perpendicular twist axes; however, a close intermolecular S–S contact (3.80 Å) is found between the neighboring TTF groups.[122] The novelty in this work is to showcase a porous molecular framework with a good charge mobility and conductivity. Despite the fascinating redox activity of this MOF, the key issue as to how charge is allowed to propagate through the crystal lattice remains to be further understood. Likely, the charge mobility can be accounted for by several mechanisms, including through-bond and through-space charge/electron transfer.[120] Nonetheless, prior to this fundamental question being fully addressed, more redox-active MOFs need to be synthesized and characterized. Akin to TTF, many TTFV derivatives show rich electron-donating properties and hence have found application in preparation of redox-

active molecular systems (see the literature review described in Chapter 1). The key objective of the work included in this chapter is to continue the research on the applicability of TTFV-based ligands in making porous redox-active nanomaterials.

3.2 Previous efforts towards TTFV-based MOFs

Previous studies by a former group member, Yunfei Wang, established the synthetic access to a class of carboxyl-substituted arene-DTFs and related TTFV derivatives.[123] Scheme 3.1 shows the detailed synthetic steps. With these compounds in hand, Yunfei Wang investigated their potential in preparing microporous coordination polymers through complexation with zinc(II) ions (see Scheme 3.2). The Zn-TTFV complexation was achieved by using an amine diffusion method to give a yellow solid product. Spectroscopic and XRD analyses on the Zn-TTFV coordination product suggested undesirable crystallinity and micromorphology. Formation of ZnO as byproduct during the synthesis of Zn-TTFV complex was found, indicating that the diffusion method using triethylamine as base is not suitable for the formation of well-defined coordination polymers or even MOFs. Other methods for complexing carboxylic TTFV with metal ions should thus be investigated.

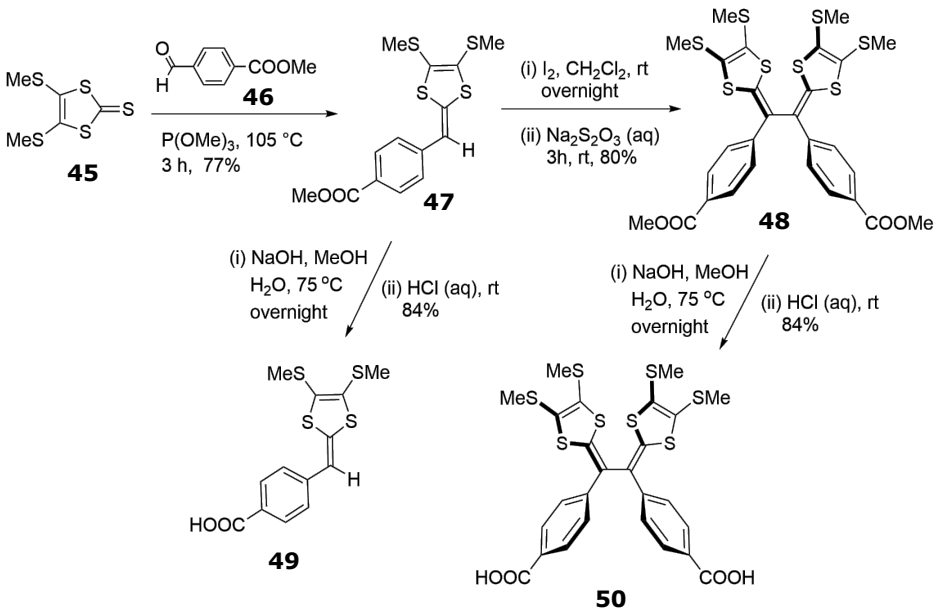

Scheme 3.1: Previous synthesis of carboxylated substituted TTFV and DTF by Yunfei Wang.

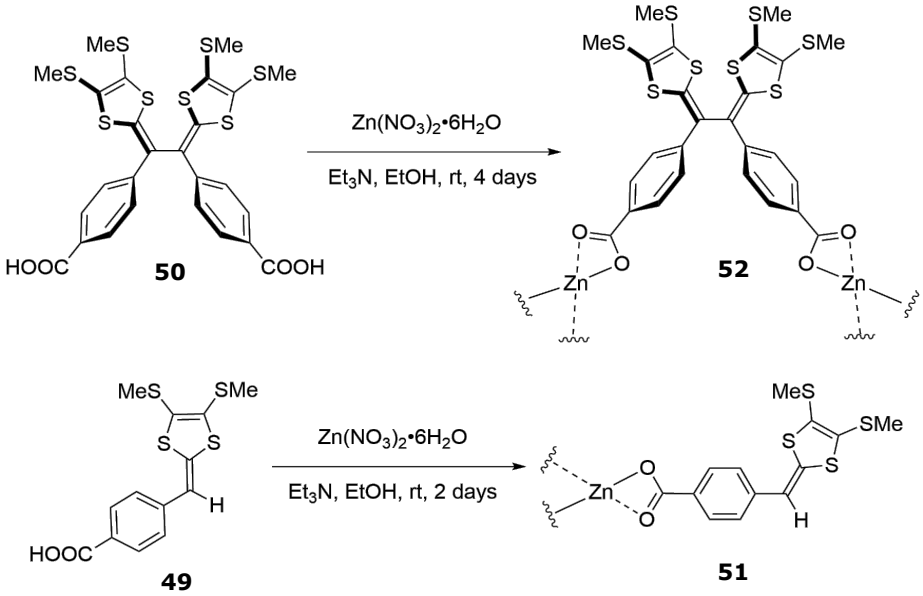

Scheme 3.2: Preparation of coordination products using carboxyl TTFV **50** and carboxyl DTF **49** as ligands.

3.3 Results and Discussion

3.3.1 Attempted Synthesis of TTFV-Based MOFs

The need for more efforts to continue the study of TTFV-based MOFs initiated by Yunfei Wang was the main objective of the work described in this chapter. As discussed above, the search for more effective reaction conditions for forming TTFV-based coordination polymers with excellent crystallinity, porosity and redox activity, at the outset of this study, remained a highly challenging topic given the fact that there had been few successful reports on the design of redox-active MOFs using TTF-based ligands.

In the previous studies done by Yunfei Wang, two major issues were identified to exert somehow "negative impact" on the formation of MOFs. First, the carboxylic-TTFV takes a twisted, pseudo-*cis* conformation according to density functional theory (DTF) calculations.[123] Such a conformation has not proven conducive to forming periodic, extended frameworks upon complexation with metal ions. Second, the low oxidation potential of TTFV as a result of its excellent electron-donating nature makes redox reactions to be effective contenders for the desired metal-ligand complexation. With these in mind, the carboxylated TTFVs utilized in the work of Chapter 2 were given favorable consideration as a new generation of TTFV-based ligands. The rationalization for this choice can be particularly substantiated by the fact that the two carboxyl groups on the phenyl group enhance the electron-withdrawing effect, as a result the conformation of TTFV changes into a nearly planar, *trans*-like geometry, which is deemed as being beneficial for the formation of more extended MOF structures. Furthermore, the reduced electron-donating properties would make it less prone to redox reactions with certain metal ions. The following sections report the experimental efforts to form coordination polymers with three different types of metal ions

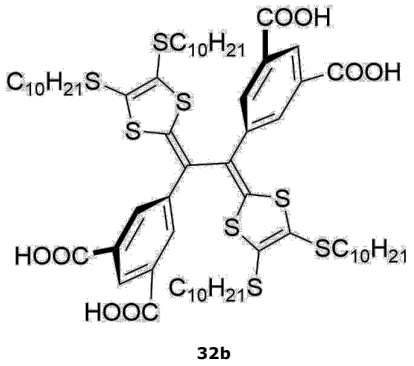

Figure 3.7: carboxyl-substituted TTFV

(i.e., Mg, Zr, and Cu) using tretrakiscarboxylic-TTFV **32b** as a redox-active ligand (Figure 3.7) .

3.3.2 Attempted Synthesis of Mg-TTFV MOFs

The use of small hard main group metals such as Mg^{2+} in MOF synthesis has been reported to form air and water stable MOF materials. One interesting aspect of Mg based materials lies in that they are cheap, light-weight, and can be easily prepared as highly porous materials.[124] In 2015, Huang and co-workers reported the construction of Mg-MOF using a pyrene-based ligand H_8L containing eight carboxylic groups (Scheme 3.3). The pyrene-cored ligand imparts the resulting MOFs with strong fluorescent properties, leading to a type of intriguing luminescent MOFs.[125] Herein, the first attempt to prepare TTFV-based redox-activie MOFs was aimed at using Mg^{2+} as the metal center, considering the good ability of Mg to complex with the carboxylic group as well as its non-oxidative nature.

The procedure reported by Huang[125] was adopted in this experimental work. A mixture of the ligand carboxyl-TTFV (5.0 mg) and $Mg(NO_3)_2$ (20.0 mg, 0.135 mmol) in DMF (3 ml) and H_2O (0.5 mL) were combined in a 10 mL glass vial, which was tightly sealed and heated in an oil bath at 85 °C for 3 days. The precipitate formed,

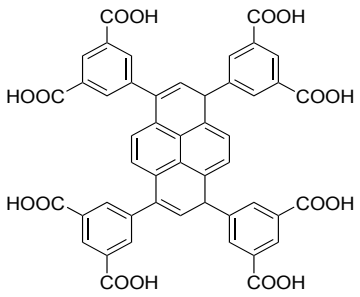

53

Scheme 3.3: Structure of H_8L

after the vial was cooled to room temperature, was collected by filtration to give a yellow solid which was completely insoluble in common organic solvents. Its solid-state structure was proven to be amorphous rather than crystalline by XRD analysis (see Figure 3.8). IR spectral analysis shows that the O–H vibrational band disappears and the C=O stretching mode shifts to a higher frequency after the reaction (Figure 3.9). It is likely that complexation of the carboxyl group with Mg happened, but it only resulted in the formation of small complexes rather than framework-like coordination polymers.

To further enhance the complexation, more forcing reactions conditions were then applied. The experimental procedure was similar to the above-mentioned approach, except that an oven was used instead of the oil bath to heat the reaction to a much higher temperature at 120 °C. Surprisingly, after 1 day of heating, transparent single crystals were formed and collected. Single crystal X-ray analysis was conducted to show that an unexpected crystal structure was successfully grown under these conditions. Instead of the expected TTFV-Mg complexation, the crystal gives an empirical formula of α-$[Mg_3(O_2CH)_6][DMF]$) and its structure is taking a three dimensional topology by edge-shared MgO_6 which is octahedrally coordinated by corner-sharing octahedral. The diffraction data was found to be identical to the MOF structure recently reported by Spanopoulos and co-workers (see Figure 3.10),[126] and further

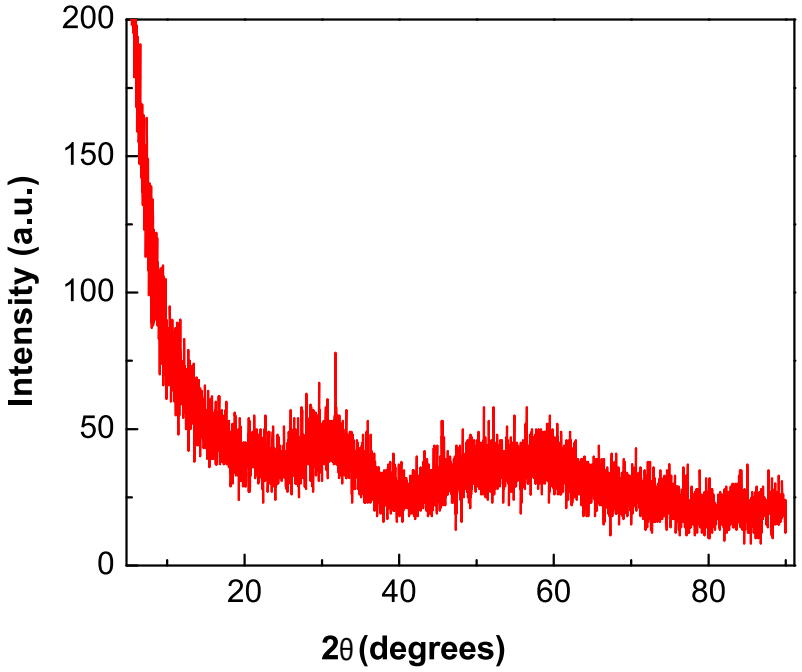

Figure 3.8: Powder XRD data for the solid complex resulting from heating **32b** and $Mg(NO_3)_2$ at 85 °C for 3 days in a sealed glass vial.

efforts to refine the single crystal data were hence abandoned. The failed inclusion of TTFV ligand into the MOF structures suggests that the solvent DMF is a more competitive ligand than the carboxylic-TTFV for Mg^{2+} ion, which makes the objective of constructing TTFV-MOF a truly challenging task. It is however worth noting that the growth of the Mg-DMF MOF crystals appeared to occur at a much faster rate than the reported method under the above conditions, since in the report of Spanopoulos the MOF growth took at least a few days to accomplish. It was noticed that the solvent DMF was lost by 20–30% after the sealed vial was heated for one day, as a result of the not-so-good sealing of the regular glass vial. The gradual solvent loss is attributed to the much faster MOF synthesis and should be favorably considered as a new strategy in the preparation other MOF structures.

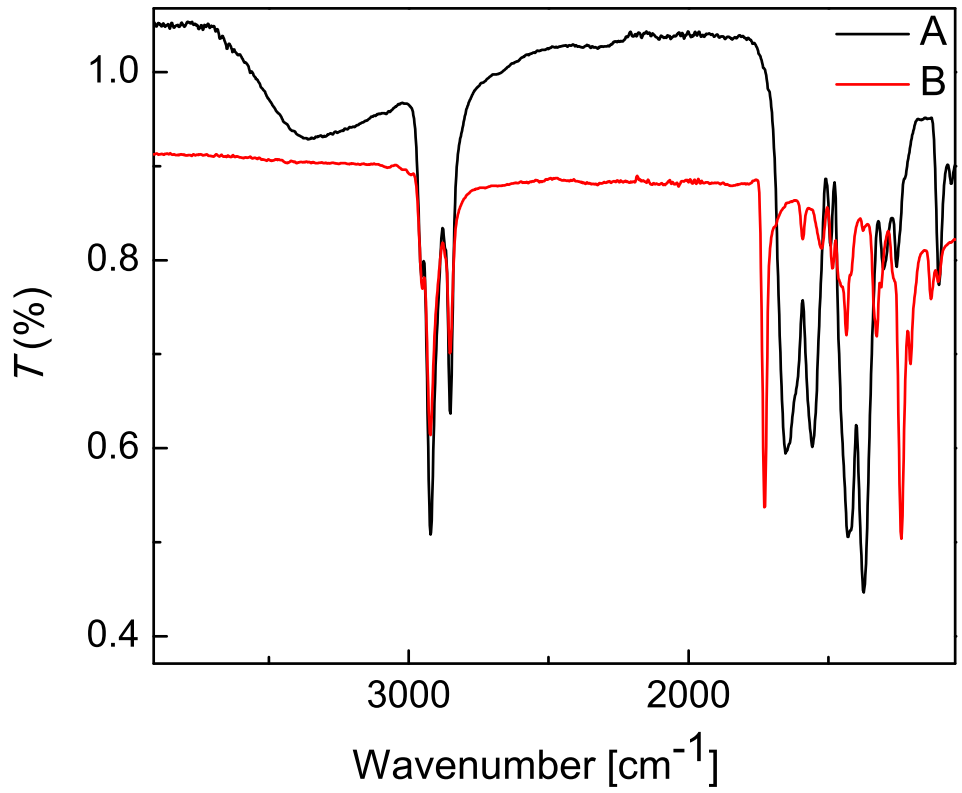

Figure 3.9: FTIR spectra of (A) carboxyl-TTFV **32b**, and (B) Mg-TTFV complexes resulting from heating **32b** and $Mg(NO_3)_2$ at 85 °C for 3 days in a sealed glass vial.

3.3.3 Attempted Synthesis of Zr-TTFV MOFs

The unsuccessful results of using Mg-TTFV complexation to form MOFs then shifted the research attention to the use of other metal ions which are more selective for binding with carboxylic groups rather than being interfered with by the solvent molecules. In this vein, zirconium ion was targeted and the following outlines the efforts and results in this respect.

It has been learned from recent literature that Zr can be used to produce MOFs with high thermal and chemical stabilities compared with other metal ions, due to the well known strong bonding between the carboxyl and high valent Zr.[127] Again,

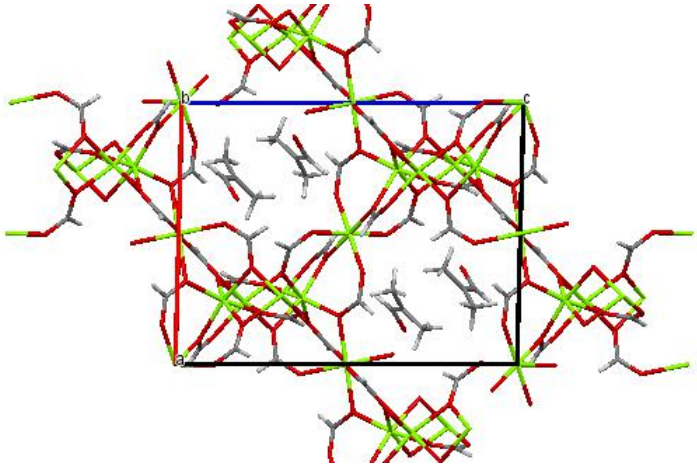

Figure 3.10: X-ray structure of α-[$Mg_3(O_2CH)_6$][DMF]) with an extended unit cell. Reproduced from reference 78 with permission from The Royal Society of Chemistry.

the standard procedure of MOF synthesis was adopted here: compound **32b** (5.0 mg) was mixed with di(cyclopentadienyl) zirconium (IV) dichloride (20.0 mg, 0.135 mmol) in DMF (3 mL). Realizing the leaking problems of the regular glass vial, a better-sealed hydrothermal autoclave reactor (Figure 3.11) was procured and utilized. The reactor has a Teflon chamber embedded in a stainless steel vessel to tolerate high temperature and pressure conditions. The reactor, after being loaded with the reactants and solvent, was placed in an oven at 120 °C for 4 days and then slowly cooled down to room temperature. Some noncrystalline black-colored precipitate was observed and then collected by filtration and rinsing multiple times with DMF and ethanol. Unfortunately, the resulting solid material was found to be amorphous but not the desired crystalline MOFs based on powder XRD analysis. The exact details for the reactions involved remain unknown at the moment due to the difficulty in characterizing the black solid. Nevertheless, the black color of the solid hints that some Zr-catalyzed reactions might take place, leading to either decomposition (e.g., desulfurization) or polymerization products.

Figure 3.11: Photograhic image of the hydrothermal autoclave reactor used in the attempted synthesis of Zr-TTFV MOFs.

3.3.4 Attempted Synthesis of Cu-TTFV MOFs

With efforts on making TTFV-based MOFs unsuccessful using both Mg^{2+} and Zr^{2+} ions, another round of exploration was launched focusing on the use of Cu^{2+} ion, on consideration that a large number of Cu-based MOFs has been successfully synthesized in the literature via the interactions of aromatic carboxylates with Cu^{2+}. It has also been well known that Cu^{2+} can coordinate with various ligands to form MOFs with highly tunable topology, porosity, and stability.[128] Under solvothermal reaction conditions similar to those used in the aforementioned synthetic work, $Cu(NO_3)_2$ was tried to complex with carboxyl-TTFV ligand **32b** in DMSO and a Teflon reactor encased in a stainless steel vessel was used to carry out the reactions. After heating the reaction mixture for 3 days at 120 °C, some non-crystalline brown precipitate was collected from the reactor by filtration and rinsed with DMSO. Once again the resulting solids were subjected to IR analysis to show evidence for carboxyl group being with the Cu^{2+} ion, which is similar to the case of the previous Mg complexation study (see Figure 3.9). However, PXRD analysis does not offer any evidence for the

samples being crystalline, which rules out the possibility of MOF formation. At this juncture, the detailed molecular structures of the resulting brown-colored solids still remain unknown.

3.3.5 Conclusions

In summary, carboxyl-TTFV **32b** has been investigated as a ligand to coordinate with three different divalent metal ions, Mg^{2+}, Zr^{2+}, and Cu^{2+}, in an attempt to form redox-active coordination polymers or MOFs. So far, the synthesis of redox-active framework-like porous materials using TTFV-based ligands has not yet been successful, and it is predicted to be a very challenging task which will require much work to be done on understanding the fundamental complexation properties of carboxylic TTFVs with various metal ions. The current studies, however, allow us to establish the following conclusions which should be of useful guidance to future work in this direction.

- The excellent electron-donating properties of TTFV (i.e., low oxidation potential) makes the TTFV ligand more susceptible to redox reaction if the metal ion used has sufficient oxidative power. This actually poses a great challenge to the desired carboxyl-metal complexation. Therefore, the future work should focus on how to balance the redox-activity to make the ligand more selective for metal complexation.

- The sulfur atoms in the TTFV unit are conceivably ligand sites for binding with metal ions. This aspect has not yet been systematically investigated, but should warrant more attention of research in the future.

- The non-planar molecular shape of the TTFV ligand as well as the long alkyl chains attached to the dithiole groups are predicted to have some negative effects

on the formation of crystalline, extended coordination polymers or MOFs. More regularly shaped and rigid TTFV ligands need to be designed and investigated in the future.

- The synthetic methods utilized in this work are mainly based on hydrothermal conditions. The tolerance of TTFV ligands to various solvents, pressure, and temperature need to thoroughly tested in future work.

- Finally, the construction of redox-active porous molecular frameworks based TTFV ligands can also be tackled through an alternative approach–covalent organic frameworks (well known as COFs)–if the metal complexation has been proven indeed an unconquerable problem for the TTFV ligands. The current results in combination with the previous work by Yunfei Wang overall have cast some light into the new intriguing class of redox-active MOFs, and it is forecast that the potential application of these novel porous materials should have a very promising future if efficient and cost-effective synthetic methodologies can be established. To this end, more efforts on the design and synthesis of TTFV-based ligands will be carried out in our future work.

3.3.6 Experimental Procedures

Chemicals were purchased from commercial suppliers and used directly without purification. The ligand **2b** was synthesized according to a previous reported synthesis in the second chapter. The 25 ml Teflon lined hydrothermal synthesis laboratory reactor was heated in an oven with temperature control. Powder X-ray diffraction (PXRD) analysis was done on a Rigaku Ultima IV x-ray diffractometer with a copper X-ray source at wavelength of 1.54 nm was used to collect the data.

Mg-TTFV 32b: A mixture of the ligand carboxyl-TTFV (0.1 g, 0.08 mmol) and $Mg(NO_3)_2$ 0.2 g in DMF (3 ml) and H_2O (0.5 ml) were combined in 10 ml glass vial ,sealed and heated in oil bath a 85°C and lifted to stand for 3 days. The precipitate formed in the vial was cooled to room temperature and washed then collected by filtration to give (43.2 mg)yellow solid product. Due to the leaking issue of the vial, the mixture was placed in a Teflon container which is sealed and kept under pressure in an oven at 120°C for one day. The brown crystals formed in the Teflon container were collected by filtration and rinsed with DMF and air dried (80.3 mg).

Zn-TTFV 32b: A solution of 5 mL of DMF , Di (cyclopentadienyl) zirconium (IV) dichloride (0.07 g, 0.23 mmol) and (0.02g, 0.16 mmol) of the ligand **32b** were combined into the hydrtherm reactor and placed in the oven at 120°C for 4 days. During this period, black precipitate was produced and then rinsed with EtOH and DMF to give (50.3 mg) black solid product.

Cu-TTFV 32b: A solution of **32b** (0.12 g, 0.09 mmol) and $Cu(NO_3)_2$ (0.41 g, 5.29 mmol) in DMSO (3 mL) was added into a Teflon container, which was sealed and left standing in oven for 3 days at 120 °C. The brown precipitate formed and collected by filtration and rinsed with DMSO to afford (40 mg) as brown solid product.

Chapter 4

Conclusions and Future Work

In this MSc thesis, a new group of carboxylated DTF and TTFV derivatives has been synthesized and investigated as redox-active $\pi-$donors and molecular building blocks. The first project (Chapter 2) demonstrates the synthesis details and characterization of these new compounds. The electronic and electrochemical properties of carboxylated DTF and TTFV are similar to those found in related DTF and TTFV derivatives. These compounds can be used as reducing agents to convert $HAuCl_4$ into Au(I) and/or AuNPs in four organic solvents, DMSO, DMF, CH_3CN and THF. Compared with TTFV, DTF has been found to be more effective at reducing $HAuCl_4$ into narrowly distributed AuNP in dipolar aprotic solvents, DMSO and DMF. The capping effects of oxidized DTFs on the surface of AuNPs via S—Au interactions are the main reason for the high stability of DTF-induced AuNPs. On the other hand, the carboxyl groups are believed to play a significant role as well. Spherical AuNPs are produced through the DTF reduction of $HAuCl_4$ with an average diameter around 32 nm. In addition, the presence of the carboxylic groups in the DTF capping agents allows the formation of large assemblies of AuNPs in solution presumably through H-bonding forces, and these assemblies can be readily dissociated into smaller individual

AuNPs by ultrasonication.

Apart from the discovery of AuNP formation, another important result found during the work of Chapter 2 is the experimental proof of Au(III)-promoted DTF dimerization in organic media, convincingly evidenced by X-ray single crystal analysis. In the literature, this aspect has been long neglected. Therefore, this thesis work does contribute critically to unravelling the mechanisms for the redox interactions of Au(III) with DTF and TTFV-based organic donors. At the physical organic chemistry level, the crystallographic studies of carboxylic ester-substituted DTF and TTFV compounds have provided an in-depth insight into the substituent effects on the ground-state conformation of these molecules. It is particularly interesting to see that the carboxylated DTF and TTFV structures investigated in this work show dramatically different conformations than other previously reported DTF and TTFV analogues. Understanding of these effects is useful for further rational design of DTF and TTFV molecular building blocks for advanced macromolecular and supramolecular structures.

In the second project (Chapter 3), the potential of carboxyl-substituted arene-DTFs and related TTFV derivatives in acting as redox-active ligands for microporous coordination polymers has been investigated. This project is the continuation of the MSc work of a former group member, Yunfei Wang. In his study, only one transition metal ion, Zn(II), was studied and the formation of coordination with carboxylic DTF and TTFV compounds was tested using the diffusion methodology with triethylamine as base. In this thesis work, three different metal ions, Mg(II), Zr(II), and Cu(II), were investigated in order to form meaningful coordination polymers or MOFs. Hydrothermal reactions were utilized in this work instead of the base diffusion method. So far, the synthetic efforts under various conditions have not yet met any succcess. Based on the data collected, it is believed that carboxylic DTF and TTFV derivatives

are not efficient ligand for metal coordination, due to many possible side reactions (e.g., redox reactions). On the other hand, a serendipitous discovery was made in the effort of making Mg(II)-based MOFs. The solvent DMF was found to complex with Mg(II) to give crystalline MOFs. Although a similar result was reported by the Spanopoulos group in 2015, the finding in this work shows that the growth time of Mg-DMF MOFs can be considerably shortened from 3 days to overnight by slow solvent leaking. This finding may be a useful strategy for MOF synthesis in future work.

Finally, on the basis of the current studies, a number of future directions can be envisioned as follows. (1) The synthesis of other noble metal particles (e.g., Ag, Pt) using DTF and TTFV derivatives as reductants and stabilizing ligands. (2) Application of the synthesized AuNPs in photocatalysis, electrocatalysis, and chemical sensing. (3) Synthesis of redox-active covalent organic frameworks (COFs) using TTFV as the active building component. (4) Metal surface adsorption and modification using the carboxylic DTF and TTFV derivatives. Again, for all these future studies, the development of efficient synthetic methods and fundamental understanding on structure-property relationships is a critical step and these should be continued as well.

Bibliography

[1] Batsanov, A. S. *Acta Cryst. C.* **2006**, *62*, o501–o504.

[2] Wudl, F.; Smith, G. M.; Hufnagel, E. J. *J. Chem. Soc. D.* **1970**, 1453–1454.

[3] Coffen, D. L.; Chambers, J. Q.; Williams, D. R.; Garrett, P. E.; Canfield, N. D. *J. Am. Chem. Soc.* **1971**, *93*, 2258–2268.

[4] Hünig, S. *Angew. Chem. Int. Ed. Engl.* **1969**, *8*, 286–286.

[5] Ferraris, J.; Cowan, D. O.; Walatka, V.; Perlstein, J. H. *J. Am. Chem. Soc.* **1973**, *95*, 948–949.

[6] Bendikov*, M.; ; Wudl*, F.; Perepichka*, D. F. *Chem. Rev.* **2004**, *104*, 4891–4946, PMID: 15535637.

[7] VandeVondele, J.; Lynden-Bell, R.; Meijer, E. J.; Sprik, M. *J. Phys. Chem. B.* **2006**, *110*, 3614–3623.

[8] Wang, Y.; Urban, C.; Rodríguez-Fernández, J.; Gallego, J. M.; Otero, R.; Martín, N.; Miranda, R.; Alcamí, M.; Martín, F. *J. Phys. Chem. A.* **2011**, *115*, 13080–13087.

[9] Cooper, W. F.; Kenny, N. C.; Edmonds, J. W.; Nagel, A.; Wudl, F.; Coppens, P. *J. Chem. Soc. D.* **1971**, 889–890.

[10] Bozio, R.; Zanon, I.; Girlando, A.; Pecile, C. *J. Chem. Phys.* **1979**, *71*, 2282–2293.

[11] Ellern, A.; Bernstein, J.; Becker, J. Y.; Zamir, S.; Shahal, L.; Cohen, S. *Chem. Mater.* **1994**, *6*, 1378–1385.

[12] Gao, F.; Zhu, F.-F.; Wang, X.-Y.; Xu, Y.; Wang, X.-P.; Zuo, J.-L. *Inorg. Chem.* **2014**, *53*, 5321–5327.

[13] Becher, J.; Jeppesen, J.; Nielsen, K. *Synth. Met.* **2003**, *133*, 309–315.

[14] Wang, C.; Dyar, S. M.; Cao, D.; Fahrenbach, A. C.; Horwitz, N.; Colvin, M. T.; Carmieli, R.; Stern, C. L.; Dey, S. K.; Wasielewski, M. R.; Stoddart, J. F. *J. Am. Chem. Soc.* **2012**, *134*, 19136–19145, PMID: 23140138.

[15] Frere, P.; Skabara, P. J. *Chem. Soc. Rev.* **2005**, *34*, 69–98.

[16] Zhao, Y.; Chen, G.; Mulla, K.; Mahmud, I.; Liang, S.; Dongare, P.; Thompson, D. W.; Dawe, L. N.; Bouzan, S. *Pure Appl. Chem.* **2012**, *84*, 1005–1025.

[17] Frère, P.; Skabara, P. J. *Chem. Soc. Rev.* **2005**, *34*, 69–98.

[18] Bendikov, M.; Wudl, F.; Perepichka, D. F. *Chem. Rev.* **2004**, *104*, 4891–4946.

[19] Moore, A. J.; Bryce, M. R. *Tetrahedron Lett.* **1992**, *33*, 1373–1376.

[20] Takahashi, K.; Nihira, T. *Tetrahedron Lett.* **1989**, *30*, 5903–5906.

[21] Khanous, A.; Gorgues, A.; Jubault, M. *Tetrahedron Lett.* **1990**, *31*, 7311–7314.

[22] Nielsen, M. B.; Sauer, S. P. *Chem. Phys. Lett.* **2008**, *453*, 136–139.

[23] Carlier, R.; Hapiot, P.; Lorcy, D.; Robert, A.; Tallec, A. *Electrochim. Acta.* **2001**, *46*, 3269–3277.

[24] Gontier, E.; Bellec, N.; Brignou, P.; Gohier, A.; Guerro, M.; Roisnel, T.; Lorcy, D. *Org. Lett.* **2010**, *12*, 2386–2389.

[25] Guerro, M.; Pham, N. H.; Massue, J.; Bellec, N.; Lorcy, D. *Tetrahedron.* **2008**, *64*, 5285–5290.

[26] Mulla, K.; Zhao, Y. *Tetrahedron Lett.* **2014**, *55*, 382–386.

[27] Lorcy, D.; Guerro, M.; Bergamini, J.-F.; Hapiot, P. *J. Phys. Chem. B.* **2013**, *117*, 5188–5194.

[28] Mulla, K.; Dongare, P.; Thompson, D. W.; Zhao, Y. *Org. Biomol. Chem.* **2012**, *10*, 2542–2544.

[29] Mulla, K.; Shaik, H.; Thompson, D. W.; Zhao, Y. *Org. Lett.* **2013**, *15*, 4532–4535.

[30] Liang, S.; Zhao, Y.; Adronov, A. *J. Am. Chem. Soc.* **2014**, *136*, 970–977.

[31] Chen, G.; Mahmud, I.; Dawe, L. N.; Zhao, Y. *Org. Lett.* **2010**, *12*, 704–707.

[32] Ripaud, E.; Leriche, P.; Cocherel, N.; Cauchy, T.; Frère, P.; Roncali, J. *Org. Biomol. Chem.* **2011**, *9*, 1034–1040.

[33] Khadem, M.; Walsh, J. C.; Bodwell, G. J.; Zhao, Y. *Org. Lett.* **2016**, *18*, 2403–2406.

[34] Chen, G.; Mahmud, I.; Dawe, L. N.; Daniels, L. M.; Zhao, Y. *J. Org. Chem.* **2011**, *76*, 2701–2715.

[35] Kubo, Y.; Sugasaki, A.; Ikeda, M.; Sugiyasu, K.; Sonoda, K.; Ikeda, A.; Takeuchi, M.; Shinkai, S. *Org. Lett.* **2002**, *4*, 925–928.

[36] Park, S.; Vosguerichian, M.; Bao, Z. *Nanoscale.* **2013**, *5*, 1727–1752.

[37] Sgobba, V.; Guldi, D. M. *Chem. Soc. Rev.* **2009**, *38*, 165–184.

[38] Avouris, P.; Freitag, M.; Perebeinos, V. *Nat. Photon.* **2008**, *2*, 341–350.

[39] Liu, X.; Wang, M.; Zhang, S.; Pan, B. *J.Environ.Sci.* **2013**, *25*, 1263–1280.

[40] Heister, E.; Brunner, E. W.; Dieckmann, G. R.; Jurewicz, I.; Dalton, A. B. *ACS Appl. Mater. Interfaces.* **2013**, *5*, 1870–1891.

[41] Prato, M.; Kostarelos, K.; Bianco, A. *Acc. Chem. Res.* **2007**, *41*, 60–68.

[42] Khadem, M.; Zhao, Y. *J. Org. Chem.* **2015**, *80*, 7419–7429.

[43] Chen, G.; Zhao, Y. *Org. Lett.* **2014**, *16*, 668–671.

[44] Steimecke, G.; Sieler, H.-J.; Kirmse, R.; Hoyer, E. *Phosphorus Sulfur Silicon Relat. Elem.* **1979**, *7*, 49–55.

[45] Parg, R. P.; Kilburn, J. D.; Ryan, T. G. *Synthesis.* **1994**, *1994*, 195–198.

[46] Schou, S. S.; Parker, C. R.; Lincke, K.; Jennum, K.; Vibenholt, J.; Kadziola, A.; Nielsen, M. B. *Synlett.* **2013**, *24*, 231–235.

[47] Christensen, C. A.; Batsanov, A. S.; Bryce, M. R. *J. Org. Chem.* **2007**, *72*, 1301–1308.

[48] Daniel, M.-C.; Astruc, D. *Chem. Rev.* **2004**, *104*, 293–346.

[49] Saha, K.; Agasti, S. S.; Kim, C.; Li, X.; Rotello, V. M. *Chem. Rev.* **2012**, *112*, 2739–2779.

[50] Wagner, F. E.; Haslbeck, S.; Stievano, L.; Calogero, S.; Pankhurst, Q.; Martinek, K.-P. *Nature.* **2000**, *407*, 691–692.

[51] Perrault, S. D.; Chan, W. C. *J. Am. Chem. Soc.* **2009**, *131*, 17042–17043.

[52] Yu, Y.-Y.; Chang, S.-S.; Lee, C.-L.; Wang, C. C. *J. Phys. Chem. B.* **1997**, *101*, 6661–6664.

[53] Braun, G. B.; Pallaoro, A.; Wu, G.; Missirlis, D.; Zasadzinski, J. A.; Tirrell, M.; Reich, N. O. *Acs Nano.* **2009**, *3*, 2007–2015.

[54] Xia, Y.; Li, W.; Cobley, C. M.; Chen, J.; Xia, X.; Zhang, Q.; Yang, M.; Cho, E. C.; Brown, P. K. *Acc. Chem. Res.* **2011**, *44*, 914–924.

[55] Huang, X.; El-Sayed, M. A. *J.Adv.Res.* **2010**, *1*, 13–28.

[56] Eustis, S.; El-Sayed, M. A. *Chem. Soc. Rev.* **2006**, *35*, 209–217.

[57] Faraday, M. *Philos. Trans. R. Soc. London.* **1857**, *147*, 145–181.

[58] Turkevich, J.; Stevenson, P. C.; Hillier, J. *Discuss Faraday Soc.* **1951**, *11*, 55–75.

[59] Brust, M.; Walker, M.; Bethell, D.; Schiffrin, D. J.; Whyman, R. *J. Chem. Soc., Chem. Commun.* **1994**, 801–802.

[60] Uehara, A.; Booth, S. G.; Chang, S. Y.; Schroeder, S. L.; Imai, T.; Hashimoto, T.; Mosselmans, J. F. W.; Dryfe, R. A. *J. Am. Chem. Soc.* **2015**, *137*, 15135–15144.

[61] Perala, S. R. K.; Kumar, S. *Langmuir.* **2013**, *29*, 9863–9873.

[62] Shon, Y.-S.; Mazzitelli, C.; Murray, R. W. *Langmuir.* **2001**, *17*, 7735–7741.

[63] Chen, S.; Templeton, A. C.; Murray, R. W. *Langmuir.* **2000**, *16*, 3543–3548.

[64] Daniel, M.-C.; Astruc, D. *Chem. Rev.* **2004**, *104*, 293–346, PMID: 14719978.

[65] Saha, K.; Agasti, S. S.; Kim, C.; Li, X.; Rotello, V. M. *Chem. Rev.* **2012**, *112*, 2739–2779.

[66] Stratakis, M.; Garcia, H. *Chem. Rev.* **2012**, *112*, 4469–4506.

[67] Zhou, W.; Gao, X.; Liu, D.; Chen, X. *Chem. Rev.* **2015**, *115*, 10575–10636.

[68] Frens, G. *Nature.* **1973**, *241*, 20–22.

[69] Turkevich, J.; Stevenson, P. C.; Hillier, J. *Discuss. Faraday Soc.* **1951**, *11*, 55–75.

[70] Kimling, J.; Maier, M.; Okenve, B.; Kotaidis, V.; Ballot, H.; Plech, A. *J. Phys. Chem. B.* **2006**, *110*, 15700–15707.

[71] Male, K. B.; Li, J.; Bun, C. C.; Ng, S.-C.; Luong, J. H. *J. Phys. Chem. C.* **2008**, *112*, 443–451.

[72] Deraedt, C.; Salmon, L.; Gatard, S.; Ciganda, R.; Hernandez, R.; Ruiz, J.; Astruc, D. *Chem. Commun.* **2014**, *50*, 14194–14196.

[73] Watson, K. J.; Zhu, J.; Nguyen, S. T.; Mirkin, C. A. *J. Am. Chem. Soc.* **1999**, *121*, 462–463.

[74] Leiva, A.; Fuentes, I.; Bossel, E.; Urzúa, M.; Méndez, M.; Pino, M.; Radić, D.; Márquez, V.; González-Nilo, F. *J. Polym. Sci. A Polym. Chem.* **2014**, *52*, 3069–3079.

[75] Sakai, T.; Alexandridis, P. *J. Phys. Chem. B.* **2005**, *109*, 7766–7777.

[76] Ray, D.; Aswal, V. K.; Kohlbrecher, J. *Langmuir.* **2011**, *27*, 4048–4056.

[77] Brust, M.; Walker, M.; Bethell, D.; Schiffrin, D. J.; Whyman, R. *J. Chem. Soc., Chem. Commun.* **1994**, 801–802.

[78] Goulet, P. J.; Lennox, R. B. *J. Am. Chem. Soc.* **2010**, *132*, 9582–9584.

[79] Uehara, A.; Booth, S. G.; Chang, S. Y.; Schroeder, S. L.; Imai, T.; Hashimoto, T.; Mosselmans, J. F. W.; Dryfe, R. A. *J. Am. Chem. Soc.* **2015**, *137*, 15135–15144.

[80] Zhou, Y.; Itoh, H.; Uemura, T.; Naka, K.; Chujo, Y. *Chem. Commun.* **2001**, 613–614.

[81] Zhou, Y.; Itoh, H.; Uemura, T.; Naka, K.; Chujo, Y. *Langmuir.* **2002**, *18*, 277–283.

[82] Inagi, S.; Naka, K.; Chujo, Y. *J. Mater. Chem.* **2007**, *17*, 4122–4135.

[83] Zhu, M.; Wang, X.; Naka, K.; Zhou, X.; Chujo, Y. *J MACROMOL SCI A.* **2006**, *43*, 1801–1805.

[84] Lanterna, A. E.; Coronado, E. A.; Granados, A. M. *Tetrahedron Lett.* **2015**, *56*, 4871 – 4876.

[85] Lorcy, D.; Carlier, R.; Robert, A.; Tallec, A.; Le Maguerès, P.; Ouahab, L. *J. Org. Chem.* **1995**, *60*, 2443–2447.

[86] Hapiot, P.; Lorcy, D.; Tallec, A.; Carlier, R.; Robert, A. *J. Phys. Chem.* **1996**, *100*, 14823–14827.

[87] Zhao, Y.; Chen, G.; Mulla, K.; Mahmud, I.; Liang, S.; Dongare, P.; Thompson, D. W.; Dawe, L. N.; Bouzan, S. *Pure Appl. Chem.* **2012**, *84*, 1005–1025.

[88] Khadem, M.; Zhao, Y. *J. Org. Chem.* **2015**, *80*, 7419–7429.

[89] Liang, S.; Zhao, Y.; Adronov, A. *J. Am. Chem. Soc.* **2014**, *136*, 970–977.

[90] Zhang, X.; Lu, Z.; Ye, L.; Zhan, C.; Hou, J.; Zhang, S.; Jiang, B.; Zhao, Y.; Huang, J.; Zhang, S. *Adv. Mater.* **2013**, *25*, 5791–5797.

[91] Wang, Y.; Zhao, Y. *Beilstein J. Org. Chem.* **2015**, *11*, 957–965.

[92] Gontier, E.; Bellec, N.; Brignou, P.; Gohier, A.; Guerro, M.; Roisnel, T.; Lorcy, D. *Org. Lett.* **2010**, *12*, 2386–2389.

[93] Khadem, M.; Walsh, J. C.; Bodwell, G. J.; Zhao, Y. *Org. Lett.* **2016**,

[94] Mulla, K.; Shaik, H.; Thompson, D. W.; Zhao, Y. *Org. Lett.* **2013**, *15*, 4532–4535.

[95] Lorcy, D.; Guerro, M.; Bergamini, J.-F.; Hapiot, P. *J. Phys. Chem. B.* **2013**, *117*, 5188–5194.

[96] Mulla, K.; Zhao, Y. *Tetrahedron Lett.* **2014**, *55*, 382–386.

[97] Mulla, K.; Dongare, P.; Thompson, D. W.; Zhao, Y. *Org. Biomol. Chem.* **2012**, *10*, 2542–2544.

[98] Chen, G.; Zhao, Y. *Org. Lett.* **2014**, *16*, 668–671.

[99] Massue, J.; Bellec, N.; Guerro, M.; Bergamini, J.-F.; Hapiot, P.; Lorcy, D. *J. Org. Chem.* **2007**, *72*, 4655–4662.

[100] Woolridge, K.; Goncalves, L. C.; Bouzan, S.; Chen, G.; Zhao, Y. *Tetrahedron Lett.* **2014**, *55*, 6362–6366.

[101] Bouzan, S.; Dawe, L. N.; Zhao, Y. *Tetrahedron Lett.* **2013**, *54*, 4666–4669.

[102] Chen, G.; Mahmud, I.; Dawe, L. N.; Zhao, Y. *Org. Lett.* **2010**, *12*, 704–707.

[103] Chen, G.; Bouzan, S.; Zhao, Y. *Tetrahedron Lett.* **2010**, *51*, 6552–6556.

[104] Kamat, P. V. *J. Phys. Chem. B.* **2002**, *106*, 7729–7744.

[105] Liu, J.; Lu, Y. *Nature Protocols.* **2006**, *1*, 246.

[106] Furukawa, H.; Cordova, K. E.; O'Keeffe, M.; Yaghi, O. M. *Science.* **2013**, *341*, 1230444.

[107] Yaghi, O. M.; Li, G.; Li, H. *Nature.* **1995**, *378*, 703–706.

[108] Cook, T. R.; Zheng, Y.-R.; Stang, P. J. *Chem. Rev.* **2012**, *113*, 734–777.

[109] Li, H.; Eddaoudi, M.; O'Keeffe, M.; Yaghi, O. M. *Nature.* **1999**, *402*, 276–279.

[110] Eddaoudi, M.; Kim, J.; Rosi, N.; Vodak, D.; Wachter, J.; O'Keeffe, M.; Yaghi, O. M. *Science.* **2002**, *295*, 469–472.

[111] Dunbar, K.; Heintz, R. A. *Prog. Inorg. Chem.* **1997**, *45*, 283–392.

[112] Gramaccioli, C. M. *Acta Crystallogr.* **1966**, *21*, 600–605.

[113] Okada, K.; Kay, M.; Cromer, D.; Almodovar, I. *J. Chem. Phys.* **1966**, *44*, 1648–1653.

[114] Jarvis, J. *Acta Crystallogr.* **1962**, *15*, 964–966.

[115] Sterling, C. *Science.* **1964**, *146*, 518–519.

[116] Robl, C. *Mater. Res. Bull.* **1992**, *27*, 99–107.

[117] Weiss, A.; Riegler, E.; Alt, I.; Böhme, H.; Robl, C. *Z. Naturforsch. B Chem. Sci.* **1986**, *41*, 18–24.

[118] Li, M.; Li, D.; O'Keeffe, M.; Yaghi, O. M. *Chem. Rev.* **2013**, *114*, 1343–1370.

[119] Stock, N.; Biswas, S. *Chem. Rev.* **2011**, *112*, 933–969.

[120] D'Alessandro, D. *Chem. Commun.* **2016**,

[121] Park, S. S.; Hontz, E. R.; Sun, L.; Hendon, C. H.; Walsh, A.; Van Voorhis, T.; Dincä, M. *J. Am. Chem. Soc.* **2015**, *137*, 1774–1777.

[122] Narayan, T. C.; Miyakai, T.; Seki, S.; Dincä, M. *J. Am. Chem. Soc.* **2012**, *134*, 12932–12935.

[123] Wang, Y.; Zhao, Y. *Beilstein J. Org. Chem.* **2015**, *11*, 957–965.

[124] Samsonenko, D. G.; Kim, H.; Sun, Y.; Kim, G.-H.; Lee, H.-S.; Kim, K. *Chem. Asian J.* **2007**, *2*, 484–488.

[125] Xie, S.; Wang, H.; Liu, Z.; Dai, R.; Huang, L. *RSC Adv.* **2015**, *5*, 7121–7124.

[126] Spanopoulos, I.; Bratsos, I.; Tampaxis, C.; Kourtellaris, A.; Tasiopoulos, A.; Charalambopoulou, G.; Steriotis, T.; Trikalitis, P. *CrystEngComm.* **2015**, *17*, 532–539.

[127] Van de Voorde, B.; Stassen, I.; Bueken, B.; Vermoortele, F.; De Vos, D.; Ameloot, R.; Tan, J.-C.; Bennett, T. D. *J. Mater. Chem. A.* **2015**, *3*, 1737–1742.

[128] Yan, Y.; Yang, S.; Blake, A. J.; Schröder, M. *Acc. Chem. Res.* **2013**, *47*, 296–307.

Appendix: NMR Spectra of New Compounds and SEM Images

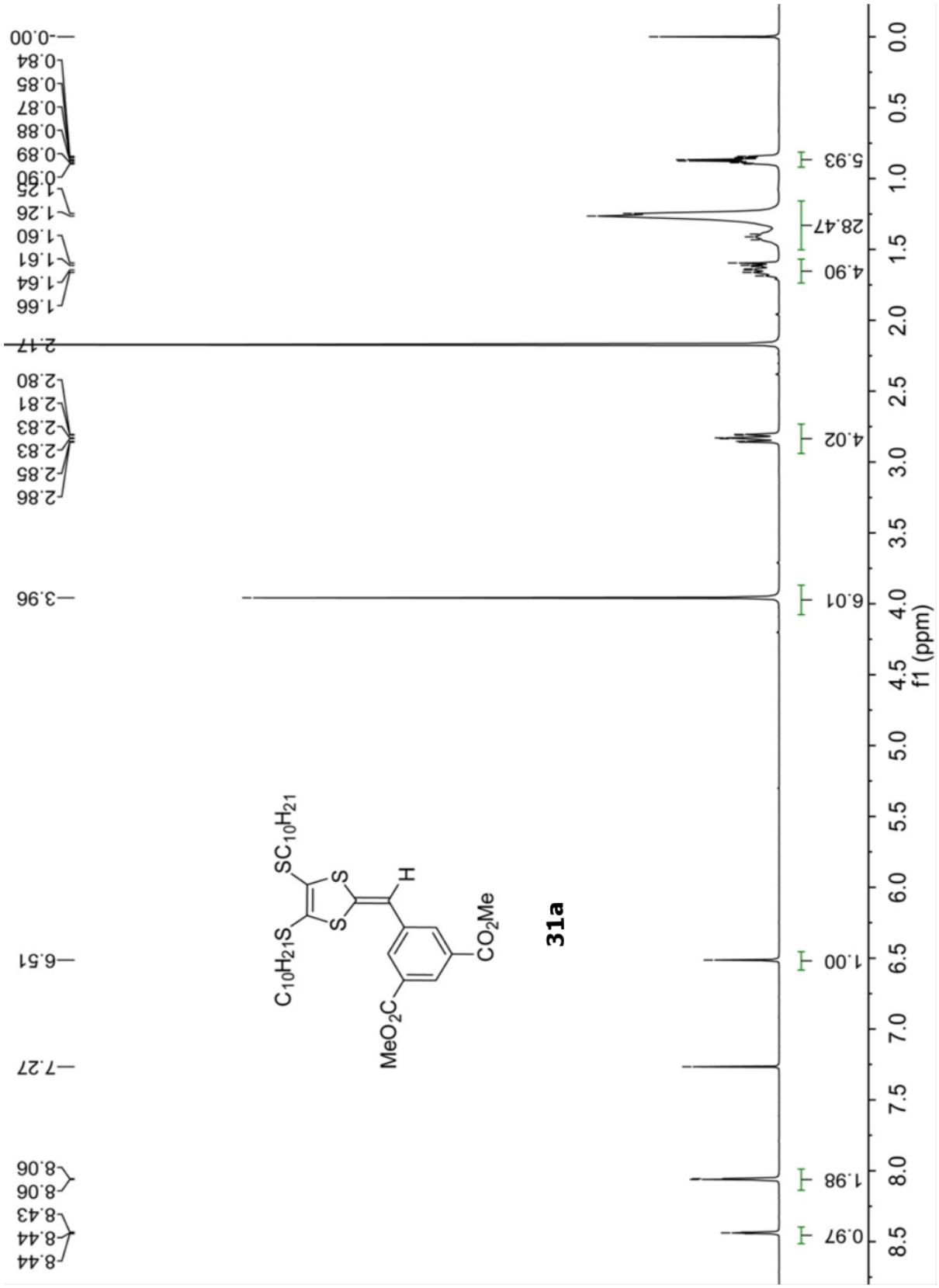

Fig. S-1 ^{1}H NMR (300 MHz, $CDCl_3$) of compound **31a**.

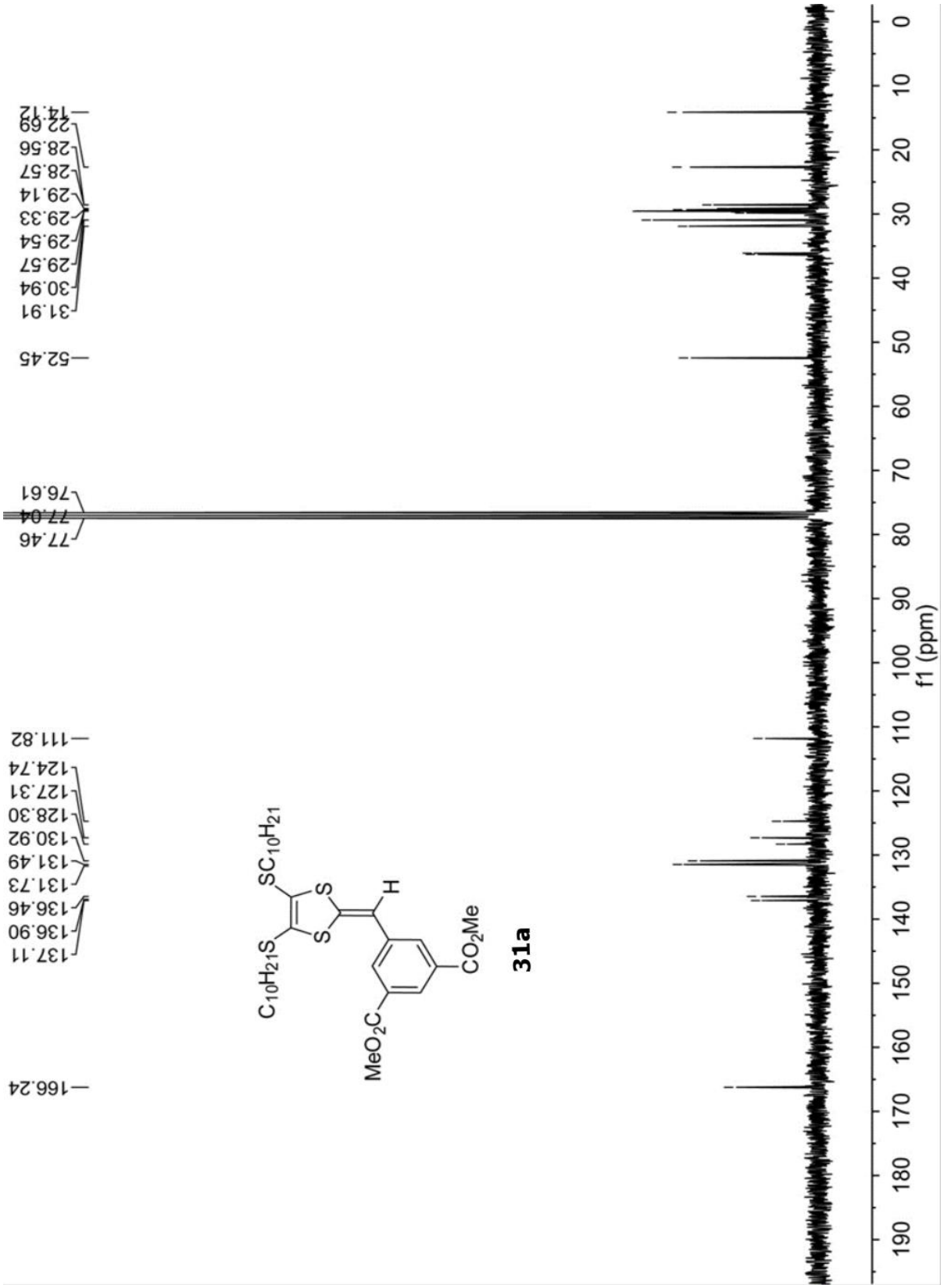

Fig. S-2 ^{13}C NMR (75 MHz, $CDCl_3$) of compound **31a**.

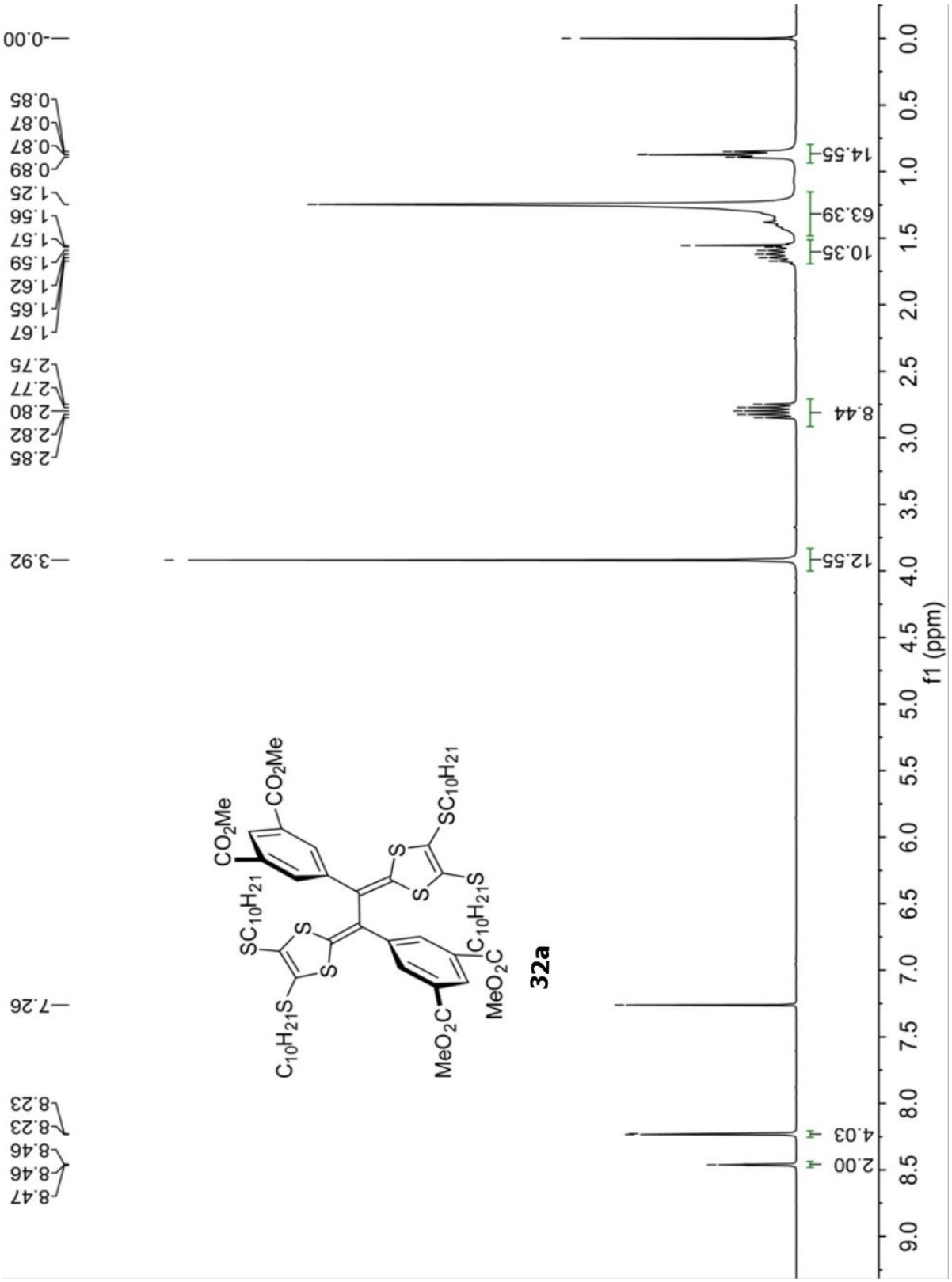

Fig. S-3 ^{1}H NMR (300 MHz, $CDCl_3$) of compound **32a**

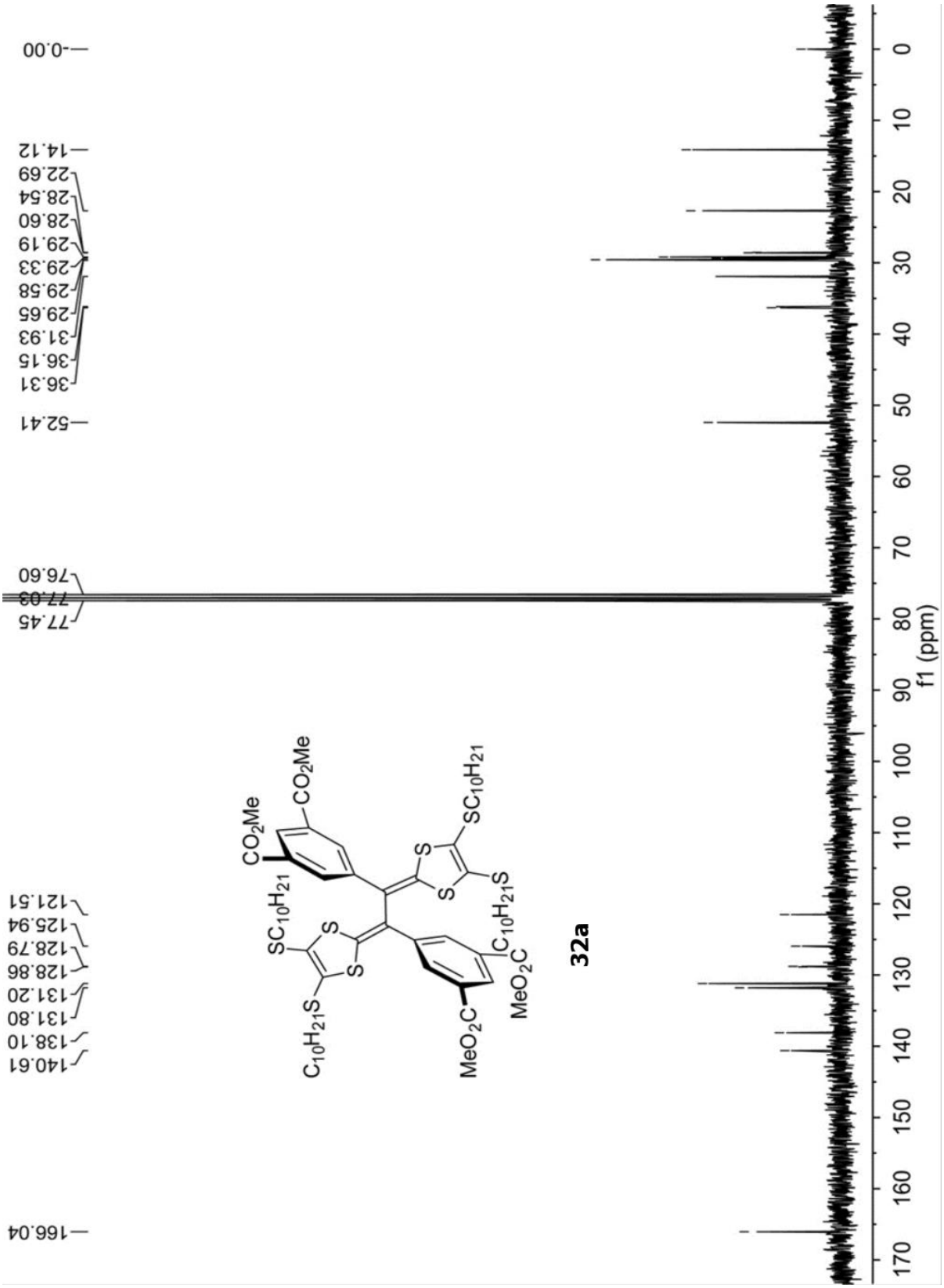

Fig. S-4 ^{13}C NMR (75 MHz, $CDCl_3$) of compound **32a**.

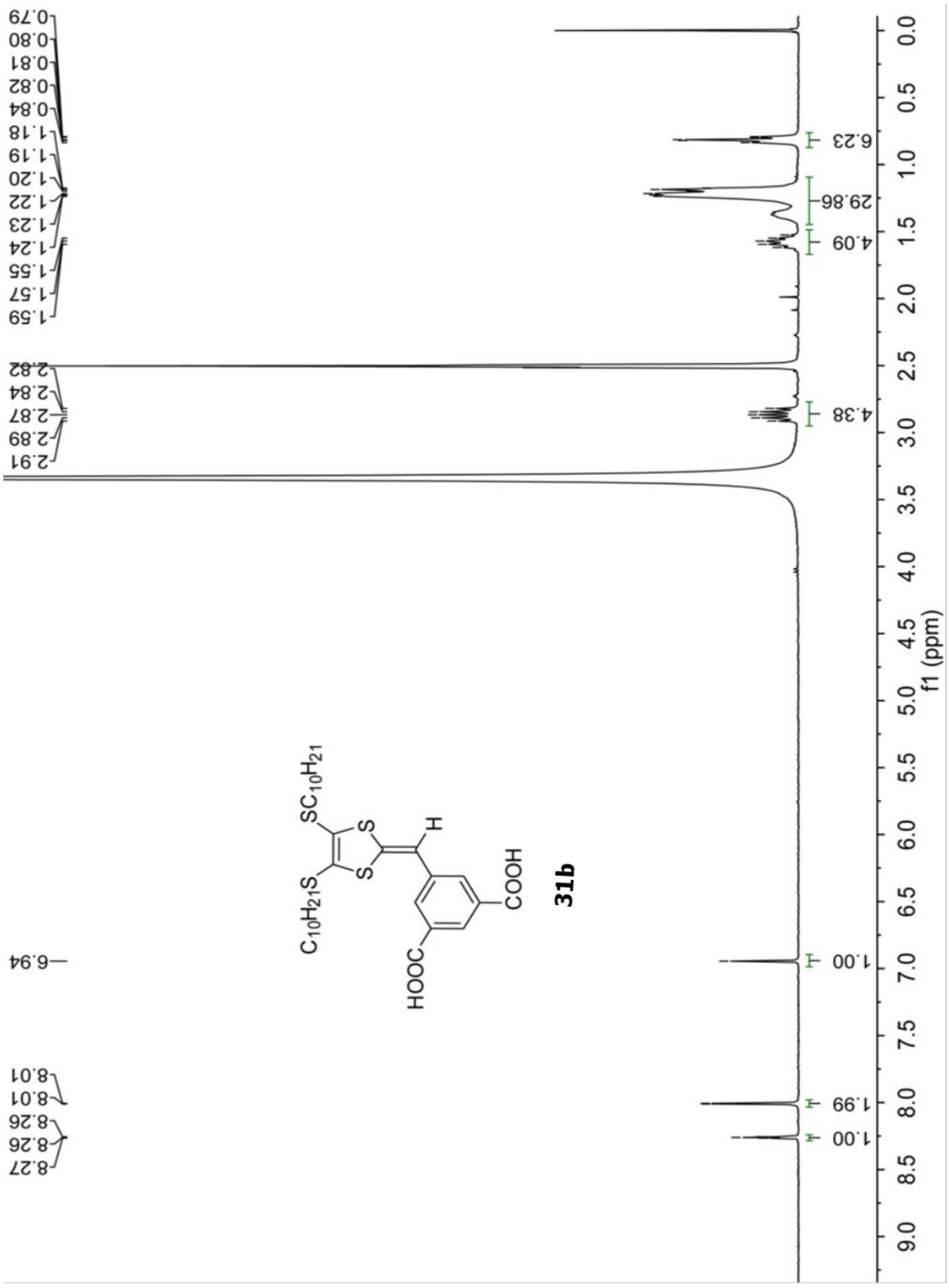

Fig. S-5 ^{1}H NMR (300 MHz, DMSO-d_6) of compound **31b**.

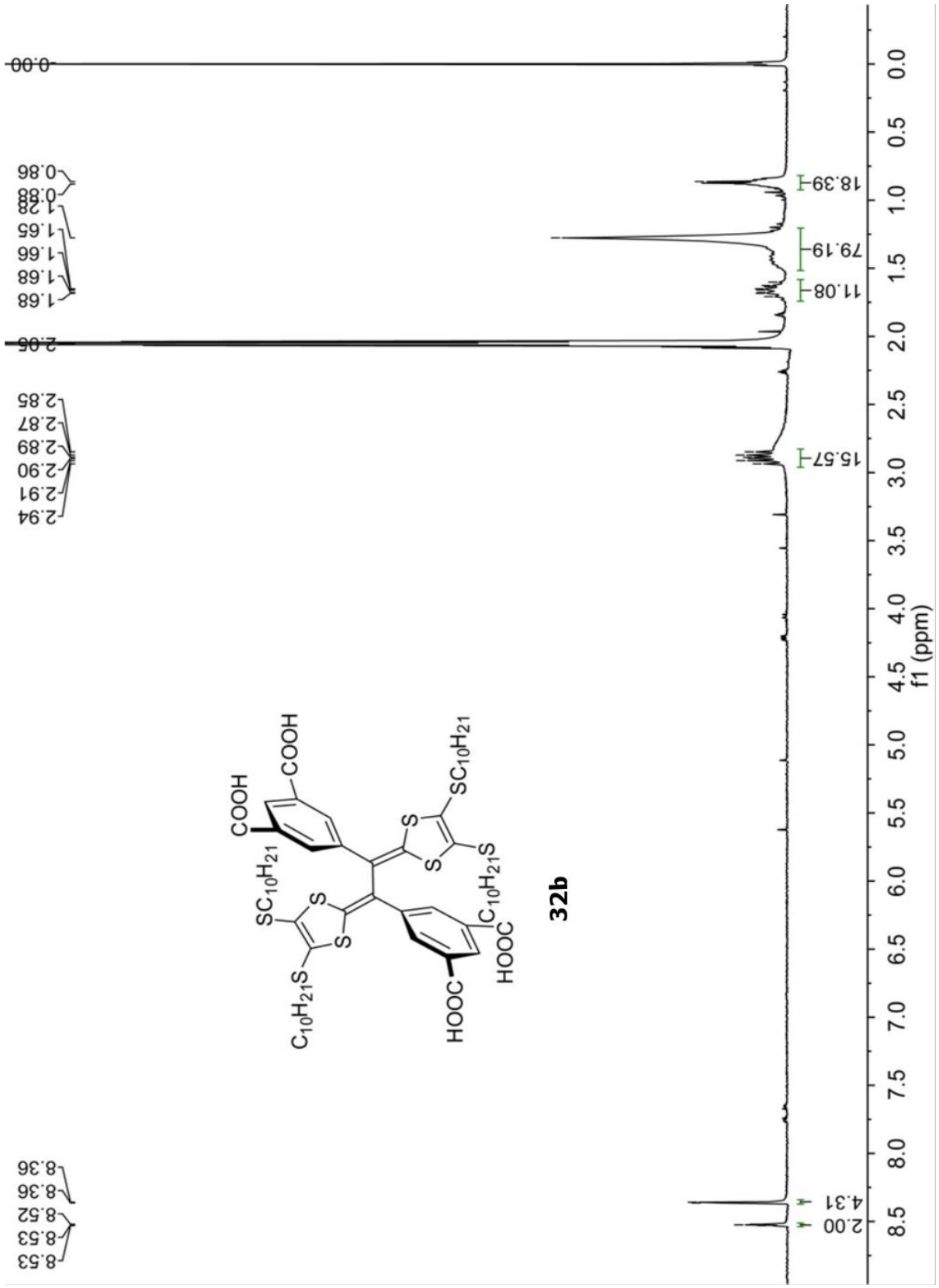

Fig. S-6 ^{1}H NMR (300 MHz, acetone-d_6) of compound **32b**

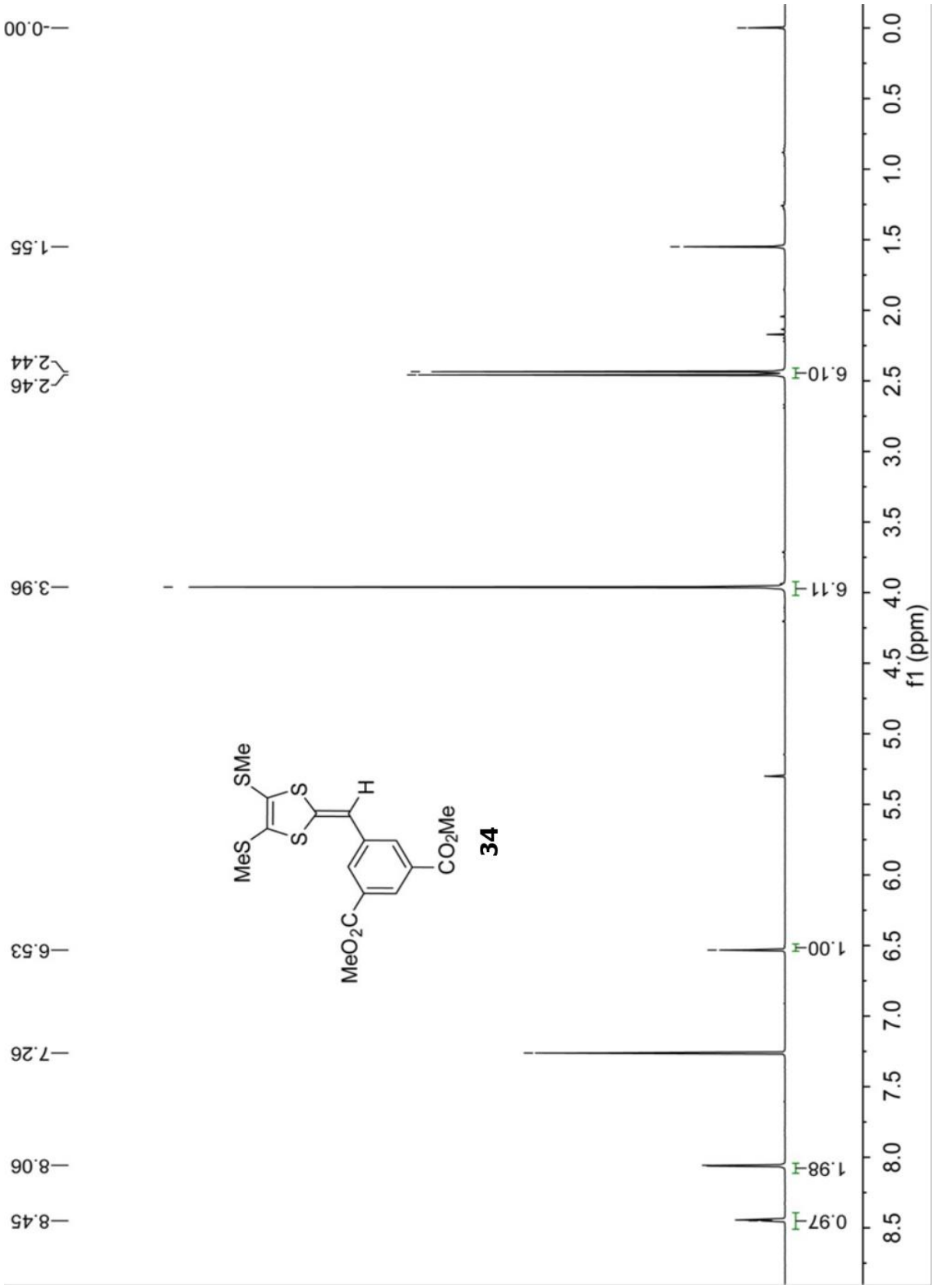

Fig. S-7 ^{1}H NMR (300 MHz, $CDCl_3$) of compound **34**.

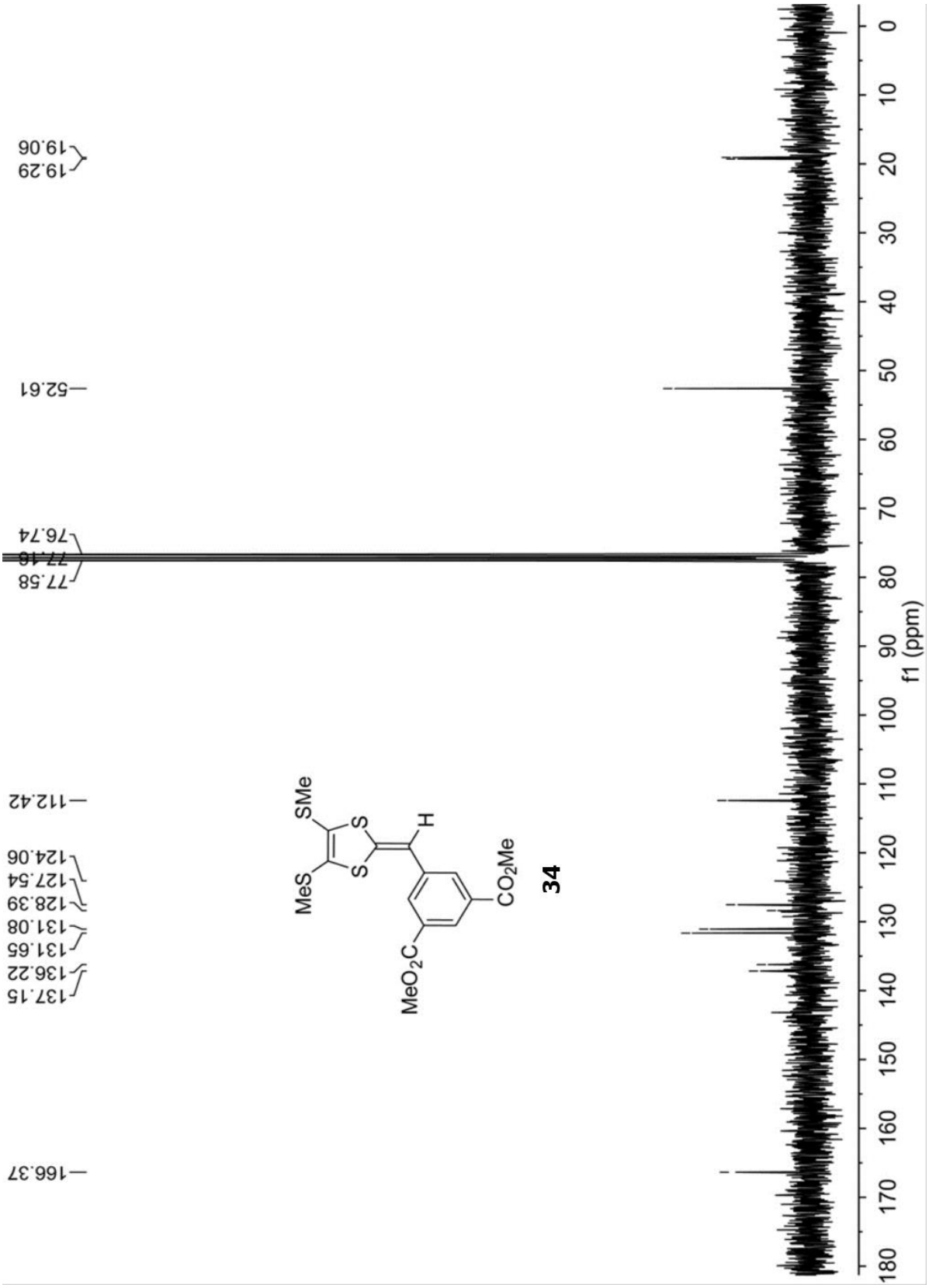

Fig. S-8 ^{13}C NMR (75 MHz, $CDCl_3$) of compound **34**.

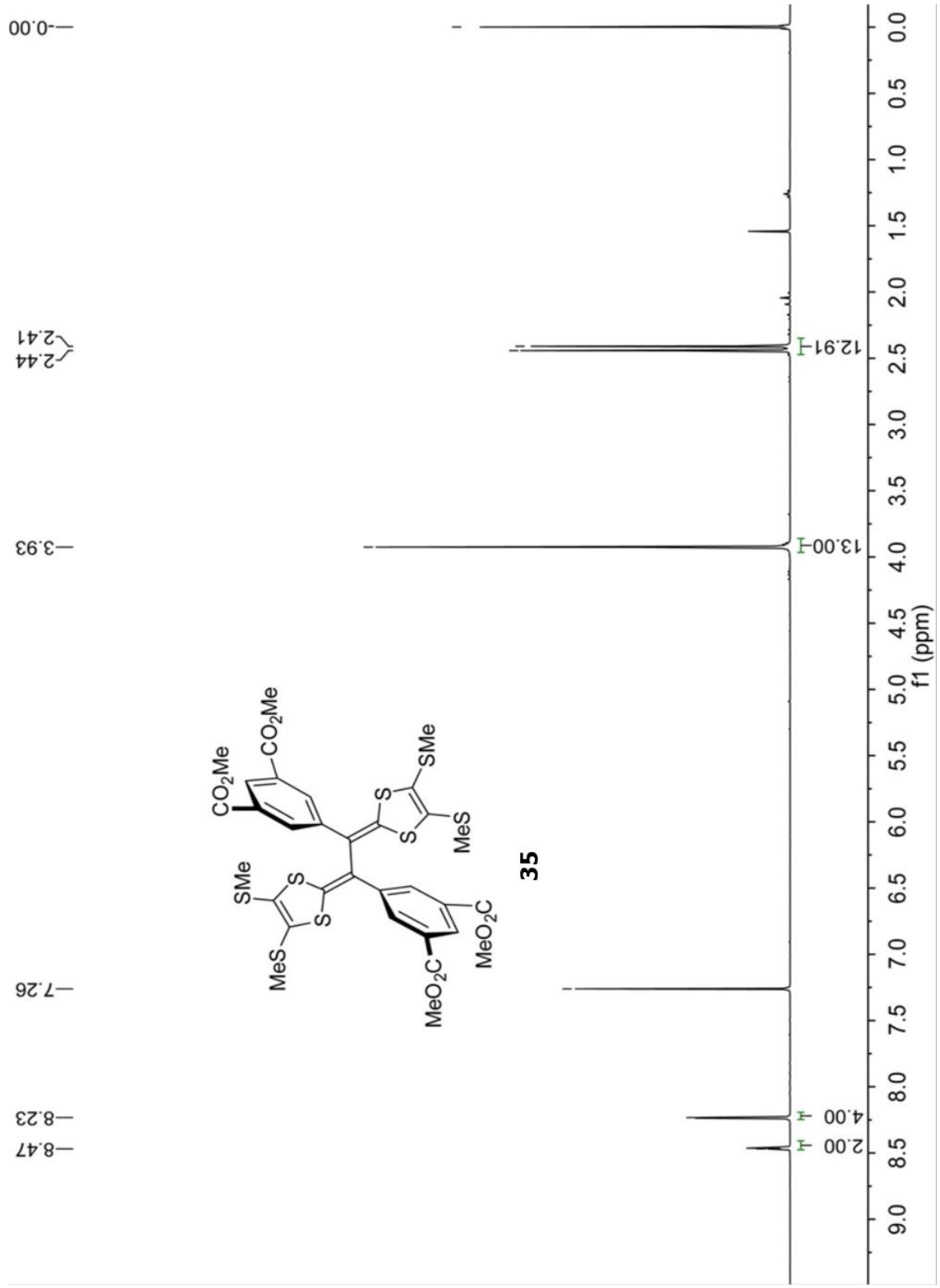

Fig. S-9 ^{1}H NMR (300 MHz, $CDCl_3$) of compound **35**

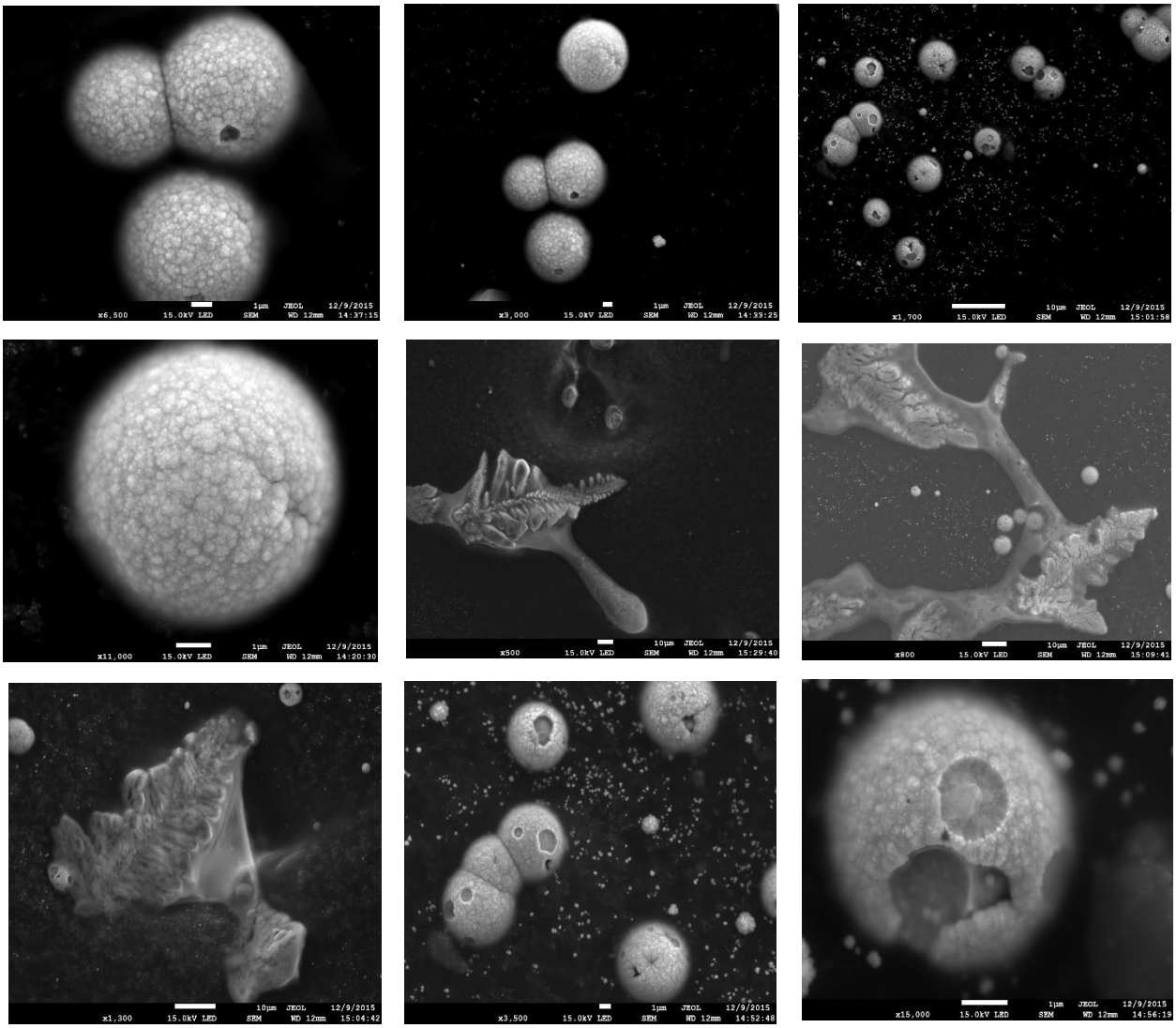

Fig. S-10 SEM images of the residuals resulting from evaporating the DMSO solutions of $HAuCl_4$ mixed with DTF **31b**.

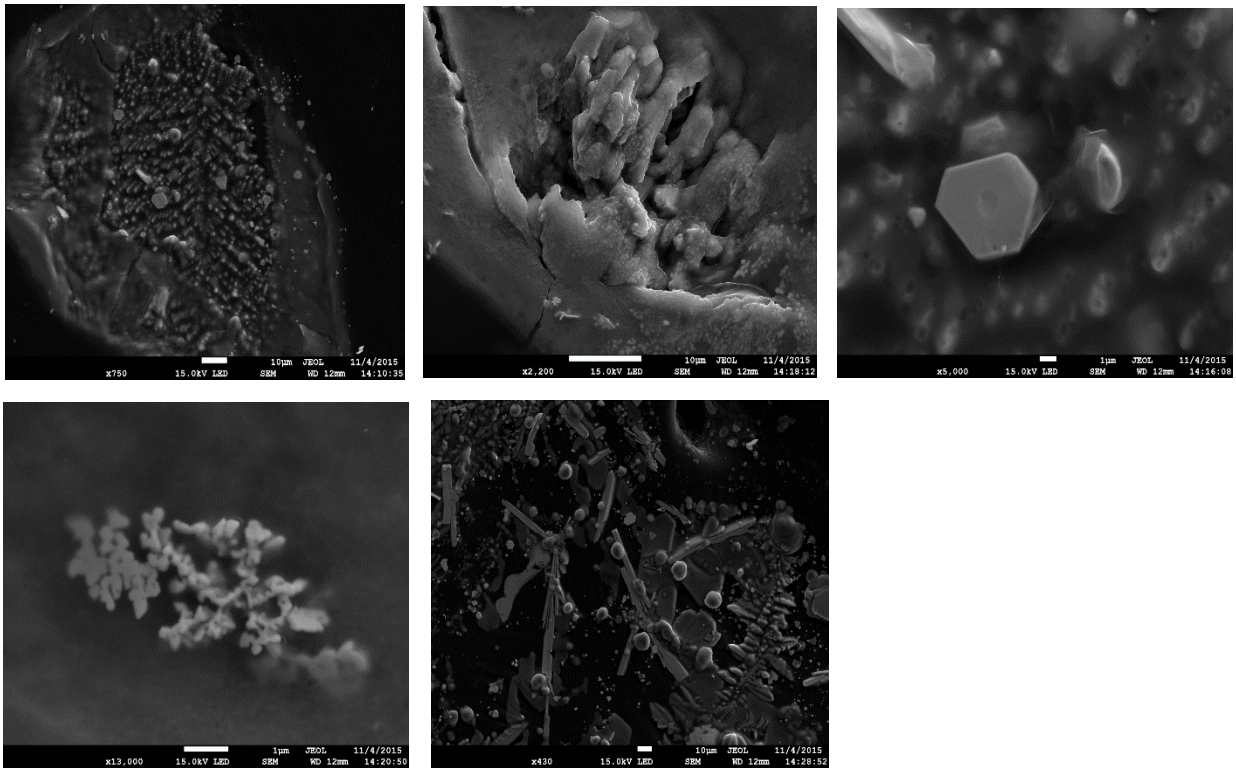

Fig. S-11 SEM images of the residuals resulting from evaporating the DMSO solutions of $HAuCl_4$ mixed with DTF **31a**.